Supplementary Information for

Electron-rich pyridines with *para*-N-heterocyclic imine substituents: ligand properties and coordination to CO_2, SO_2, BCl_3 and Pd^{II} complexes

Jonas H. Franzen[a], Lukas F. B. Wilm[b], Philipp Rotering[a], Klaus Wurst[a], Michael Seidl[a], and Fabian Dielmann[a]

[a] Institut für Allgemeine, Anorganische und Theoretische Chemie, Leopold-Franzens-Universität Innsbruck, Innrain 80-82, 6020 Innsbruck (Austria)
e-mail: fabian.dielmann@uibk.ac.at
homepage: https://www.uibk.ac.at/en/aatc/ag-dielmann/univ-prof-dr-fabian-dielmann/

[b] Institut für Anorganische und Analytische Chemie, Universität Münster
Corrensstrasse 30, 48149 Münster (Germany)

CONTENTS:

Synthetic Details **3**

Preparation of Pyridines 1 and 2 **4**

Preparation of Dication 3 **9**

Reactions of 1 with CO_2 **13**

Preparation of Coordination Compounds 4-8 **23**

Preparation of Compounds 9-13 **30**

Demethylation reactions of LB–Me iodide salts 9-12 **34**

Determination of the Huynh Electronic Parameter **41**

Computational Details **43**

X-ray Diffraction Studies **54**

Single-crystal X-ray structure analysis of 1: 55

Single-crystal X-ray structure analysis of 2: 56

Single-crystal X-ray structure analysis of 3: 57

Single-crystal X-ray structure analysis of 4: 58

Single-crystal X-ray structure analysis of 5: 59

Single-crystal X-ray structure analysis of 6: 60

Single-crystal X-ray structure analysis of 7: 61

Single-crystal X-ray structure analysis of 8: 62

Single-crystal X-ray structure analysis of 12: 63

Single-crystal X-ray structure analysis of 13: 64

References **65**

Synthetic Details

General remarks: If not mentioned otherwise, all manipulations were performed under an inert atmosphere of dry argon, using standard Schlenk and drybox techniques. Dry and oxygen-free solvents were employed. ^{1}H, ^{11}B, ^{13}C and ^{15}N spectra were recorded at 300 K in the solvent indicated on Bruker AVANCE I 400, Bruker AVANCE III 400, Bruker AVANCE II 200, Bruker AVANCE NEO 500 or Bruker AVANCE IV 400 spectrometers. Chemical shifts are given in parts per million (ppm) relative to $SiMe_4$ (TMS) in $CDCl_3$ (^{1}H, ^{13}C), 15% BF_3 x Et_2O in $CDCl_3$ (^{11}B) or NH_3 (^{15}N) and were referenced internally to the residual solvent signals. HEP values were referenced to the solvent residual signal of $CDCl_3$ at 77.7 ppm relative to TMS.[1–3] NMR multiplicities are abbreviated as follows: s = singlet, d = doublet, t = triplet, sept = septet, m = multiplet, br = broad signal. Mass spectra were obtained with an Orbitrap LTQ XL (Thermo Scientific) spectrometer. IR spectra were obtained on a Bruker ALPHA II FT-IR Spectrometer. Intensities of the signals are abbreviated as follows: w = weak, m = medium, s = strong, vs = very strong1,3-Diisopropyl-4,5-dimethyl-2-chloroimidazolium tetrafluoroborate[4], 2,6-dimethyl-4-pyridinamine[5] and $[PdBr_2(BiPr)]_2$[6] were prepared following literature procedures. Sulfur dioxide was purchased from Messer Griesheim GmbH (47805 Krefeld, Germany) as SO_2 3.8 (99.98%). Carbon dioxide was purchased from Westfalen AG (48155 Münster, Germany) as CO_2 4.5 (99.995%). All other compounds were purchased from commercial sources.

Preparation of Pyridines **1** and **2**

Compound 1: 1,3-Diisopropyl-4,5-dimethyl-2-chlorimidazolium tetrafluoroborate[4] (1.00 g, 3.29 mmol, 1.00 eq.), pyridine-4-amine (0.310 g, 3.29 mmol, 1.00 eq.) and KF (1.15 g, 19.8 mmol, 6.00 eq.) were suspended in MeCN (50 mL) and heated up in a pressure tube for 3 d at 160 °C. The reaction mixture was allowed to cool down to room temperature, the solids were filtered off and the volatiles of the filtrate were removed under reduced pressure. The residue was suspended in hot *n*-hexane (2 x 30 mL, 60 °C) and filtered hot. The solution was concentrated by half *in vacuo* and stored at –18 °C yielding **1** as colorless crystals in 82.0% yield (0.795 g, 2.92 mmol).

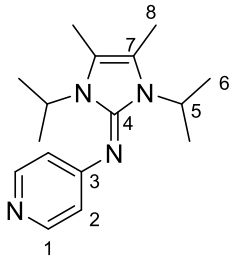

^{1}H NMR (400.03 MHz, MeCN-d_3): δ = 7.83–7.85 (m, 2H, H-2), 6.16–6.18 (m, 2H, H-1), 4.38 (sept, $^{3}J_{HH}$ = 7.1 Hz, 2H, H-5), 2.16 (s, 6H, H-8), 1.34 (d, $^{3}J_{HH}$ = 7.1 Hz, 12H, H-6) ppm.

^{13}C{^{1}H} NMR (100.60 MHz, MeCN-d_3): δ = 161.3 (s, C-3), 151.0 (s, C-4), 150.4 (s, C-2), 119.9 (s, C-7), 113.4 (s, C-2), 48.3 (s, C-5), 21.0 (s, C-6), 10.1 (s, C-8) ppm.

2D NMR experiments were performed for the assignment of the resonances.

HRMS (ESI): m/z calculated for $[C_{16}H_{25}N_4]^+$ $(M+H)^+$ 273.20737, found 273.20743.

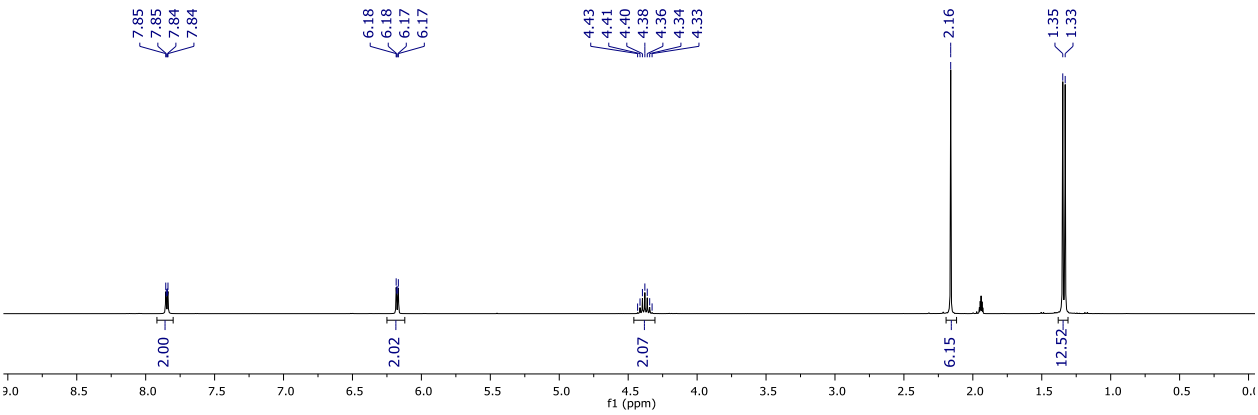

Figure S1: ^{1}H NMR spectrum (in MeCN-d_3, 300 K, 400.03 MHz) of **1**.

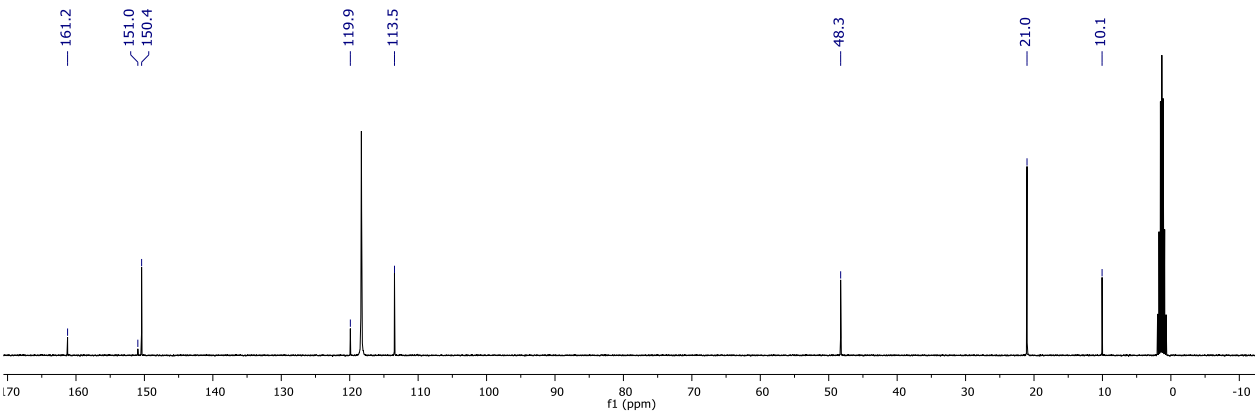

Figure S2: $^{13}C\{^{1}H\}$ NMR spectrum (in MeCN-d_3, 300 K, 100.60 MHz) of **1**.

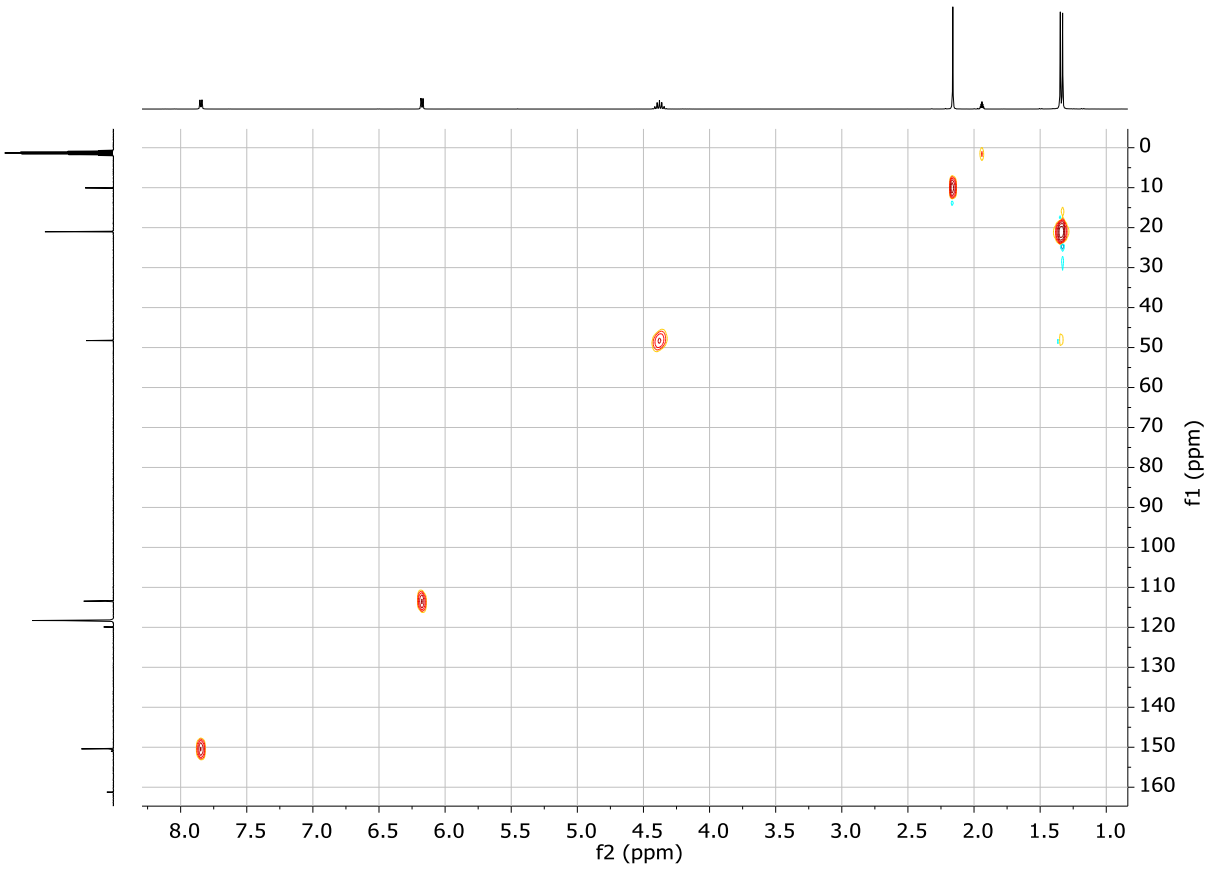

Figure S3: ^{1}H-$^{13}C\{^{1}H\}$ HSQC NMR spectrum (in MeCN-d_3, 300 K, 400.23 MHz, 100.60 MHz) of **1**.

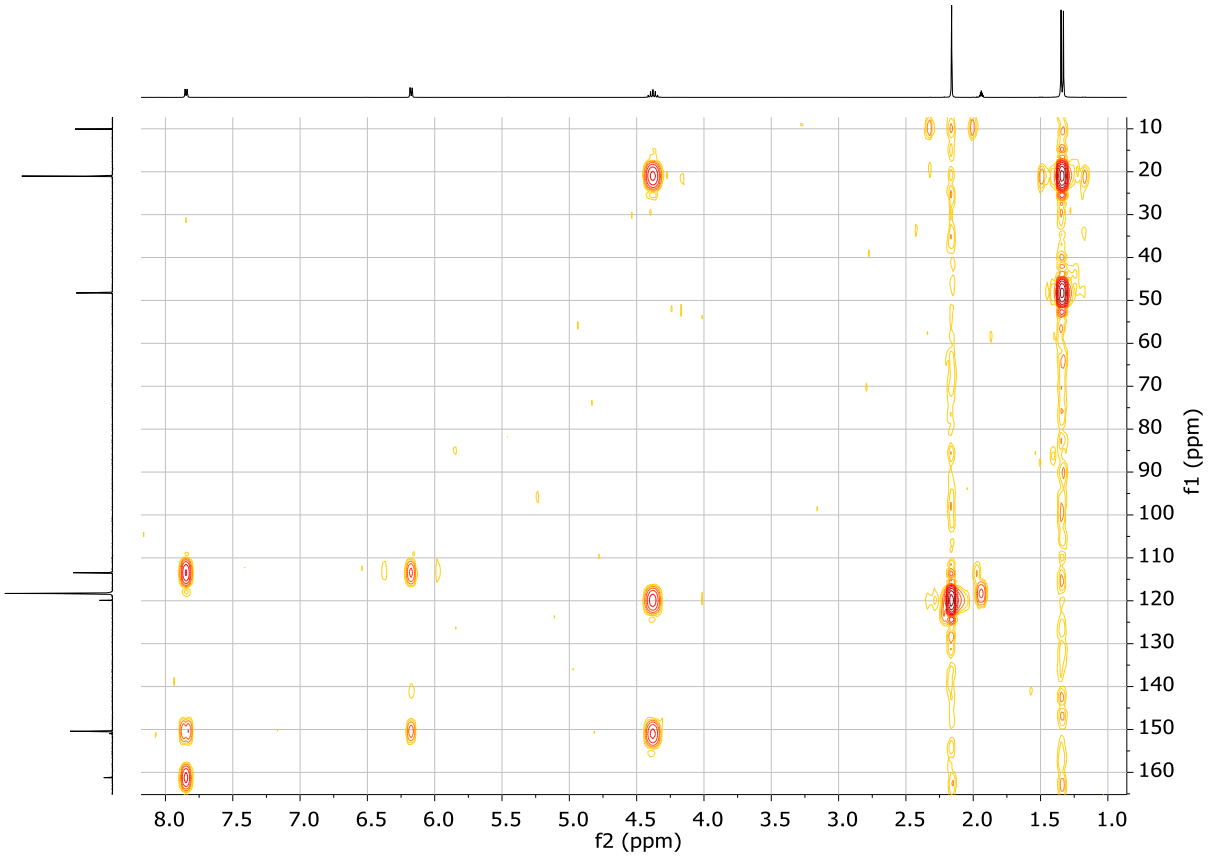

Figure S4: ^{1}H-^{13}C{^{1}H} HMBC NMR spectrum (in MeCN-d_3, 300 K, 400.23 MHz, 100.60 MHz) of **1**.

Compound 2: 1,3-Di-*tert*-butyl-2-chlorimidazolinium tetrafluoroborate[4] (3.24 g, 10.6 mmol, 1.00 eq.), pyridine-4-amine (1.00 g, 10.6 mmol, 1.00 eq.) and KF (3.70 g, 63.8 mmol, 6.00 eq.) were suspended in MeCN (50 mL) and stirred at 90 °C for 3 d in a pressure tube. While cooling down to room temperature, a colorless solid formed in the reaction mixture. The volatiles were removed under reduced pressure and the product was subsequently extracted with hot *n*-hexane (3 x 20 mL, 60 °C). The combined fractions of *n*-hexane were concentrated by half under reduced pressure and stored at –18 °C yielding **2** as colorless crystals in 72.0% total yield (2.10 g, 7.65 mmol).

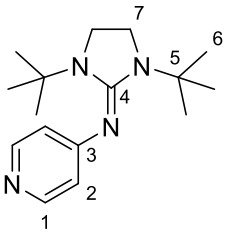

^{1}H NMR (400.03 MHz, C_6D_6) δ = 8.48–8.50 (m, 2H, H-2), 6.49–6.51 (m, 2H, H-1), 2.69 (s, 4H, H-7), 1.09 (s, 18H, C-6) ppm.

^{13}C NMR (100.60 MHz, C_6D_6) δ = 158.6 (s, C-4), 157.9 (s, C-3), 150.5 (s, C-2), 115.1 (s, C-1), 55.7 (s, C-5), 42.6 (s, C-7), 28.3 (s, C-6) ppm.

2D NMR experiments were performed for the assignment of the resonances.

HRMS (ESI): m/z calculated for $[C_{16}H_{27}N_4]^+$ $(M+H)^+$ 275.22302, found 275.2227.

Elemental Analysis: calculated (%) for $C_{16}N_4H_{26}$: C 70.03, N 20.42, H 9.55, found C 70.09, N 20.34, H 9.53.

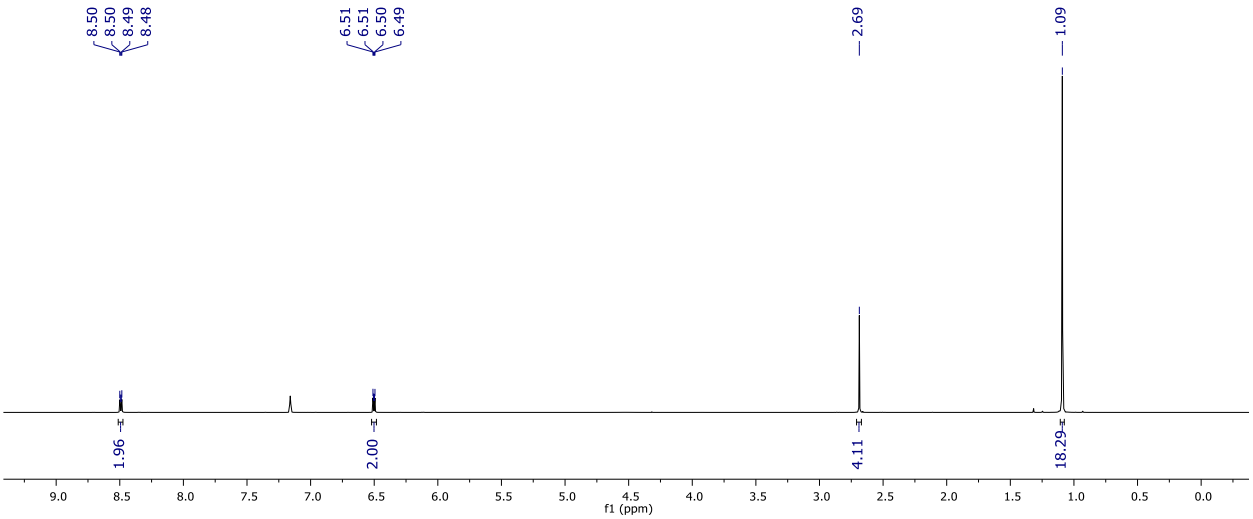

Figure S5: ^{1}H NMR spectrum (in C_6D_6, 300 K, 400.03 MHz) of **2**.

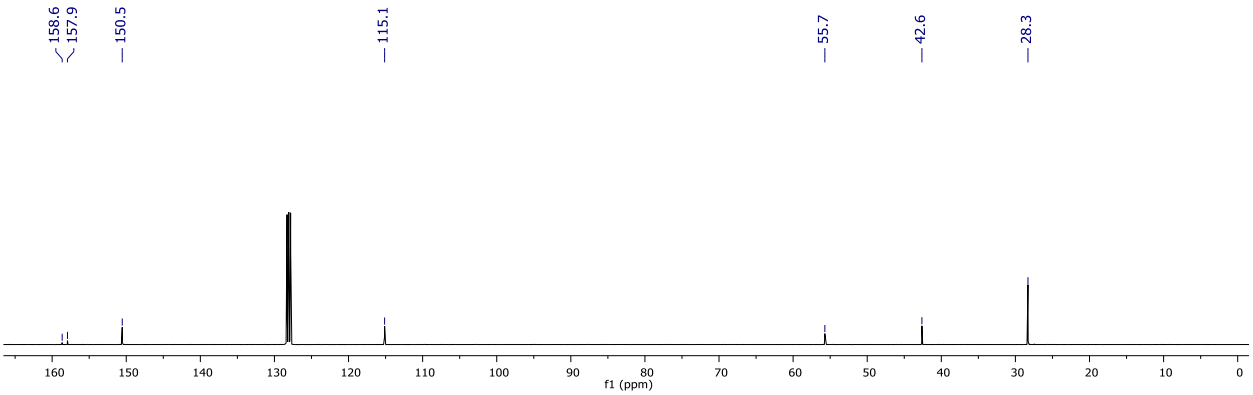

Figure S6: ^{13}C{H} NMR spectrum (in C_6D_6, 297 K, 100.60 MHz) of **2**.

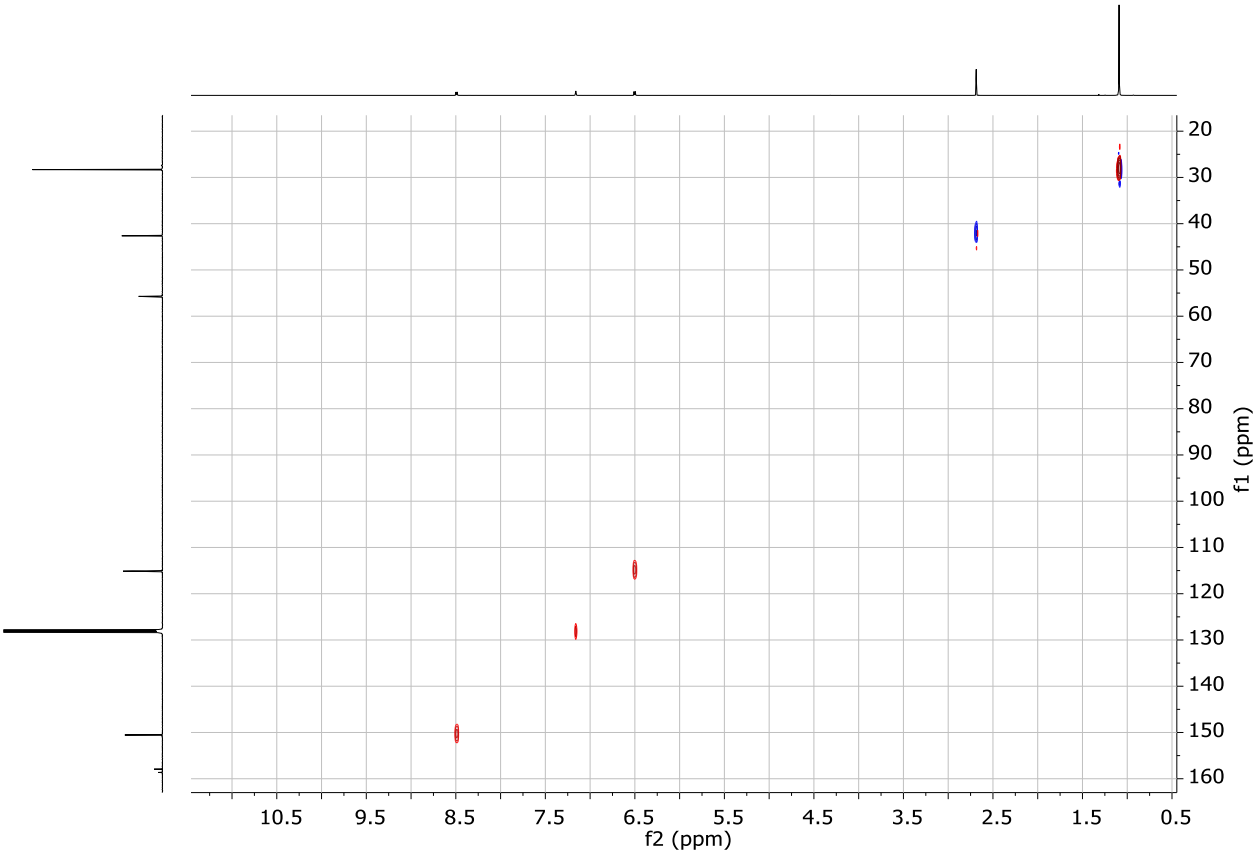

Figure S7: ^{1}H-$^{13}C\{^{1}H\}$ HSQC NMR spectrum (in C_6D_6, 300 K, 400.03 MHz, 100.60 MHz) of **2**.

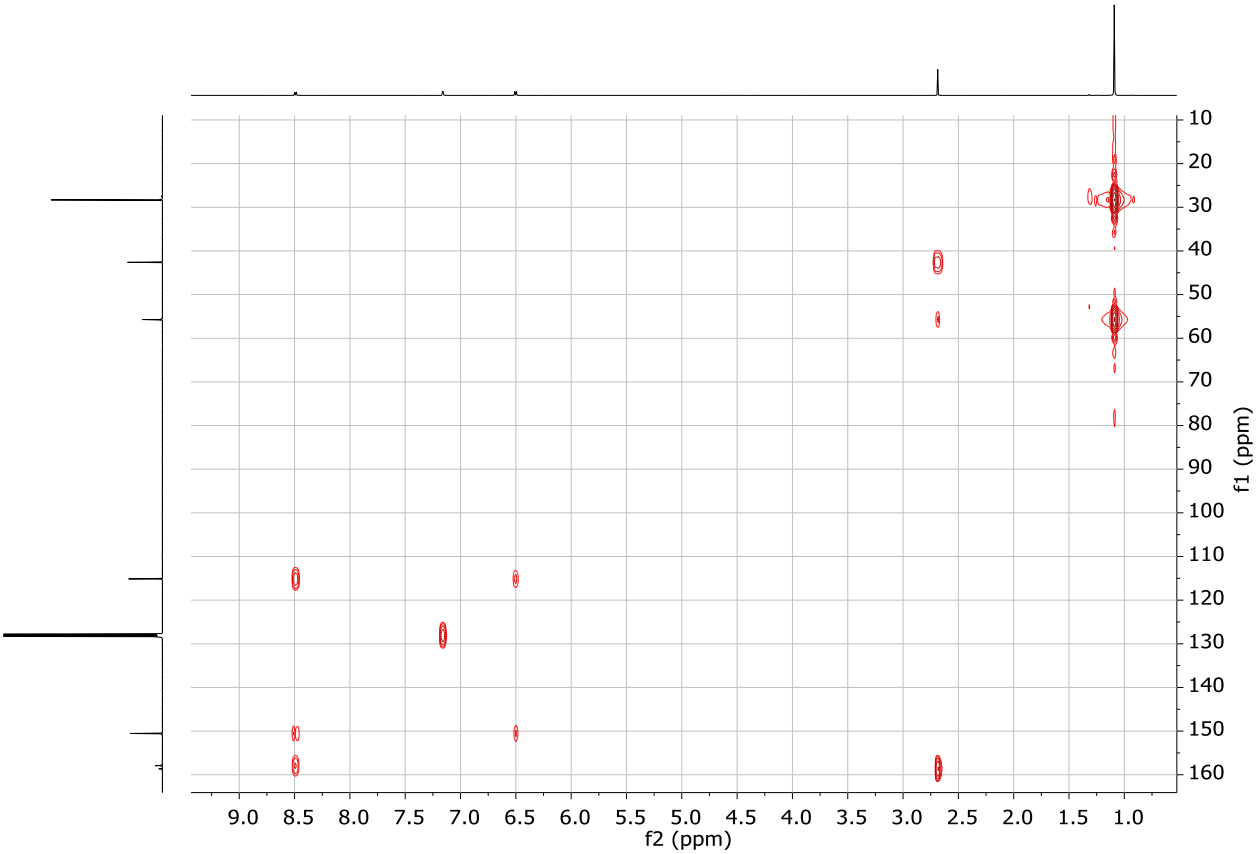

Figure S8: ^{1}H-^{13}C{^{1}H} HMBC NMR spectrum (in C_6D_6, 300 K, 400.03 MHz, 100.60 MHz) of **2**.

Preparation of Dication **3**

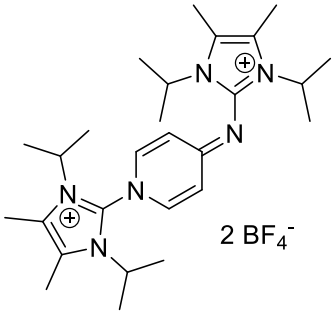

1,3-Diisopropyl-4,5-dimethyl-2-chloroimidazolium tetrafluoroborate[4] (200 mg, 659 µmol, 1.00 eq.), pyridine-4-amine (62.0 mg, 659 µmol, 1.00 eq.) and KF (230 mg, 3.95 mmol, 6.00 eq.) were suspended in MeCN (10 mL), Et_3N (133 mg, 183 µL, 1.32 mmol, 2.00 eq.) was added and the reaction mixture was stirred for 3 d at room temperature. $CHCl_3$ (20 mL) was added and the suspension was filtrated. The organic phase was washed with an aqueous solution of $NaBF_4$ (750 mg in 15 mL H_2O, 10.4 eq.) and subsequently with H_2O (10 mL). The volatiles of the organic phase were removed under reduced pressure, the residue was washed with THF (2 x 10 mL) and after drying at 50 °C *in vacuo* for 16 h, **3** was obtained as a light-yellow solid in 41 % yield (167 mg, 267 µmol).

^{1}H NMR (400.03 MHz, MeCN-d_3): δ = 7.59 (br, 2H, H_{aryl}), 6.78 (br, 1H, CH_{aryl}), 6.25 (br, 1H, CH_{aryl}), 4.49 (sept, $^{3}J_{HH}$ = 7.1 Hz, 2H, *i*Pr-CH), 4.37 (sept, $^{3}J_{HH}$ = 7.0 Hz, 2H, *i*Pr-CH), 2.38 (s, 6H, imidazole-CH_3), 2.26 (s, 6H, imidazole-CH_3), 1.46 (d, $^{3}J_{HH}$ = 7.0 Hz, 12H, *i*Pr-CH_3), 1.44 (br, 12H, *i*Pr-CH_3) ppm.

^{13}C{^{1}H} NMR (100.60 MHz, MeCN-d_3): δ = 164.7 (s, $NC_q(CH_{aryl})_2$), 146.7 (s, N_3C_q), 140.9 (s, br, CH_{aryl}), 133.9 (s, N_3C_q), 128.7 (s, imidazole-C_q), 123.7 (s, imidazole-C_q), 113.0 (s, br, CH_{aryl}), 53.4 (s, *i*Pr-CH), 50.1 (s, *i*Pr-CH), 21.3 (s, *i*Pr-CH_3), 20.5 (s, br, *i*Pr-CH_3), 9.9 (s, imidazole-CH_3), 9.8 (s, imidazole-CH_3) ppm.

^{19}F NMR (376.44 MHz, MeCN-d_3): δ = –151.9 (s)

^{19}F{^{1}H} NMR (376.44 MHz, MeCN-d_3): δ = –151.9 (s)

^{11}B NMR (100.60 MHz, MeCN-d_3): δ = –1.2 (s).

^{11}B{^{1}H} NMR (100.60 MHz, MeCN-d_3): δ = –1.2(s)

HRMS (ESI): m/z calculated for $[C_{27}H_{44}N_6]^{2+}$ $(M)^{2+}$ 226.18082, found 226.18147; calculated $[C_{27}H_{44}N_6BF_4]^{+}$ $(M+BF_4)^{+}$ 539.36512, found 539.36725.

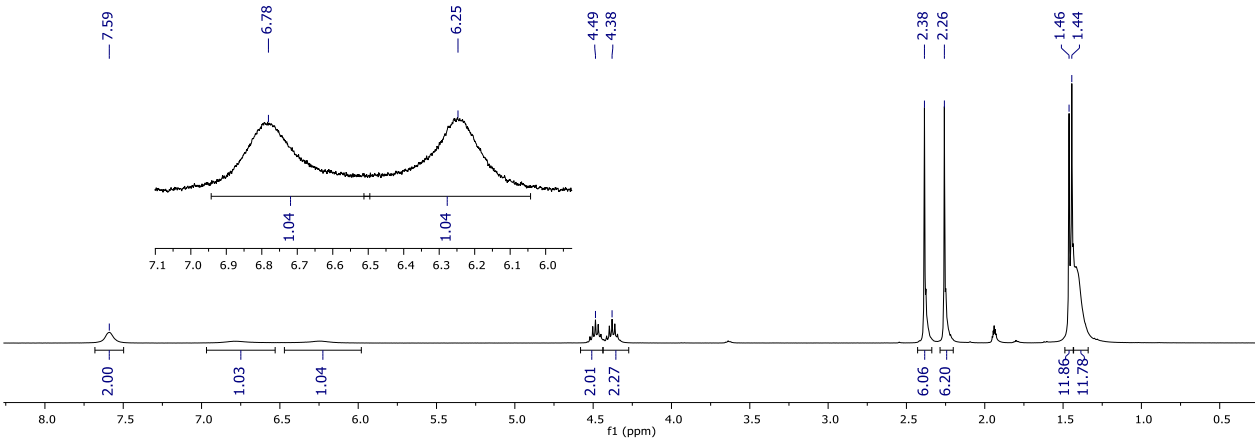

Figure S9: ^{1}H NMR spectrum (in MeCN-d_3, 300 K, 400.03 MHz) of **3**.

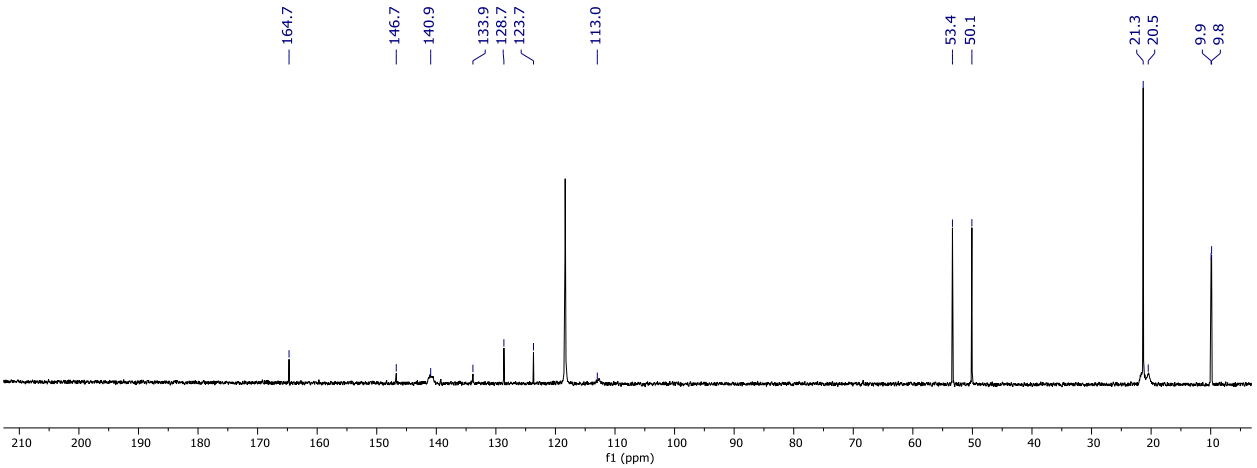

Figure S10: $^{13}C\{^{1}H\}$ NMR spectrum (in MeCN-d_3, 300 K, 100.60 MHz) of **3**.

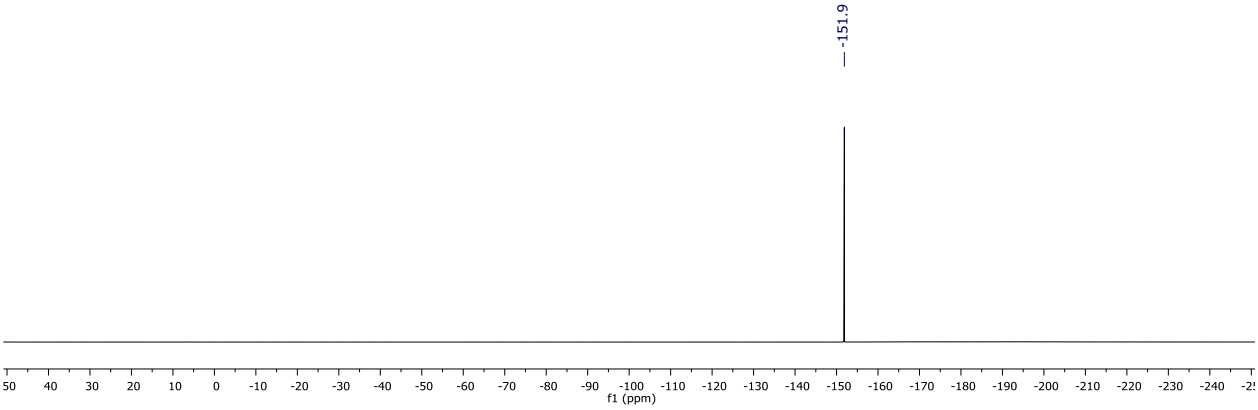

Figure S11: ^{19}F NMR spectrum (in MeCN-d_3, 300 K, 376.44 MHz) of **3**.

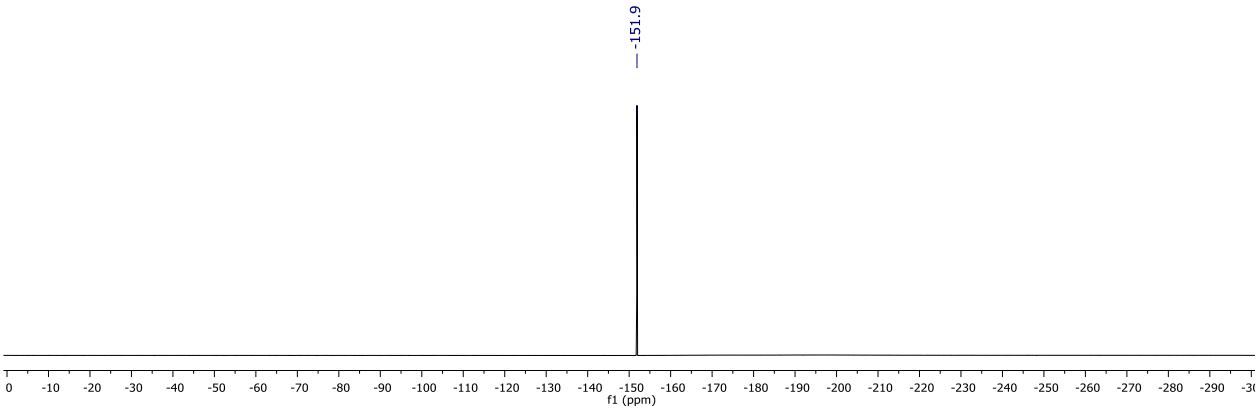

Figure S12: $^{19}F\{^{1}H\}$ NMR spectrum (in MeCN-d_3, 300 K, 376.44 MHz) of **3**.

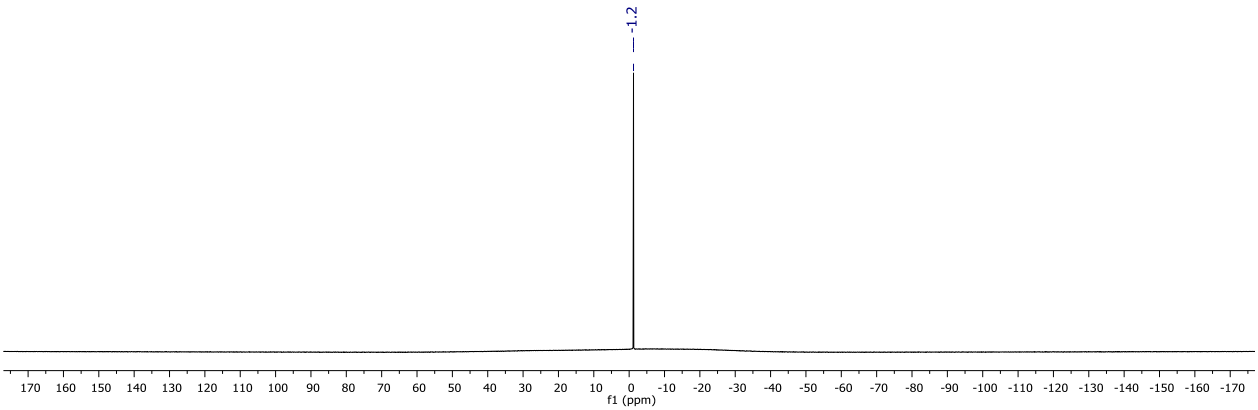

Figure S13: ^{11}B NMR spectrum (in MeCN-d_3, 300 K, 128.38 MHz) of **3**.

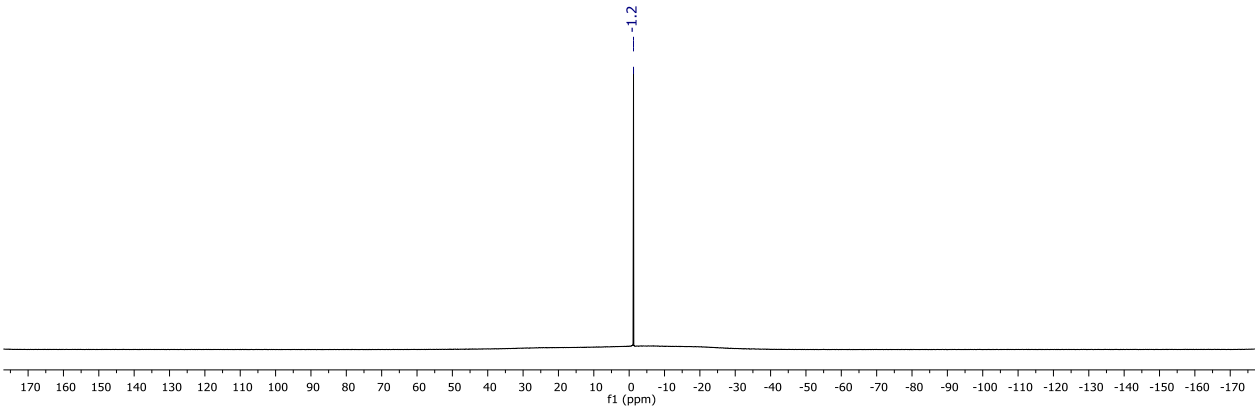

Figure S14: ^{11}B{^{1}H} NMR spectrum (in MeCN-d_3, 300 K, 128.38 MHz) of **3**.

Reactions of **1** with CO_2

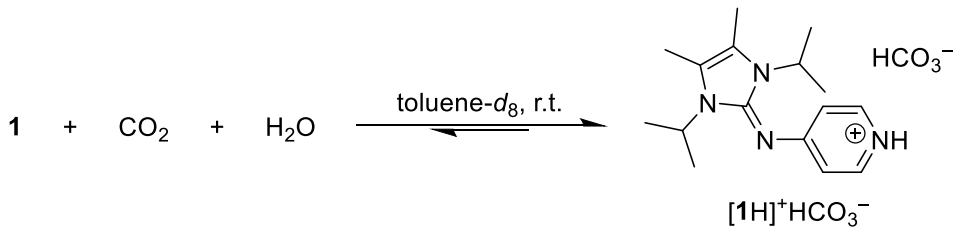

Scheme 1: Reaction of **1** with CO_2 and H_2O to form the bicarbonate salt [**1**H]$^+$HCO$_3^-$.

In an NMR tube, a solution of **1** (20.0 mg, 73.3 µmol, 1.0 eq.) in toluene-d_8, to which H_2O (2.00 µL, 110 µmol, 1.5 eq.) was added, was pressurized with 4 bar CO_2 and shaken vigorously to mix the two phases. Then, the NMR tube was put in an ultrasonic bath for 10 minutes which caused the formation of a voluminous white precipitate. No precipitate formed under the exclusion of H_2O. When carefully heated with a heat gun set to 80 °C, the solid rapidly dissolved releasing CO_2 in the process and reformed when the solution cools down to room temperature. After releasing the excess CO_2 from the sealed NMR tube, the bicarbonate salt [**1**H]$^+$HCO$_3^-$ is partially dissolved releasing CO_2 in the process over a period of 16 h.

The synthesis of [**1**H]$^+$HCO$_3^-$ was repeated in a PTFE-sealed Schlenk flask. Argon was passed through the suspension to drive out CO_2. This led to a complete dissolution of the solid under reconversion to the starting material **1** (Figure S15) after 16 h.

[**1**H]$^+$HCO$_3^-$ appears to be only stable under an atmosphere of CO_2. Attempts to remove the solvent under reduced pressure resulted in the isolation of **1**.

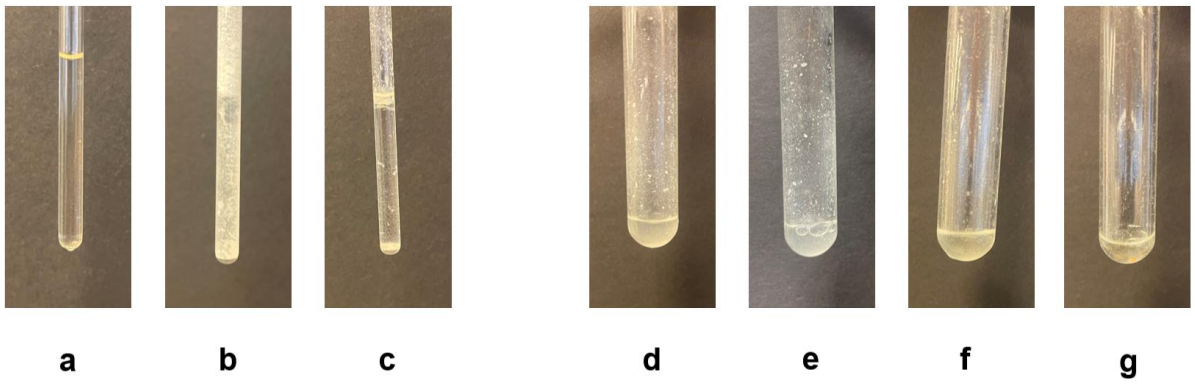

Figure S15: Formation and dissociation of [**1**H]$^+$HCO$_3^-$ from a solution of **1** in toluene-d_8 in a PTFE-sealed NMR tube (left): clear solution of **1** in toluene-d_8 (**a**), precipitate after pressurizing with 4 bar CO_2 in the presence of 1.5 eq. H_2O (**b**), suspension after 16 h after releasing the excess CO_2 atmosphere (**c**). The reaction was repeated in a PTFE-sealed Schlenk flask (right): precipitation of [**1**H]$^+$HCO$_3^-$ after pressurizing with 4 bar CO_2 (**d**), continuous evolution of CO_2 after release of excess CO_2 (**e**), resulting suspension after releasing excess CO_2 (**f**), clear solution of **1** after exchanging the CO_2 atmosphere by passing Argon through the suspension (**g**).

The reaction of **1** with CO_2 and H_2O was repeated in the more polar solvent DMF-d_7 and monitored via ^1H and $^{13}C\{^1H\}$ NMR spectroscopy. The stacked spectra are depicted in Figure S16 and Figure S17, respectively. For the NMR spectra of **1** and **1**+CO_2, anhydrous DMF-d_7 was employed. **1** (20.0 mg, 73.3 µmol, 1.0 eq.) was dissolved in DMF-d_7 and H_2O (2.00 µL, 110 µmol, 1.5 eq.) was added before the NMR tube was pressurized with 4 bar of CO_2. Upon addition of H_2O, no significant shifts were observed in the ^1H NMR or $^{13}C\{^1H\}$ NMR spectrum for the resonances of **1**. The new signal at 3.58 ppm is assigned to H_2O. However, after pressurizing the water-containing sample with 4 bar CO_2, significant broadening and shift of the resonance to 4.14 ppm occurs in the ^1H NMR spectrum. This indicates a dynamic process, presumably the reversible formation of the pyridinium bicarbonate salt. Also, the proton shifts of the pyridine moiety are deshielded and appear at higher frequencies. A similar, yet smaller shift is observed as well in the absence of water.

Similarly, the $^{13}C\{^1H\}$ NMR spectra of the resonance of CO_2 appears as a broad signal at 126.3 ppm in the presence of water and as a sharp signal in the absence of water, consistent with a reversible formation of pyridinium bicarbonate in solution. Furthermore, the ^{13}C signals of the aromatic carbon atoms are shifted in both cases, more so in the presence of water. No additional resonance indicating the formation of the bicarbonate salt $[\mathbf{1}H]^+HCO_3^-$ was observed in the $^{13}C\{^1H\}$ NMR spectrum.

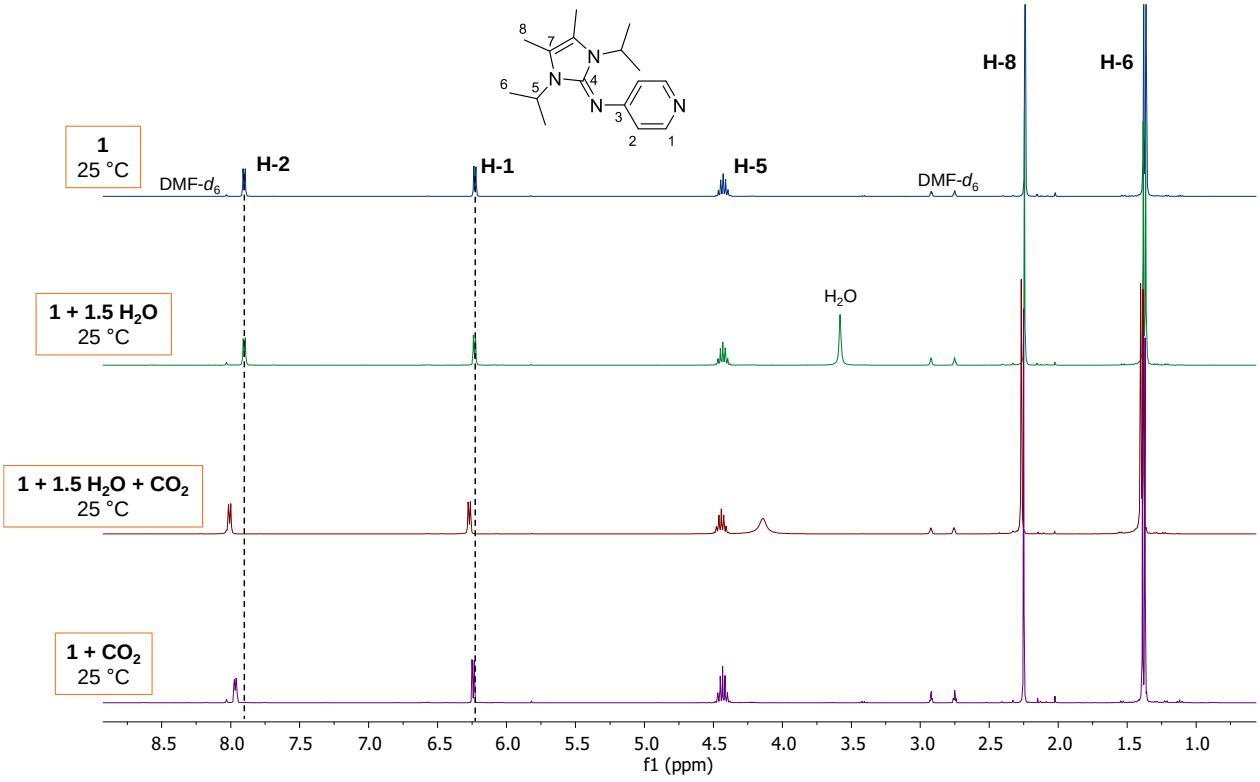

Figure S16: Stacked ^1H NMR spectra (400.03 MHz) of **1**, **1**+H_2O, **1**+H_2O+CO_2 and **1**+CO_2 in DMF-d_7 measured at 25 °C. Dotted lines are centered at the resonances of **1** to visualize the shift.

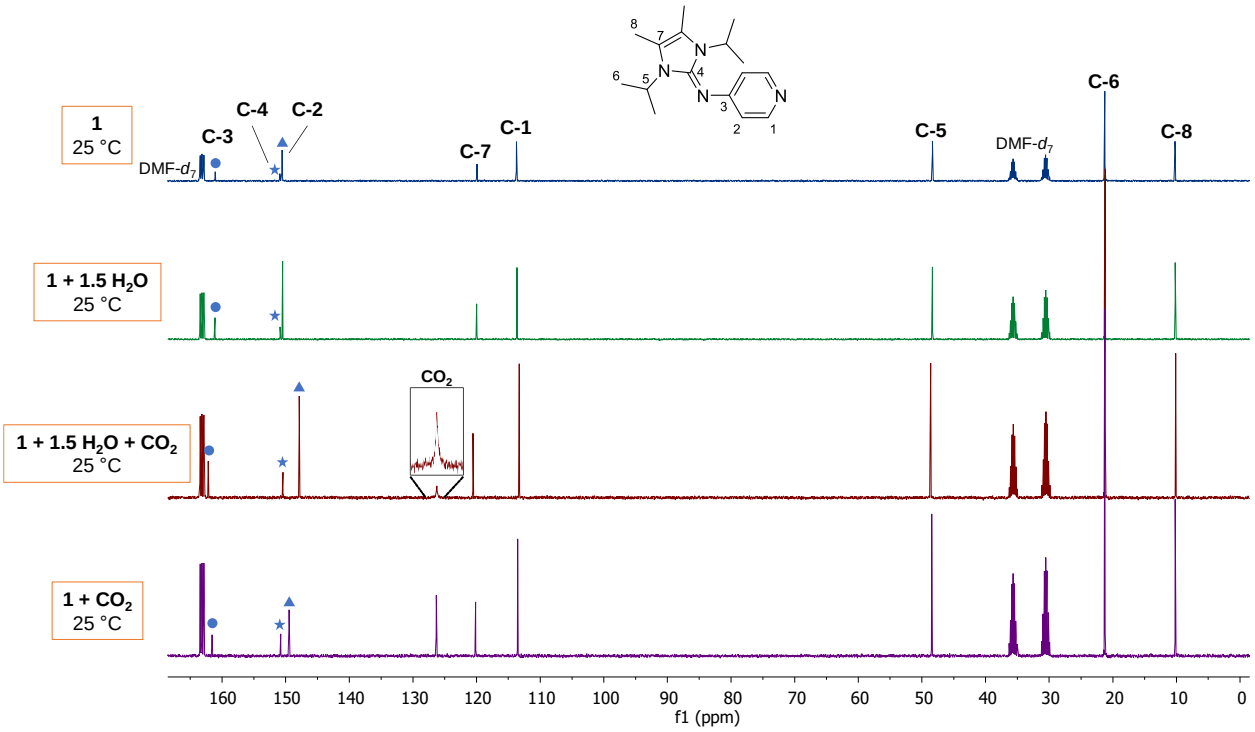

Figure S17: Stacked $^{13}C\{^{1}H\}$ NMR spectra (100.60 MHz) of **1**, **1**+H_2O, **1**+H_2O+CO_2 and **1**+CO_2 in DMF-d_7 measured at 25 °C. The C-2, C-3 and C-4 resonances are highlighted individually to visualize the shift.

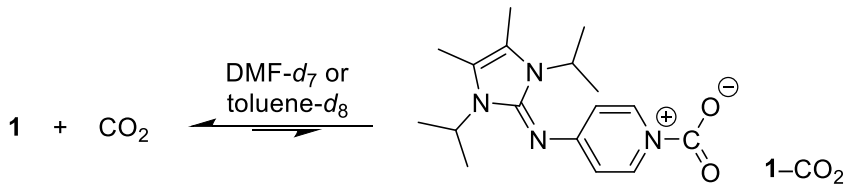

Scheme 2: Reaction of **1** with CO_2 to form the **1**–CO_2 adduct.

In an NMR tube, initial investigations of the formation of a CO_2 adduct with **1** were carried out in toluene-d_8. Due to the low polarity of toluene, the inner salt **1**–CO_2 was expected to precipitate from a solution of **1** (20.0 mg, 73.3 µmol) in toluene-d_8 after being subjected to an 0.8 bar atmosphere of $^{13}CO_2$ in an NMR tube. Instead, no formation of a solid was observed even at low temperatures down to –50 °C. Another sample of **1** (20.0 mg, 73.3 µmol) was dissolved in DMF-d_7 and pressurized with 4 bar CO_2. Due to the higher polarity of DMF, the formation of a **1**–CO_2 adduct is expected to be favored and to stay in solution. Both samples were subjected to variable temperature ^1H and $^{13}C\{^1H\}$ NMR experiments to spectroscopically investigate the **1**–CO_2 adduct formation. For comparison and to verify that changes in the NMR spectra are caused by the interaction with CO_2, the same variable temperature NMR experiments of **1** in toluene-d_8 and DMF-d_7 were carried out in the absence of CO_2.

Toluene-d_8: Figure S18 shows the stacked ^1H NMR spectra of **1** and **1**+CO_2 in toluene-d_8. The variable temperature ^1H NMR experiments show that at lower temperatures, the resonances of the pyridine protons are slightly downfield shifted whereas the resonances of the NHI protons are slightly highfield shifted. In both cases, the signals broaden at low temperatures down to –50 °C. This is likely because the rotation of the NHI group around the exocyclic N–C bond is hindered. Yet, the broadening of the signals is more pronounced in the sample with $^{13}CO_2$. The ^1H resonances of all protons at different temperatures for **1** and **1**+CO_2 are listed in table 1.

Table 1: ^1H NMR shifts of **1** and **1**+$^{13}CO_2$ in toluene-d_8 at given temperatures.

	H-1	**H-2**	**H-5**	**H-6**	**H-8**
1, 25 °C	6.54	8.41	4.31	1.04	1.61
1, –10 °C	6.59	8.50	4.28	1.01	1.53
1, –30 °C	6.61	8.54	4.30	0.99	1.50
1, –50 °C	6.63	8.58	4.42	0.93	2.09
1+CO_2, 25 °C	6.53	8.41	4.32	1.04	1.61
1+CO_2, –10 °C	6.54	8.42	4.28	1.01	1.58
1+CO_2, –30 °C	6.56	8.47	4.27	1.00	1.55
1+CO_2, –50 °C	6.52	8.53	4.32	0.95	1.52

Figure S19 shows the stacked $^{13}C\{^1H\}$ NMR spectra of **1** and **1**+CO_2 in toluene-d_8. The variable $^{13}C\{^1H\}$ NMR experiments show that the resonances of the pyridine moiety are not shifted at different temperatures in the absence of $^{13}CO_2$. In the presence of $^{13}CO_2$ the carbon resonances are more broadened at –10 °C and at lower temperatures. Also, the C-3 resonance is shifted to higher frequencies and the C-2 resonance is shifted to lower frequencies. Notably, the $^{13}CO_2$ is only shifted at –50 °C from 125.4 ppm to 125.8 ppm. We assume that the broadening and the shift of the signals is caused by the interaction of **1** with CO_2. Given the low polarity of toluene, the possible formation of the inner salt **1**–CO_2 is expected to be disfavored and appears to be only detectable at temperatures ≤ –50 °C. The ^{13}C resonances of all carbon atoms at different temperatures for **1** and **1**+$^{13}CO_2$ are listed in table 2.

Table 2: $^{13}C\{^{1}H\}$ NMR shifts of **1** and **1**+CO_2 in toluene-d_8 at given temperatures.

	C-1	**C-2**	**C-3**	**C-4**	**C-5**	**C-6**	**C-7**	**C8**	**$^{13}CO_2$**
1, 25 °C	114.1	151.2	160.3	150.6	47.7	21.0	118.3	10.0	–
1, –10 °C	114.1	151.2	160.3	150.4	47.7	21.0	118.3	9.9	–
1, –30 °C	114.0	151.2	160.3	150.3	47.6	20.9	118.3	9.9	–
1, –50 °C	114.0	151.2	160.3	150.2	47.6	20.8	118.4	9.9	–
1+CO_2, 25 °C	114.1	151.2	160.3	150.6	47.7	21.0	118.3	9.9	125.3
1+CO_2, –10 °C	114.0	150.7	162.6	150.3	47.7	20.9	118.6	10.0	125.2
1+CO_2, –30 °C	113.9	150.2	162.7	150.8	47.7	21.0	118.6	9.9	125.2
1+CO_2, –50 °C	113.7	150.0	162.9	150.2	47.7	21.0	118.2	9.9	**125.8**

DMF-d_7: The same experiments were repeated in DMF-d_7 as a more polar solvent to stabilize the **1**–CO_2 adduct. Figure S20 shows the stacked ^{1}H NMR spectra of **1** and **1**+CO_2 in DMF-d_7. At 25 °C, pressurizing the DMF-d_7 solution of **1** with 4 bar CO_2, leads to a small shift of the H-2 resonance from 7.90 ppm (**1)** to 7.97 ppm (**1**+CO_2) (Table 3). At low temperatures down to –50 °C, a significant shift to 8.84 ppm (**1**+CO_2) and only a small shift to 7.97 ppm (**1**) of the H-2 resonance is observed. Also, the resonance of the H-1 proton is shifted from 6.23 ppm to 6.38 ppm (**1**+CO_2). The deshielding of the pyridine protons agrees with the interaction of the pyridine-N atom with the Lewis acid CO_2. In both samples **1** and **1**+CO_2, the signals of the H-5 protons are broadened at low temperatures likely due to hindered rotation of the NHI group around the exocyclic N–C bond.

Table 3: ^{1}H NMR shifts of **1** and **1**+CO_2 in DMF-d_7 at given temperatures.

	H-1	**H-2**	**H-5**	**H-6**	**H-8**
1, 25 °C	6.23	7.90	4.43	1.37	2.24
1, –10 °C	6.22	7.91	4.39	1.35	2.24
1, –30 °C	6.23	7.94	4.37	1.34	2.24
1, –50 °C	**6.23**	**7.97**	4.34	1.32	2.25
1+CO_2, 25 °C	6.24	7.97	4.43	1.38	2.25
1+CO_2, –10 °C	6.29	8.18	4.40	1.38	2.28
1+CO_2, –30 °C	6.34	8.39	4.38	1.38	2.30
1+CO_2, –50 °C	**6.38**	**8.48**	4.36	1.37	2.31

Figure S21 depicts the stacked $^{13}C\{^{1}H\}$ NMR spectra of **1** and **1**+CO_2 in DMF-d_7. The variable $^{13}C\{^{1}H\}$ NMR experiments show that the resonances are not significantly shifted at different temperatures in the absence of CO_2. At 25 °C, pressurizing the DMF-d_7 solution of **1** with 4 bar CO_2, leads to a small shift of the C-2 resonance from 150.6 ppm (**1)** to 149.5 ppm (**1**+CO_2). At low temperatures down to –50 °C, a significant shift to a lower frequency of 139.5 ppm (**1**+CO_2) of the C-2 resonance is observed (table 4). All other aromatic ^{13}C resonances undergo small shifts to higher or lower frequencies in **1**+CO_2 which is not observed for **1**. Also, the CO_2 signal is shifted to higher frequencies from 126.3 ppm to 128.4 ppm.

Collectively, these results suggest that **1** interacts with CO_2, likely forming the **1**–CO_2 adduct which appears to be only stable at low temperatures. The equilibrium of this reaction lies on the side of the reactants, and we were thus not able to isolate the **1**–CO_2 adduct.

Table 4: $^{13}C\{^{1}H\}$ NMR shifts of **1** and **1**+CO_2 in DMF-d_7 at given temperatures.

	C-1	**C-2**	**C-3**	**C-4**	**C-5**	**C-6**	**C-7**	**C8**	**CO_2**
1, 25 °C	113.7	**150.6**	161.1	150.9	48.3	21.3	119.9	10.2	–
1, –10 °C	113.6	150.2	161.1	150.7	48.3	21.2	120.0	10.2	–
1, –30 °C	113.4	149.5	161.4	150.4	48.4	21.1	120.2	10.1	–
1, –50 °C	113.2	148.6	161.7	150.1	48.5	21.0	120.4	10.0	–
1+CO_2, 25 °C	113.5	**149.5**	161.6	150.8	48.5	21.2	120.2	10.2	**126.3**
1+CO_2, –10 °C	112.8	145.2	163.3	150.0	48.8	21.1	121.0	10.0	127.5
1+CO_2, –30 °C	112.2	141.3	164.8	149.3	49.1	21.1	121.7	9.9	128.0
1+CO_2, –50 °C	112.0	**139.5**	165.5	148.8	49.2	21.0	122.0	9.8	**128.4**

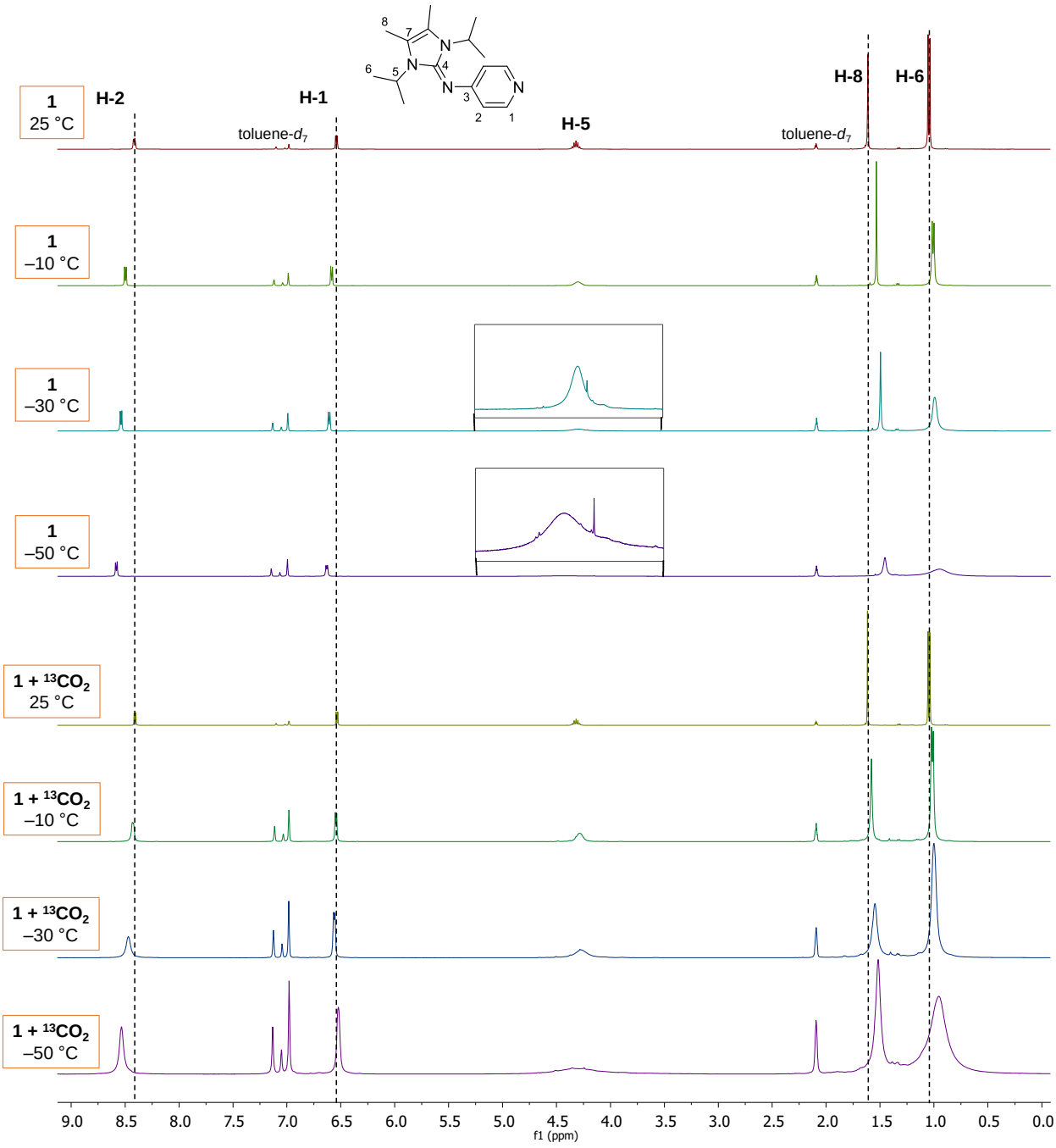

Figure S18: Stacked ^{1}H NMR spectra (400.03 MHz) of **1** and **1**+$^{13}CO_2$ in toluene-d_8 measured at given temperatures. Dotted lines are centered at the resonances of **1** measured at 25 °C to visualize the shift.

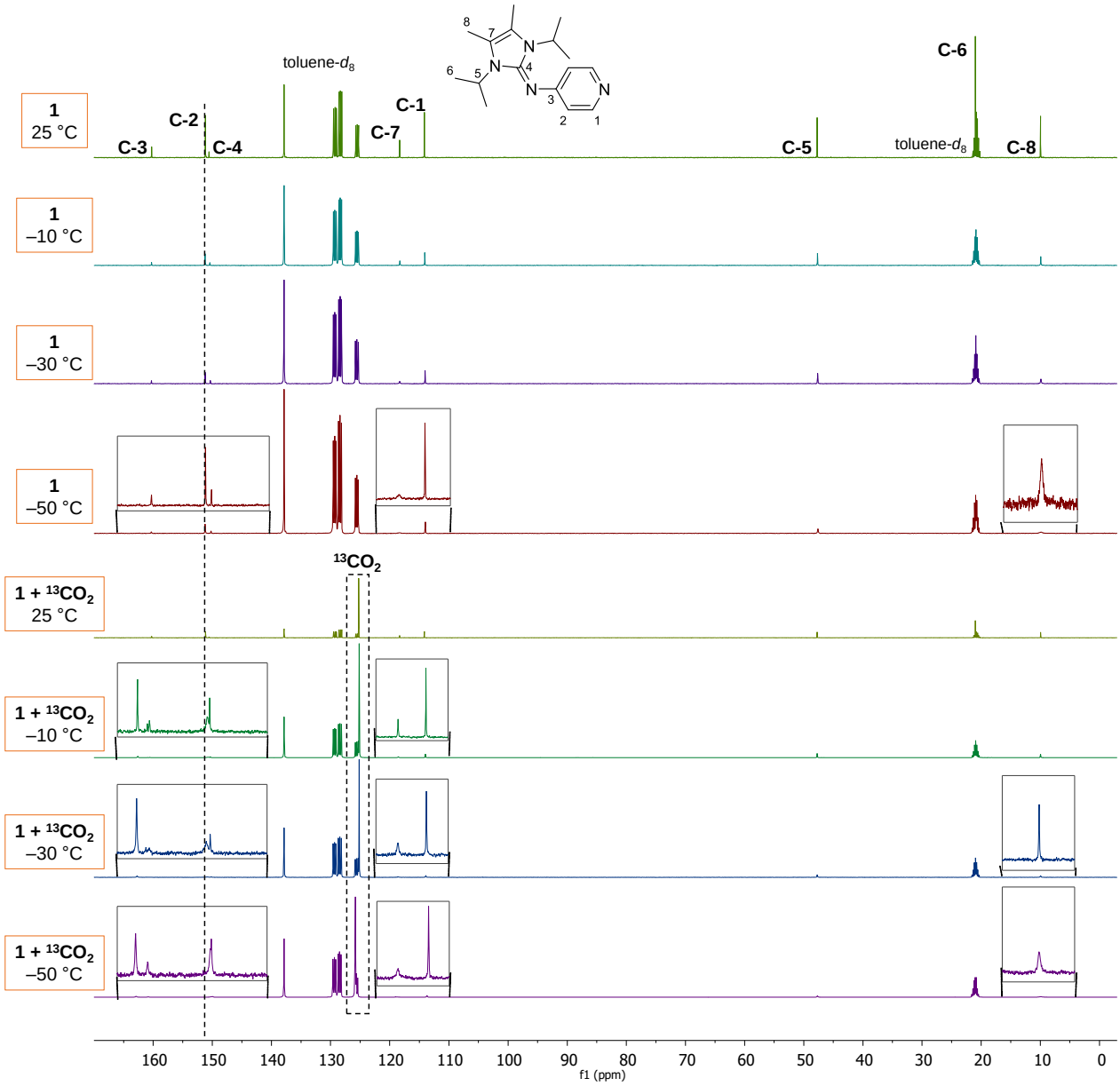

Figure S19: Stacked $^{13}C\{^{1}H\}$ NMR (100.60 MHz) spectra of **1** and **1**+$^{13}CO_2$ in toluene-d_8 measured at given temperatures. The dotted line is centered at the C-2 resonance of **1** measured at 25 °C to visualize the shift. The resonance of $^{13}CO_2$ overlaps with the solvent signal of toluene-d_8 and is highlighted in a dotted frame.

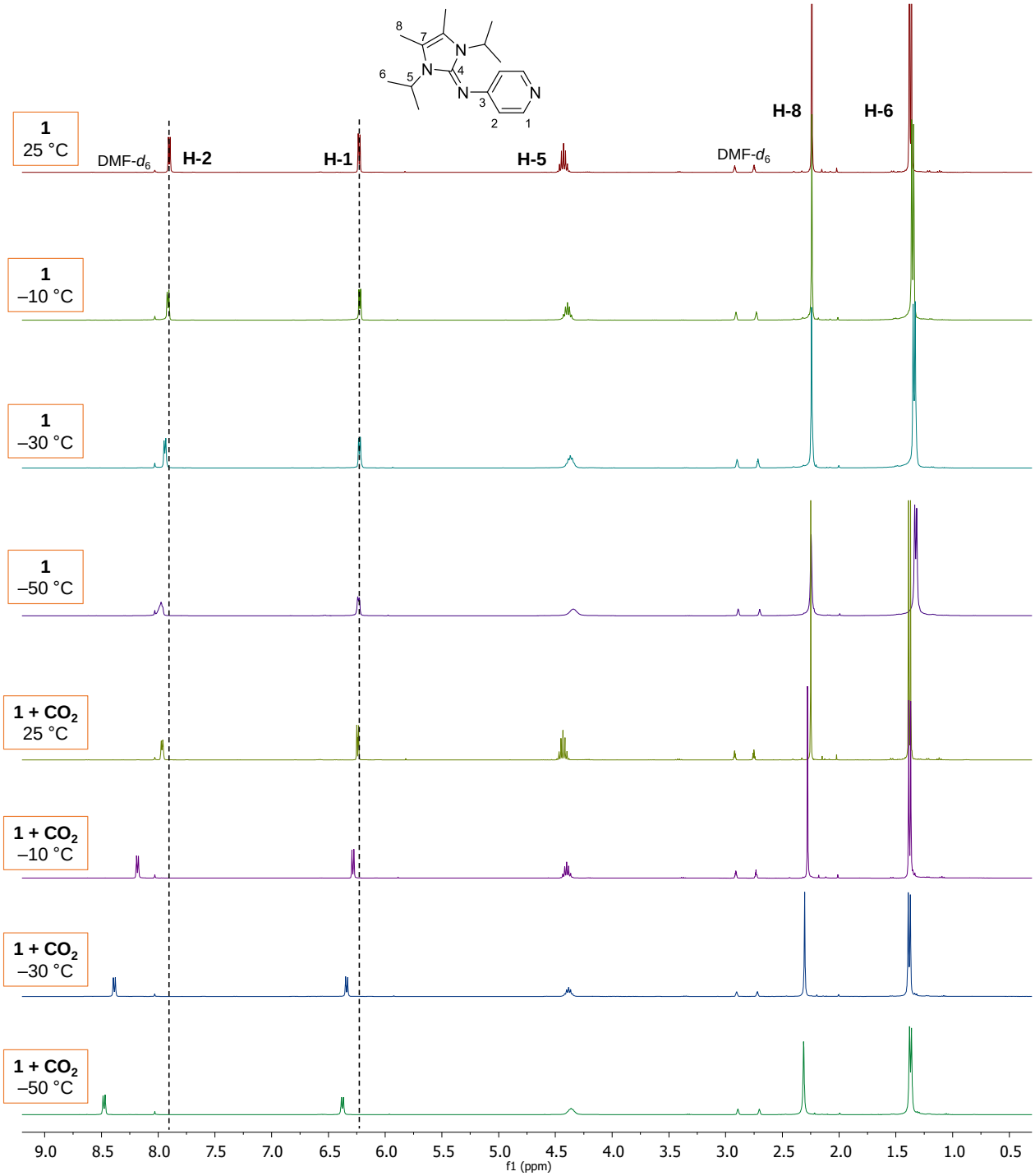

Figure S20: Stacked ^{1}H NMR (400.03 MHz) spectra of **1** and **1**+CO_2 in DMF-d_7 measured at given temperatures. Dotted lines are centered at the resonances of **1** measured at 25 °C to visualize the shift.

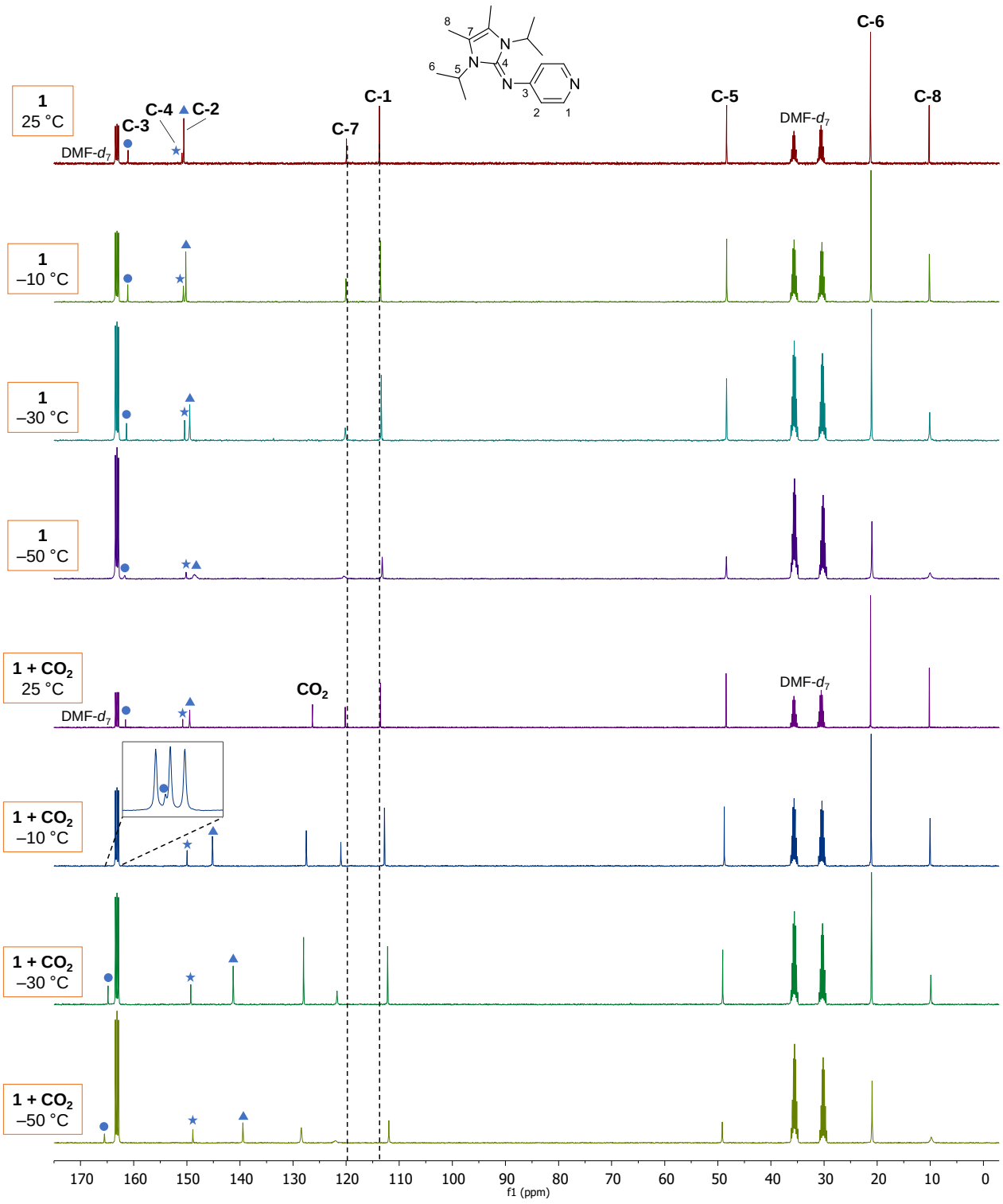

Figure S21: Stacked $^{13}C\{^{1}H\}$ NMR (100.60 MHz) spectra of **1** and **1**+CO_2 in DMF-d_7 measured at given temperatures. Dotted lines are centered at the resonances of **1** measured at 25 °C (C-1, C-7) to visualize the shift. The C-3 signal overlaps with a DMF-d_7 resonance (**1**+CO_2, –10 °C) and the C-2, C-3 and C-4 resonances are highlighted individually to visualize the shift.

Preparation of Coordination Compounds **4-8**

Compound 4: **1** (80.0 mg, 294 µmol) was dissolved in *n*-pentane and the solution was pressurized with two bar SO_2 pressure. The excess solvent was decanted off and the light-yellow solid was dried by letting pentane evaporate at room temperature. **4** was isolated in a 99% (98.9 mg, 294 µmol) yield.

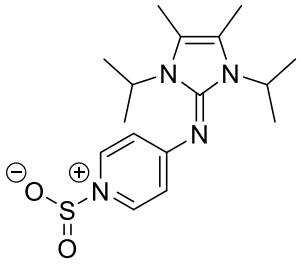

^{1}H NMR (400.13 MHz, THF-d_8): δ = 7.94–7.95 (m, 2H, CH_{aryl}), 6.50–6.37 (m, 2H, CH_{aryl}), 4.42 (sept, $^3J_{HH}$ = 7.0 Hz, 2H, *i*Pr-CH), 2.28 (s, 6H, imidazole-CH_3), 1.42 (d, $^3J_{HH}$ = 7.0 Hz, 12H, *i*Pr-CH_3) ppm.

^{13}C{^{1}H} NMR (100.62 MHz, THF-d_8): δ = 162.9 (s, $NC_q(CH_{aryl})_2$), 147.8 (s, N_3C_q), 140.3 (s, CH_{aryl}), 122.6 (s, imidazole-C_q), 111.9 (s, CH_{aryl}), 49.6 (s, *i*Pr-CH), 21.5 (s, *i*Pr-CH_3), 10.0 (s, imidazole-CH_3) ppm.

HRMS (ESI): m/z calculated for $[C_{16}H_{25}N_4]^+$ $(M–SO_2+H)^+$ 273.2074, found 273.2067.

IR (neat): $\tilde{\nu}$ = 1004 (s), 1035 (s), 1059 (m), 1091 (vs), 1138 (s), 1193 (vs), 1213 (s), 1275 (w), 1336 (m), 1352 (m), 1371 (s), 1390 (s), 1432 (s), 1454 (s), 1497 (vs), 1526 (vs), 1613 (m), 1646 (w), 2876 (w), 2935 (w), 2977 (w) cm^{-1}.

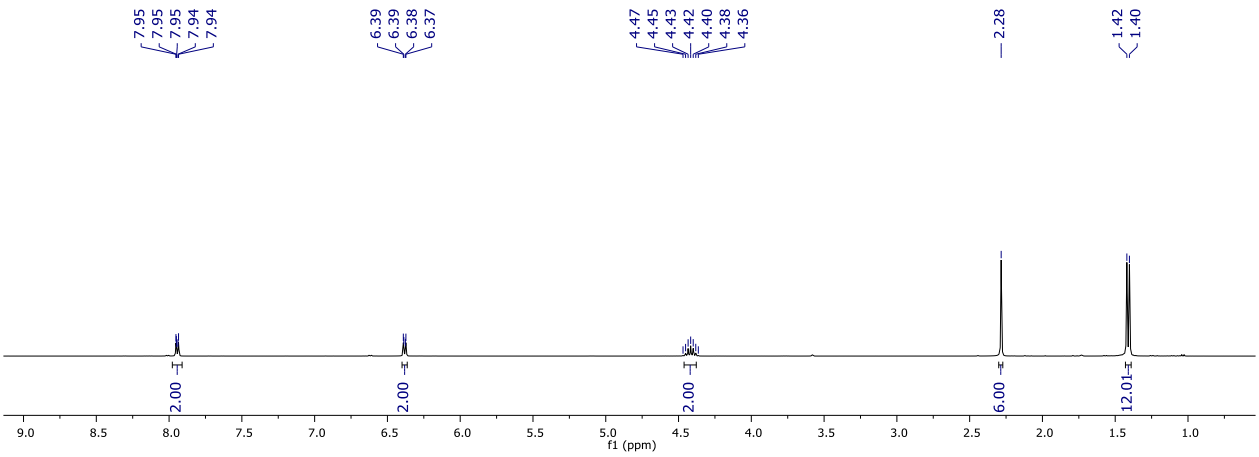

Figure S22: ^{1}H NMR spectrum (in THF-d_8, 300 K, 400.13 MHz) of **4**.

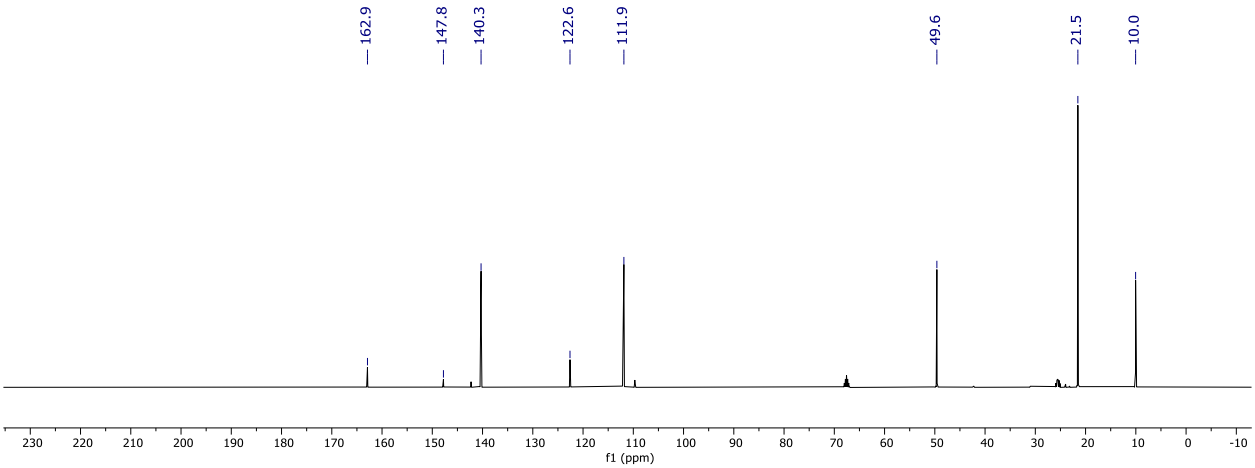

Figure S23: $^{13}C\{^{1}H\}$ NMR spectrum (in THF-d_8, 300 K, 100.62 MHz) of **4**.

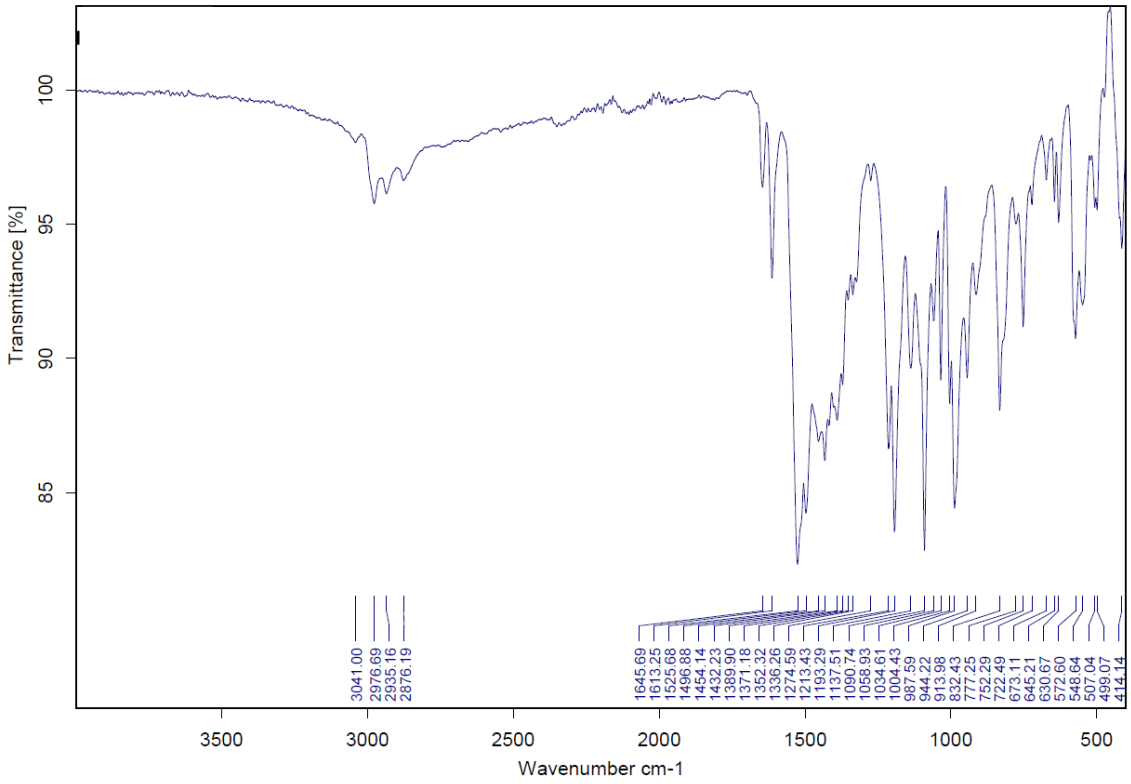

Figure S24: FT-IR spectrum (neat) of **4**.

Compound 5: **1** (100 mg, 367 µmol, 3.00 eq.) was dissolved in toluene (2 mL) and BCl_3 (14.3 mg, 122 µL, 122 µmol, 1 M in *n*-hexane, 1.00 eq.) was added at –78 °C to the stirring solution. The reaction mixture was stirred for 16 h at room temperature and the colorless precipitate was filtered off. The solid was washed with DCM (1 x 4 mL) and dried *in vacuo*. **5** was isolated in a 19.4% (36.0 mg, 71.1 µmol) yield. Due to its low solubility, compound **7** was not characterized via ^{13}C NMR spectroscopy.

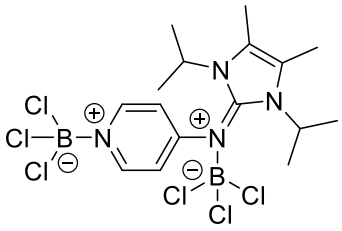

^{1}H NMR (400.13 MHz, DMSO-d_6): δ = 8.92 (d, $^{3}J_{HH}$ = 5.4 Hz, 2H, CH_{aryl}), 7.45 (br, 2H, CH_{aryl}), 4.55 (sept, $^{3}J_{HH}$ = 7.0 Hz, 2H, *i*Pr-CH), 2.45 (s, 6H, imidazole-CH_3), 1.53 (d, $^{3}J_{HH}$ = 7.0 Hz, 6H, *i*Pr-CH_3), 1.40 (d, $^{3}J_{HH}$ = 7.0 Hz, 6H, *i*Pr-CH_3) ppm.

^{11}B NMR (128.38 MHz, DMSO-d_6): δ = 7.7 (s), 5.8 (s) ppm.

^{11}B{^{1}H} NMR (128.38 MHz, DMSO-d_6): δ = 7.7 (s), 5.8 (s) ppm.

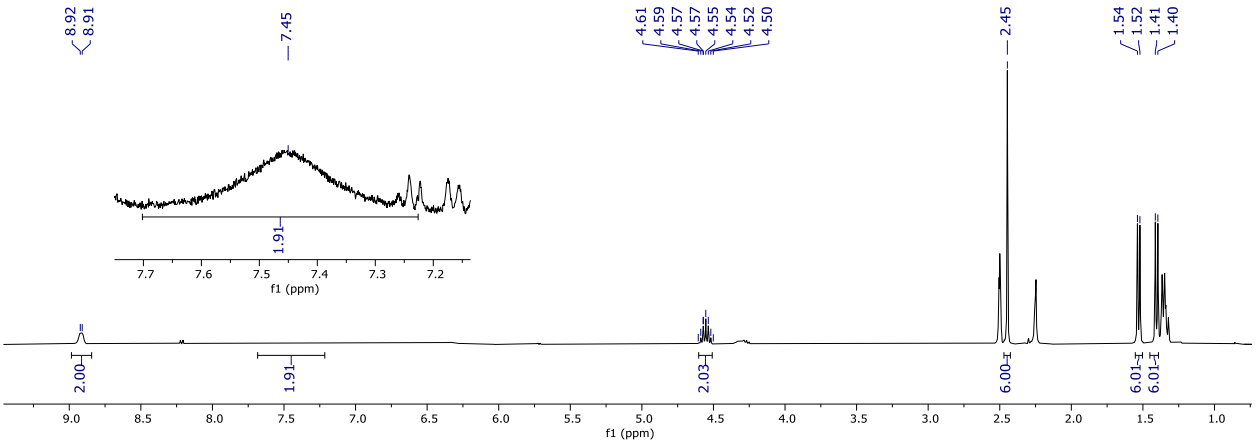

Figure S25: ^{1}H NMR spectrum (in DMSO-d_6, 300 K, 400.13 MHz) of **5**.

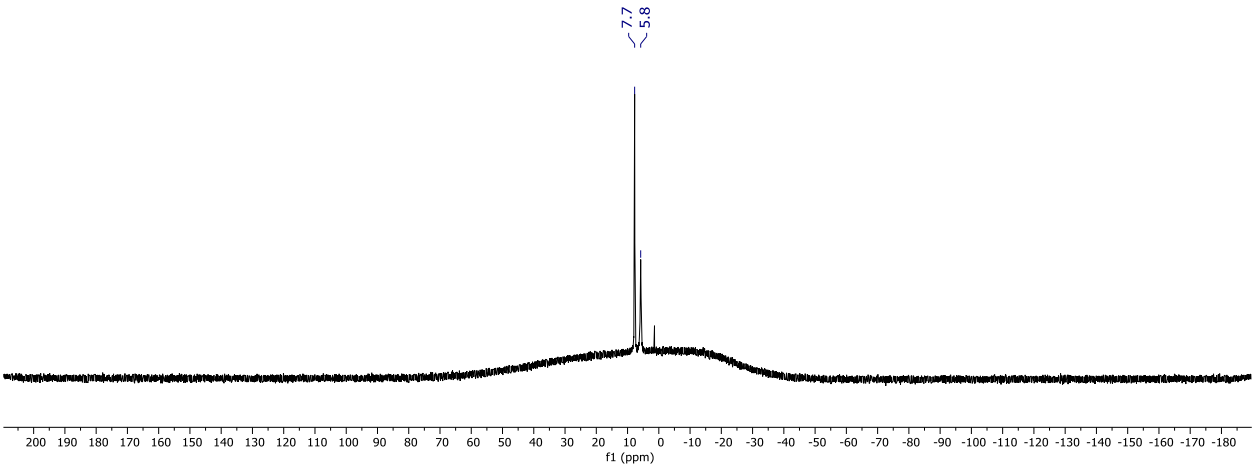

Figure S26: ^{11}B NMR spectrum (in DMSO-d_6, 300 K, 128.38 MHz) of **5**.

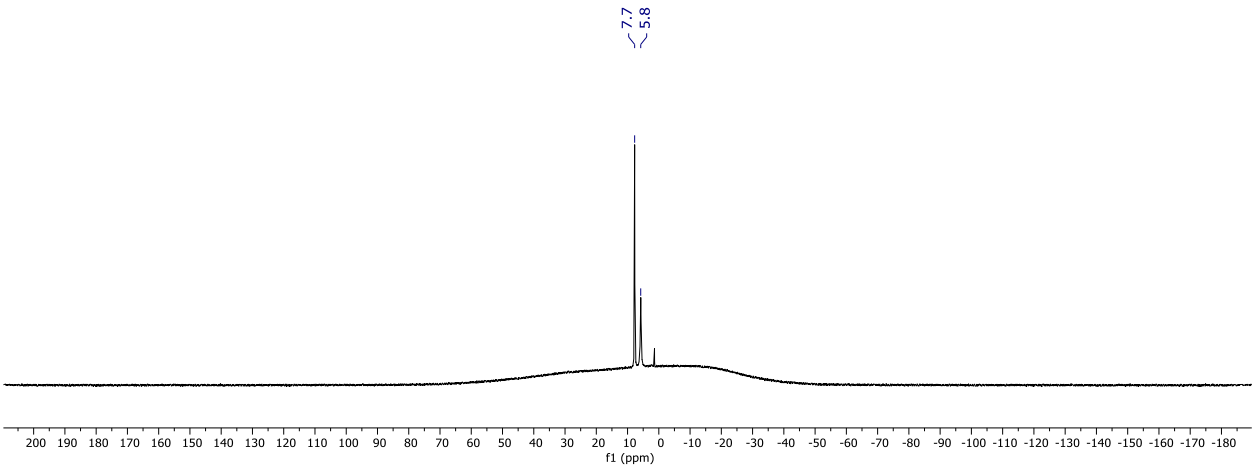

Figure S27: $^{11}B\{^{1}H\}$ NMR spectrum (in DMSO-d_6, 300 K, 128.38 MHz) of **5**.

Compound 6: **1** (55.0 mg, 202 µmol, 2.00 eq.) was dissolved in THF (5 mL) and $PdCl_2(PhCN)_2$ (38.7 mg, 101 µmol, 1.00 eq.) was added to the stirring solution. The reaction mixture was stirred for 16 h at room temperature and the yellow precipitated was filtered off and dried *in vacuo*. **6** was isolated in 96.0% (70.0 mg, 96.9 µmol) yield.

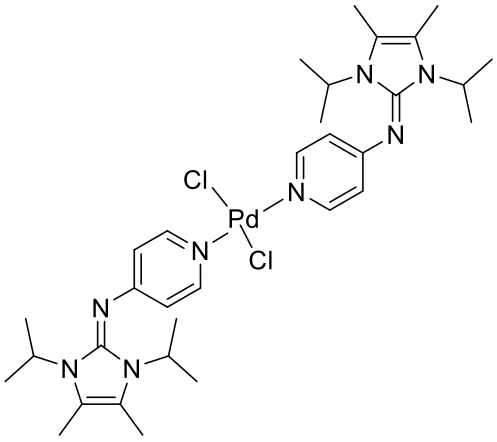

^{1}H NMR (400.03 MHz, MeCN-d_3): δ = 7.75–7.77 (m, 4H, CH_{aryl}), 6.01–6.03 (m, 4H, CH_{aryl}), 4.34 (sept, $^{3}J_{HH}$ = 6.9 Hz, 4H, *i*Pr-CH), 2.18 (s, 12H, imidazole-CH_3), 1.35 (d, $^{3}J_{HH}$ = 7.0 Hz, 24H, *i*Pr-CH_3) ppm.

^{13}C{^{1}H} NMR (100.60 MHz, MeCN-d_3): δ = 162.4 (s, $NC_q(CH_{aryl})_2$), 151.9 (s, CH_{aryl}), 130.4 (s, N_3C_q), 121.0 (s, imidazole-C_q), 113.4 (s, CH_{aryl}), 48.8 (s, *i*Pr-CH), 21.2 (s, *i*Pr-CH_3), 10.0 (s, imidazole-CH_3) ppm.

HRMS (ESI): m/z calculated for $[C_{64}H_{98}Cl_4N_{16}Pd_2]^{2+}$ $(M+H)_2^{2+}$ 723.24739, found 723.24852.

Elemental analysis: calculated (%) for $[C_{32}H_{48}Cl_2N_8Pd]$: C 53.23, H 6.70, N 15.52, found C 52.95, H 6.62, N 15.37.

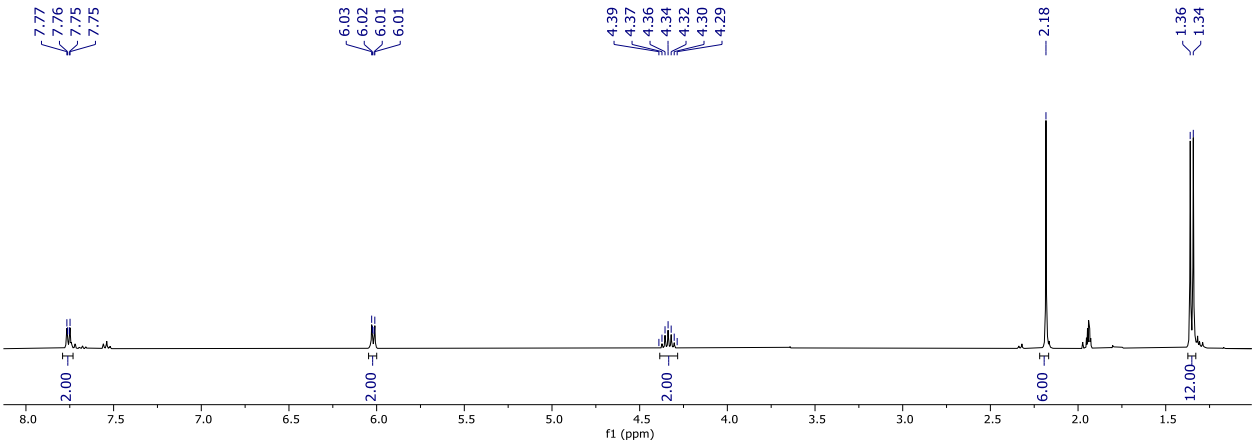

Figure S28: ^{1}H NMR spectrum (in MeCN-d_3, 300 K, 400.03 MHz) of **6**.

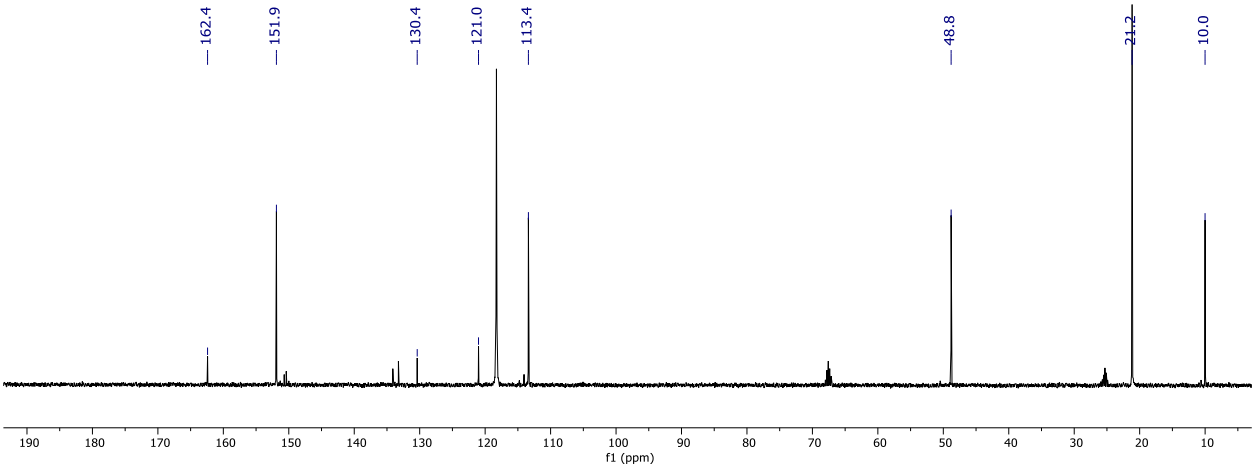

Figure S29: ^{13}C{^{1}H} NMR spectrum (in MeCN-d_3, 300 K, 100.60 MHz) of **6**.

Compound 7: **1** (16.3 mg, 59.8 µmol, 2.00 eq.) was dissolved in toluene (5 mL) and $[PdBr_2(BiPr)]_2$[6] (28.0 mg, 29.9 µmol, 1.00 eq.) was added to the stirred solution. The reaction mixture was stirred for 16 h at room temperature and the volatiles were removed under reduced pressure. **7** was isolated in a quantitative yield (44.4 mg, 59.8 µmol) as a yellow solid.

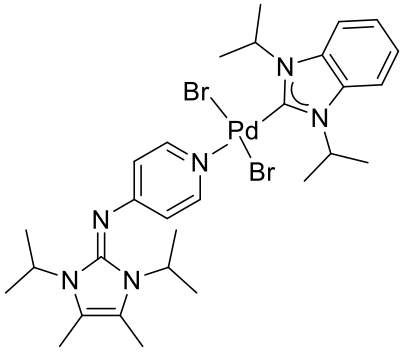

^{1}H NMR (400.03 MHz, $CDCl_3$): δ = 8.33–8.35 (m, 2H, CH_{aryl}), 7.53–7.55 (m, 2H, benzimidazole-CH_{aryl}), 7.15–7.17 (m, 2H, benzimidazole-CH_{aryl}), 6.39 (sept, $^{3}J_{HH}$ = 7.0 Hz, 2H, benzimidazole-*i*Pr-CH), 6.11–6.13 (m, 2H, CH_{aryl}), 4.43 (sept, $^{3}J_{HH}$ = 7.0 Hz, 2H, imidazole-*i*Pr-CH), 2.18 (s, 6H, imidazole-CH_3), 1.77 (d, $^{3}J_{HH}$ = 7.1 Hz, 12H, benzimidazole-*i*Pr-CH_3), 1.38 (d, $^{3}J_{HH}$ = 7.1 Hz, 12H, imidazole-*i*Pr-CH_3) ppm.

$^{13}C\{^{1}H\}$ NMR (100.60 MHz, $CDCl_3$): δ = 162.7 (s, $PdC_{benzimidazole}$), 161.1 (s, $NC_q(CH_{aryl})_2$), 151.4 (s, CH_{aryl}), 133.7 (s, benzimidazole-C_q), 129.1 (s, N_3C_q), 122.0 (s, benzimidazole-CH_{aryl}), 119.7 (s, imidazole-C_q), 112.5 (s, CH_{aryl}), 112.4 (s, benzimidazole-CH_{aryl}), 54.4 (s, benzimidazole-*i*Pr-CH), 47.9 (s, imidazole-*i*Pr-CH), 21.2 (s, imidazole-*i*Pr-CH_3), 20.7 (s, benzimidazole-*i*Pr-CH_3), 10.0 (s, imidazole-CH_3) ppm.

HRMS (ESI): m/z calculated for $[C_{29}H_{43}N_6Br_2Pd]^+$ $(M+H)^+$ 741.09378, found 741.09561.

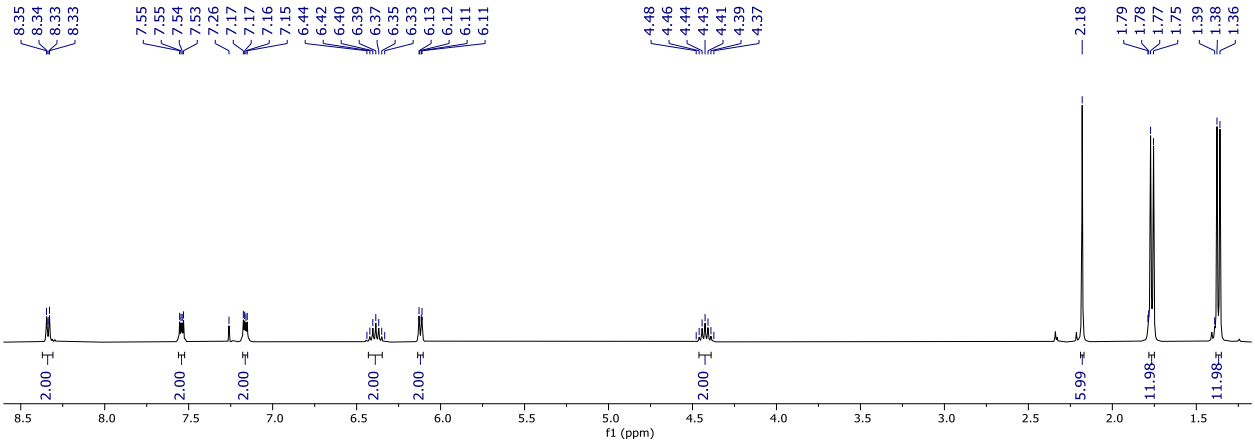

Figure S30: ^{1}H NMR spectrum (in $CDCl_3$, 300 K, 400.03 MHz) of **7**.

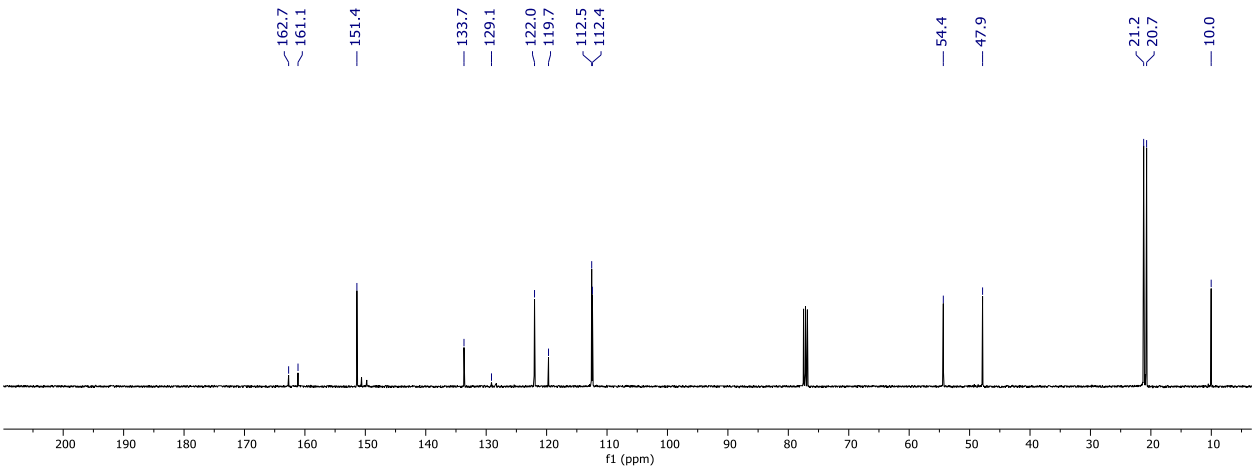

Figure S31: $^{13}C\{^{1}H\}$ NMR spectrum (in $CDCl_3$, 300 K, 100.60 MHz) of **7**.

Compound 8: **1** (16.4 mg, 59.8 µmol, 2.00 eq.) was dissolved in toluene (5 mL) and $[PdBr_2(BiPr)]_2$[6] (28.0 mg, 29.9 µmol, 1.00 eq.) was added to the stirring solution. The reaction mixture was stirred for 16 h at room temperature and the volatiles were removed under reduced pressure. **8** was isolated in a quantitative yield (44.4 mg, 59.8 µmol) as a yellow solid.

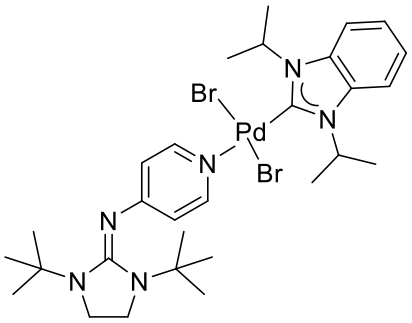

^{1}H NMR (400.13 MHz, $CDCl_3$): δ = 8.36–8.38 (m, 2H, pyridine-CH_{aryl}), 7.52–7.58 (m, 2H, benzimidazole-CH_{aryl}), 7.15–7.19 (m, 2H, benzimidazole-CH_{aryl}), 6.39 (sept, $^3J_{HH}$ = 7.0 Hz, 2H, *i*Pr-CH), 6.03–6.05 (m, 2H, pyridine-CH_{aryl}), 3.50 (s, 4H, imidazole-CH_2), 1.77 (d, $^3J_{HH}$ = 7.0 Hz, 12H, *i*Pr-CH_3), 1.27 (s, 18H, 6 x *t*Bu-CH_3) ppm.

^{13}C{^{1}H} NMR (75 MHz, $CDCl_3$): δ = 162.6 (s, N_3C_q), 162.6 (s, $PdC_{benzimidazole}$), 157.6 (s, $NC_q(CH_{aryl})_2$), 151.4 (s, CH_{aryl}), 133.7 (s, benzimidazole-C_q), 122.0 (s, benzimidazole-CH_{aryl}), 113.0 (s, CH_{aryl}), 112.6 (s, benzimidazole-CH_{aryl}), 56.2 (s, *t*Bu-C_q), 54.4 (s, *i*Pr-CH), 42.6 (s, imidazole-CH_2), 28.6 (s, *t*Bu-CH_3), 20.7 (s, *i*Pr-CH_3) ppm.

HRMS (ESI): m/z calculated for $[C_{29}H_{45}N_6Br_2Pd]^+$ $(M+H)^+$ 743.1081, found 743.1077.

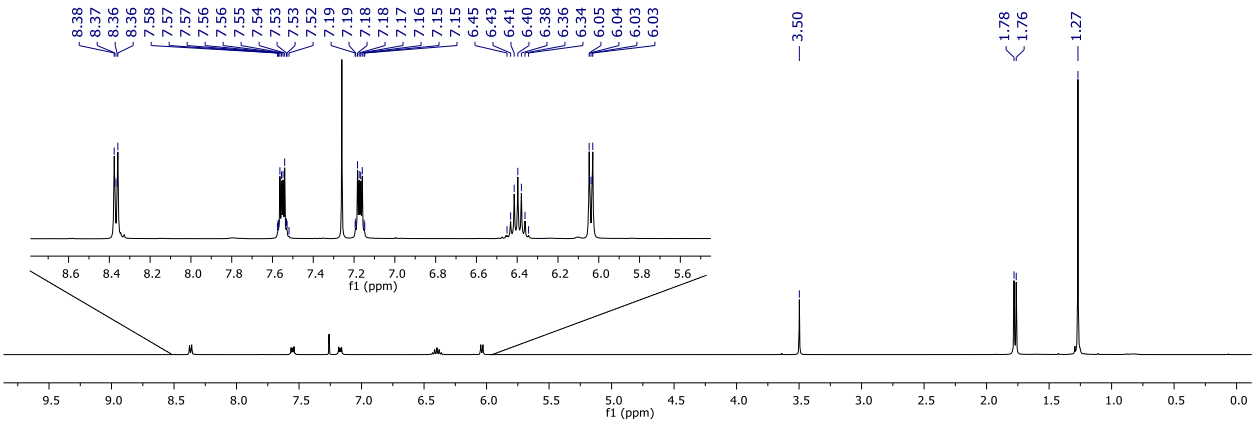

Figure S32: ^{1}H NMR spectrum (in $CDCl_3$, 300 K, 400.03 MHz) of **8**.

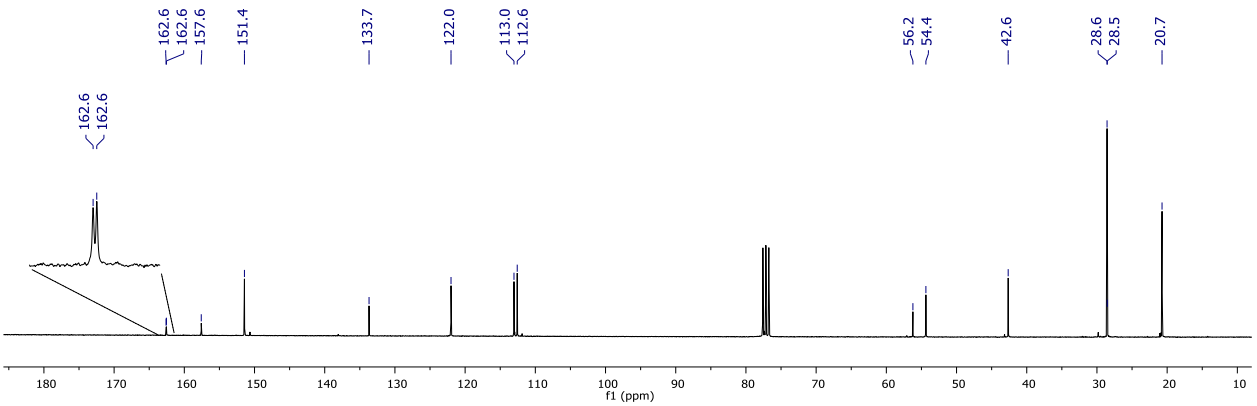

Figure S33: $^{13}C\{^{1}H\}$ NMR spectrum (in $CDCl_3$, 300 K, 100.60 MHz) of **8**.

Preparation of Compounds **9-13**

Compound 9: Pyridine-*N*-methyl iodide was synthesized according to a literature-known procedure.[7] The white solid was dried *in vacuo* at 160 °C for 16 h prior to use in demethylation reactions.

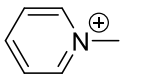

^{1}H NMR (400.23 MHz, CD_3CN) δ = 8.86–8.88 (m, 2H, CH_{aryl}), 8.53 (tt, J_{HH} = 7.8, 1.5 Hz, 1H, CH_{aryl}), 8.05 (t, J_{HH} = 7.1 Hz, 2H, CH_{aryl}), 4.39 (s, 3H, CH_3) ppm.

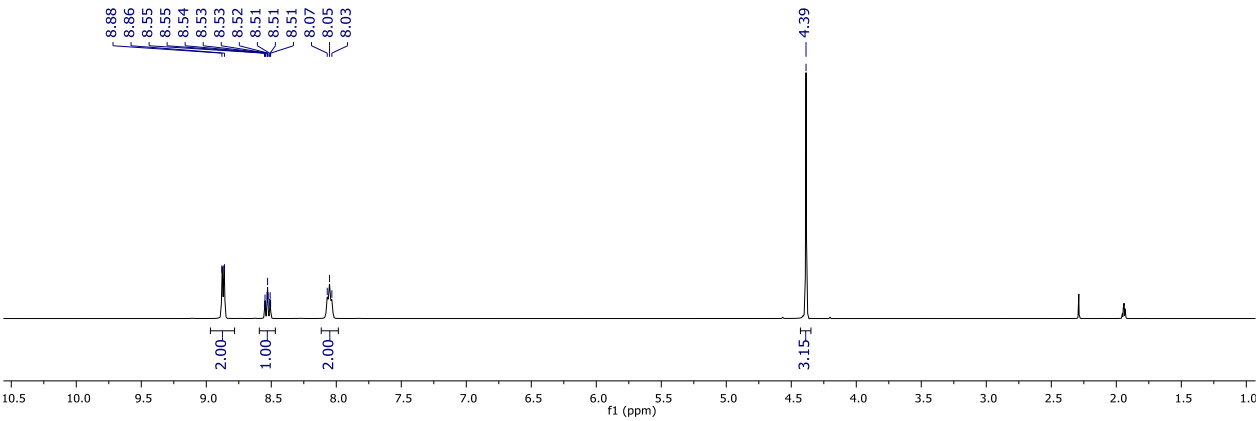

Figure S34: ^{1}H NMR spectrum (in MeCN-d_3, 298.1 K, 400.23 MHz) of **9**.

Compound 10: 4-Picoline-*N*-methyl iodide was synthesized according to a literature-known procedure.[8] The off-white solid was dried *in vacuo* at 160 °C for 16 h prior to use in demethylation reactions.

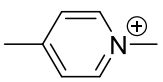

^{1}H NMR (400.23 MHz, CD_3CN) δ = 8.74–8.77 (m, 2H, CH_{aryl}), 7.86 (d, J_{HH} = 6.2 Hz, 2H, CH_{aryl}), 4.32 (s, 3H, N–CH_3), 2.59 (s, 3H, CH_3) ppm.

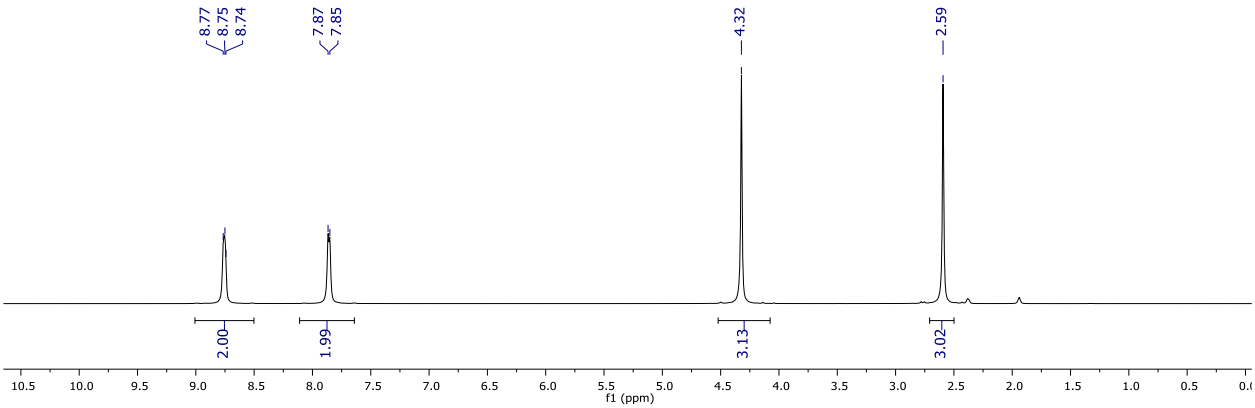

Figure S35: ^{1}H NMR spectrum (in MeCN-d_3, 298.1 K, 400.23 MHz) of **10**.

Compound 11: 4-Dimethylaminopyridine-*N*-methyl iodide was synthesized according to a literature-known procedure[9] using toluene as solvent for the reaction. The off-white solid was dried *in vacuo* at 160 °C for 16 h prior to use in demethylation reactions.

^{1}H NMR (400.23 MHz, CD_3CN) δ = 7.98–8.02 (m, 2H, CH_{aryl}), 6.85–6.89 (m, 2H, CH_{aryl}), 3.90 (s, 3H, CH_3), 3.17 (s, 6H, $N(CH_3)_2$).

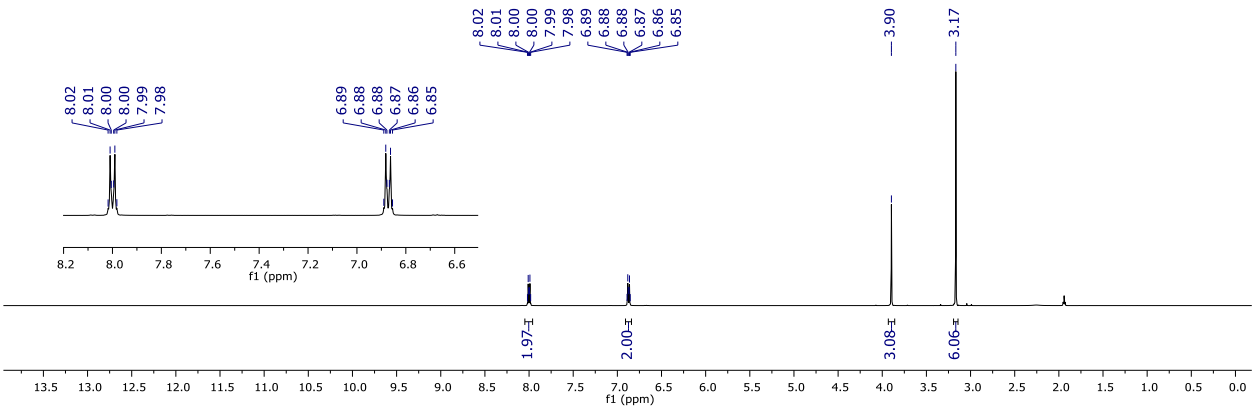

Figure S36: ^{1}H NMR spectrum (in MeCN-d_3, 298.1 K, 400.23 MHz) of **11**.

Compound 12: To a toluene (10 mL) solution of **2** (500 mg, 1.82 mmol, 1.0 eq.) iodomethane (0.113 mL, 1.82 mmol, 1.0 eq.) was slowly added dropwise at room temperature. The resulting suspension was allowed to stir for 3 h, then filtered off and the residue was washed with diethyl ether (3 x 10 mL). The product was dried *in vacuo* at 110 °C for 16 h prior to use in demethylation reactions and obtained as a white solid in 85% yield (644 mg, 1.55 mmol).

^{1}H NMR (400.23 MHz, CD_3CN) δ = 7.55–7.58 (m, 2H, CH_{aryl}), 6.22–6.26 (m, 2H, CH_{aryl}), 3.70 (s, 4H, CH_2), 3.67 (s, 3H, NCH_3), 1.27 (s, 18H, *t*Bu-CH_3) ppm.

^{13}C{^{1}H} NMR (100.62 MHz, CD_3CN) δ = 165.9 (s, N_3C_q), 159.0 (s, $NC_q(CH_{aryl})_2$), 142.5 (s, CH_{aryl}), 113.5 (s, CH_{aryl}), 57.3 (s, *t*Bu-C_q), 44.3 (s, NCH_3), 44.1 (s, imidazole-CH_2), 28.6 (s. *t*Bu-CH_3) ppm.

HRMS (ESI): m/z calculated for $[C_{17}H_{29}N_4]^+$ $(M\text{-}I^-)^+$ 289.2387, found 298.2382.

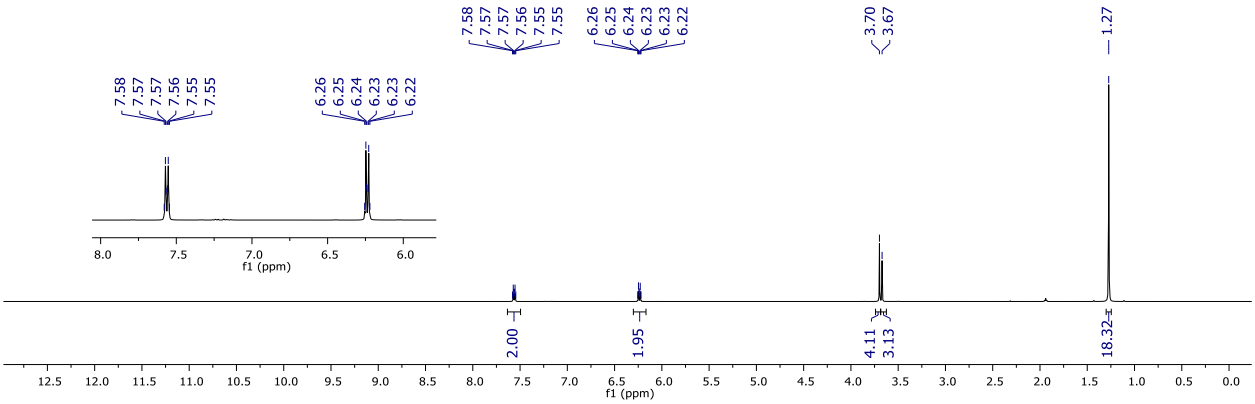

Figure S37: ^{1}H NMR spectrum (in MeCN-d_3, 298.1 K, 400.23 MHz) of **12**.

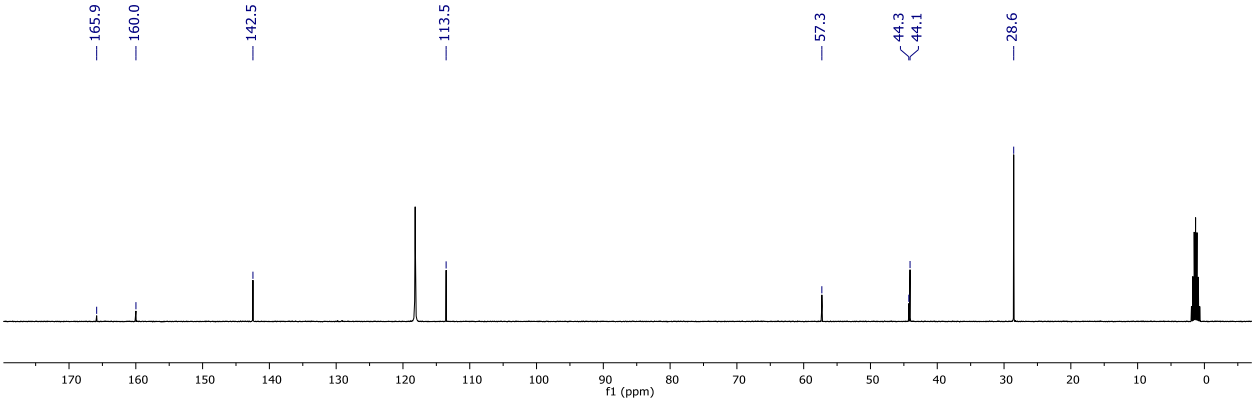

Figure S38: ^{13}C{^{1}H} NMR spectrum (in MeCN-d_3, 298.1 K, 100.62 MHz) of **12**.

Compound 13: To a toluene (10 mL) solution of **1** (210.0 mg, 0.770 mmol, 1.0 eq.) a 0.765 M stock solution of iodomethane in toluene (1.01 mL, 0.770 mmol, 1.0 eq.) was slowly added dropwise at room temperature. The solution was stirred at room temperature for 16 h which resulted in the formation of a yellow oil that was separated from the toluene solution. The volatiles were removed *in vacuo* at 70 °C. Et_2O (10 mL) was added to the viscous oil and the suspension was sonicated for 20 minutes before the solvent was filtered off. This procedure was repeated three times to remove residual toluene from the oil yielding a yellow solid. Compound **13** was then dried *in*

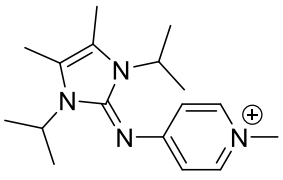

vacuo at 120 °C for 16 h to fully remove the residual toluene and was isolated as yellow solid in 58% yield (0.183 mg, 0.447 mmol).

^{1}H NMR (400.23 MHz, CD_3CN) δ = 7.57 (d, J_{HH} = 7.5 Hz, 2H, CH_{aryl}), 6.26 (d, J_{HH} = 7.2 Hz, 2H, CH_{aryl}), 4.31 (hept, $^{3}J_{HH}$ = 7.0 Hz, 2H, *i*Pr-CH), 3.70 (s, 3H, NCH_3), 2.21 (s, 6H, imidazole-CH_3), 1.35 (d, $^{3}J_{HH}$ = 7.0 Hz, 12H, *i*Pr-CH_3) ppm.

^{13}C{^{1}H} NMR (100.62 MHz, CD_3CN) δ = 164.0 (s, $NC_q(CH_{aryl})_2$), 148.5 (s, N_3C_q), 142.5 (s, CH_{aryl}), 122.2 (s, imidazole-C_q), 113.4 (s, CH_{aryl}), 49.2 (s, *i*Pr-CH), 44.3 (s, NCH_3), 20.9 (s, *i*Pr-CH_3), 9.8 (s, imidazole-CH_3).

HRMS (ESI): m/z calculated for $[C_{17}H_{28}N_4]^+$ $(M\text{-}I)^+$ 287.2230 found 287.2230.

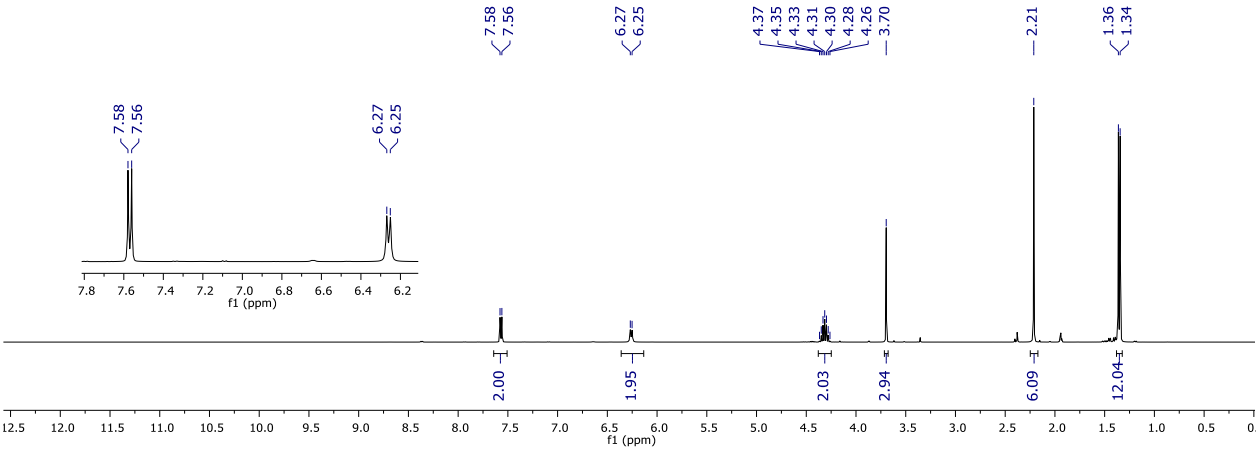

Figure S39: ^{1}H NMR spectrum (in MeCN-d_3, 298.1 K, 400.23 MHz) of **13**.

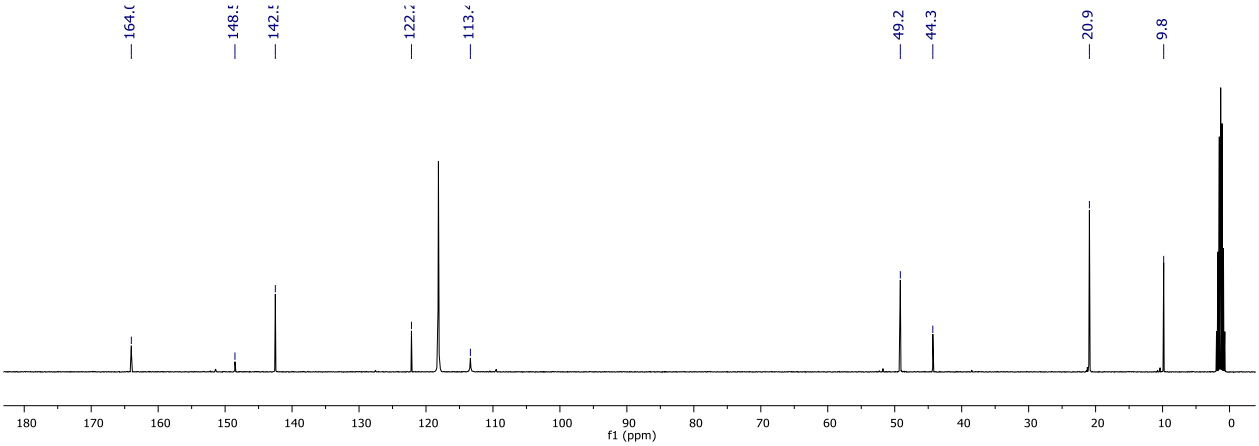

Figure S40: ^{13}C{^{1}H} NMR spectrum (in MeCN-d_3, 298.1 K, 100.62 MHz) of **13**.

Demethylation reactions of LB–Me iodide salts **9-12**

General procedure: Demethylation reactions were carried out under inert atmosphere and using 1 eq. of **1** (~15 mg) and 1 eq. of the *N*-methylated iodide salt **9-12**. Also, the same protocol was used for demethylation reactions of 1 eq. DMAP (~15 mg) with 1 eq. of the iodide salts **9** and **10**, respectively. MeCN-d_3 was used as the solvent and PTFE-sealed NMR tubes were employed to allow heating higher than the boiling point of the solvent. The reaction progress was monitored by ^{1}H NMR spectroscopy. The following figures show the stacked NMR spectra of the demethylation reactions after heating the respective reaction mixture at a given temperatures for a given time. After prolonged heating at 160 °C, all reaction mixtures turned orange or brown, yet the analysis of the ^{1}H NMR spectra revealed only minor amounts of impurities that are indicative of side reactions.

Demethylation reaction using DMAP as Lewis-base.

(1)

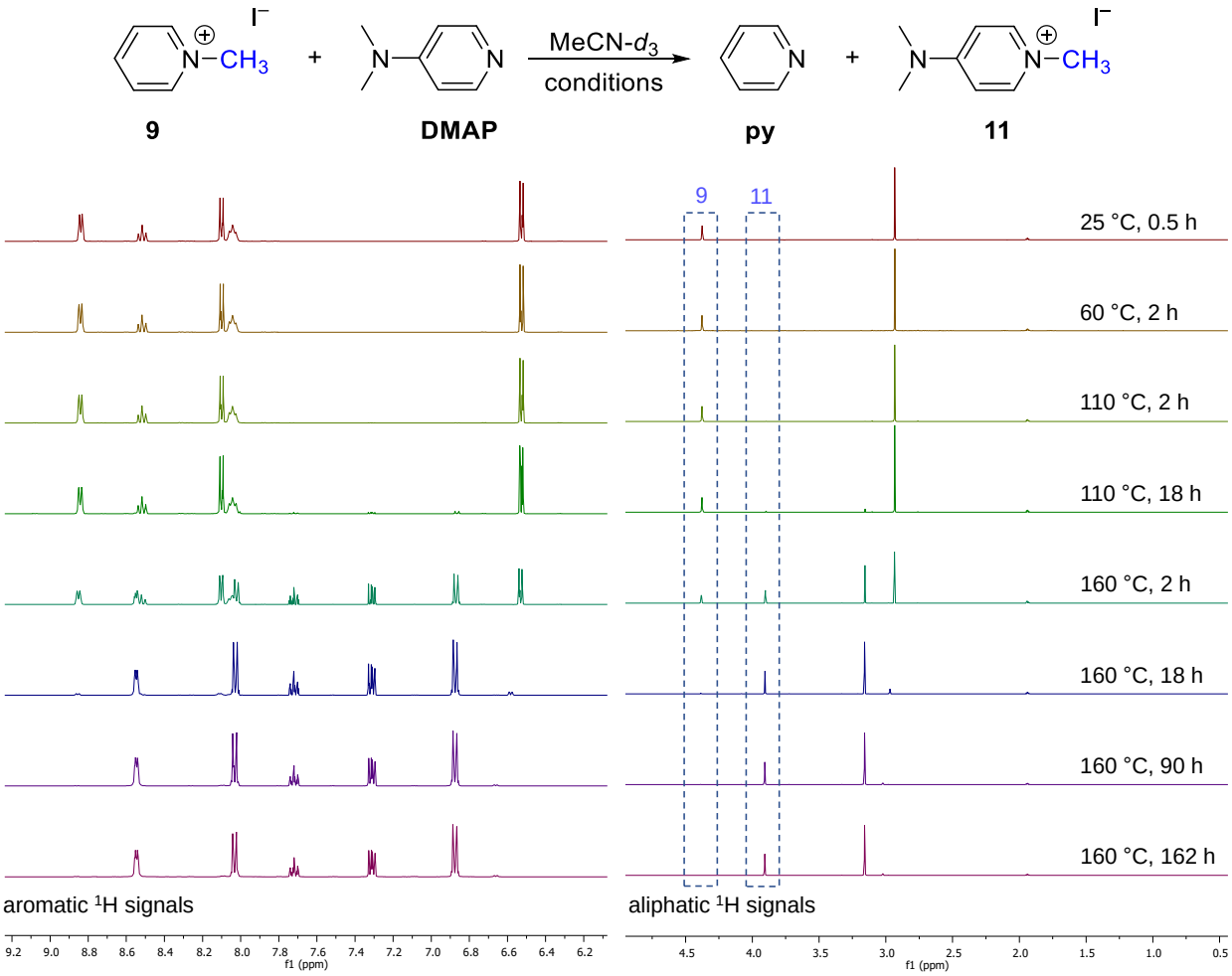

Figure S41: Stacked ^{1}H NMR spectra of the demethylation reaction of **9** with DMAP in MeCN-d_3 recorded after heating at a given temperature for a given time. The aromatic ^{1}H signals (left) are depicted with a 7-fold scaling for better visibility of the signals. Characteristic resonances corresponding to the consumption of **9** and the formation of **11** are highlighted in dotted frames.

^{1}H NMR analysis shows that the transfer of the methyl group is 98.9 % complete after continuous heating at 160 °C for a total of 162 h.

(2)

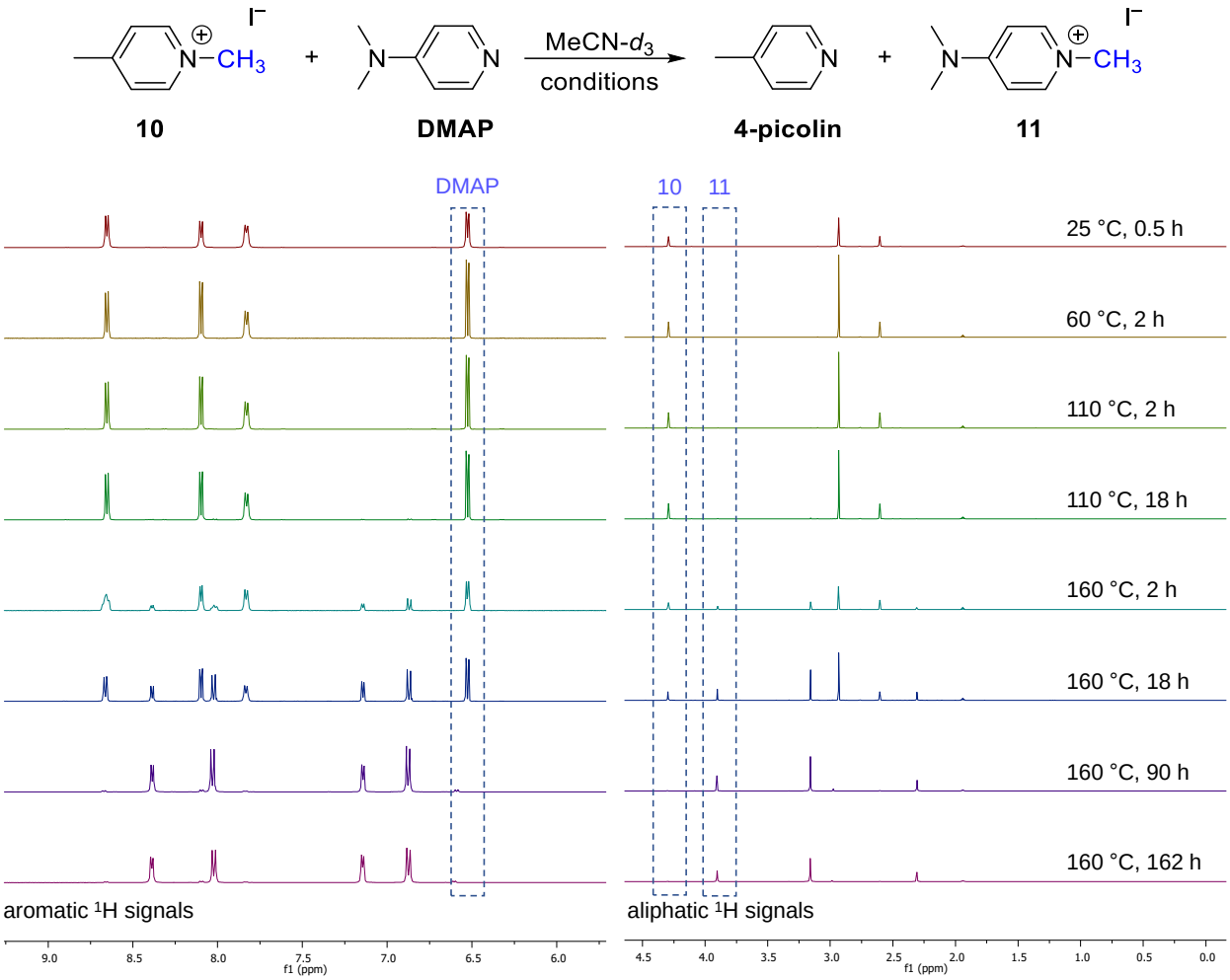

Figure S42: Stacked ^{1}H NMR spectra of the demethylation reaction of **10** using DMAP in MeCN-d_3 recorded after heating at a given temperature for a given time. The aromatic ^{1}H signals (left) are depicted with a 13-fold scaling for better visibility of the signals. Characteristic resonances corresponding to the consumption of **10** and the formation of **11** are highlighted in dotted frames.

^{1}H NMR analysis shows that the transfer of the methyl group is 94.6 % complete after continuous heating at 160 °C for a total of 162 h.

Demethylation reaction using 1 as Lewis-base.

(3)

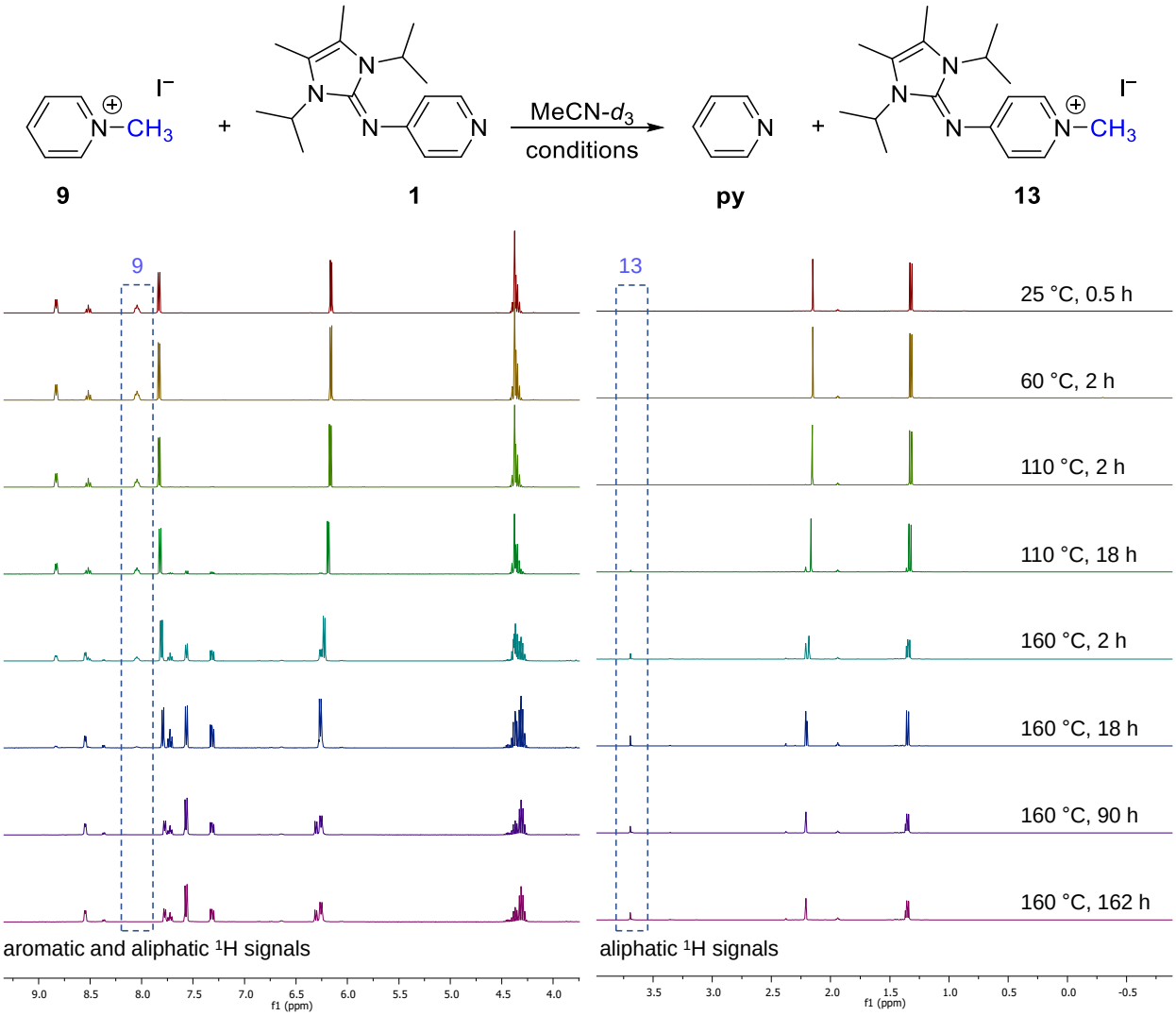

Figure S43: Stacked ^{1}H NMR spectra of the demethylation reaction of **9** using **1** in MeCN-d_3 recorded after heating at a given temperature for a given time. The aromatic and some aliphatic ^{1}H signals (left) are depicted with a 10-fold scaling for better visibility of the signals. Characteristic resonances corresponding to the consumption of **9** and the formation of **13** are highlighted in dotted frames.

In the ^{1}H NMR spectra of the reaction mixture, the methyl resonance of **9** overlaps with the signal from the *iso*-propyl group of **1**. ^{1}H NMR analysis shows that the transfer of the methyl group is quantitative after continuous heating at 160 °C for a total of 162 h.

(4)

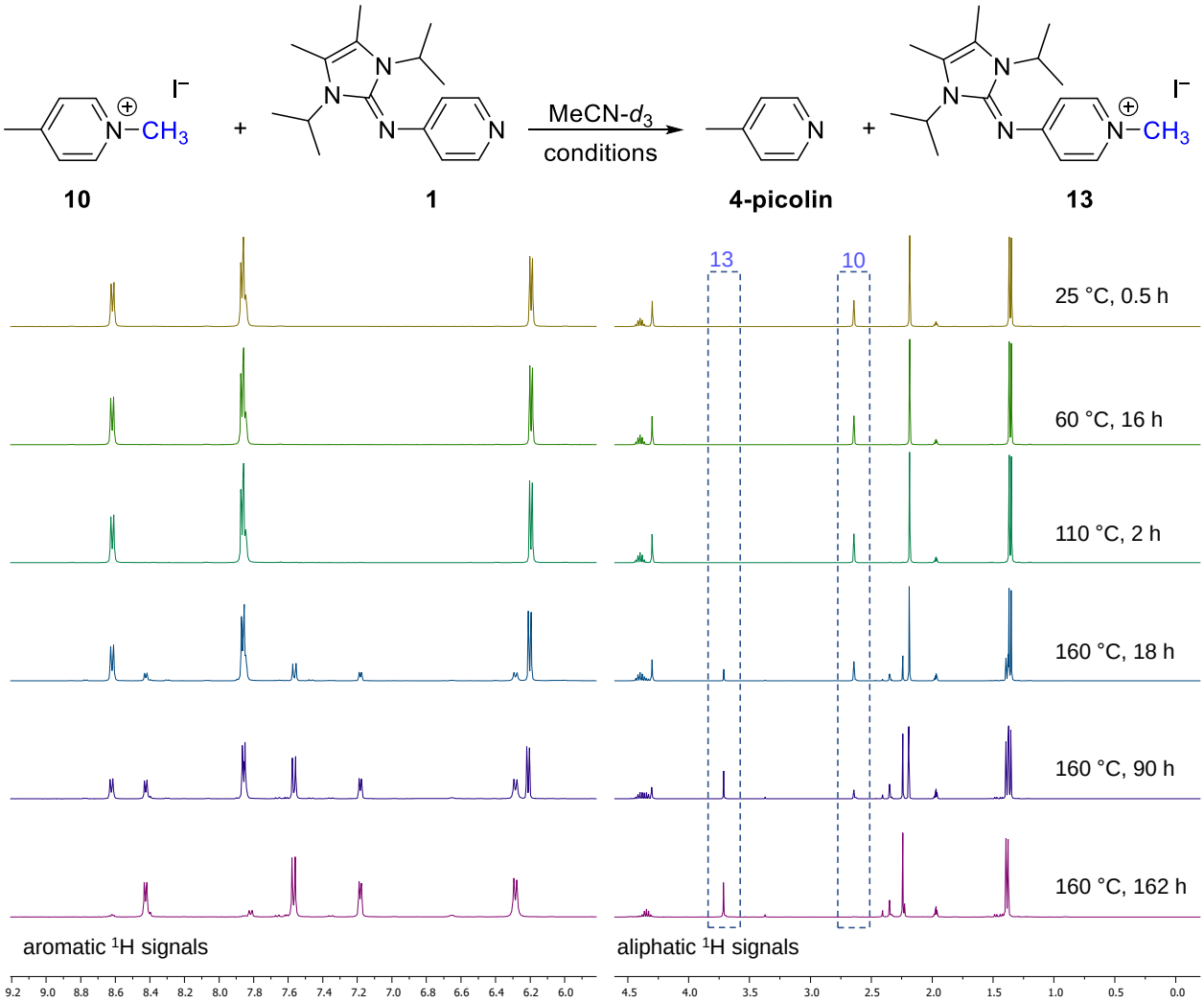

Figure S44: Stacked ^{1}H NMR spectra of the demethylation reaction of **10** using **1** in MeCN-d_3 after heating at given a given temperature for a given time. The aromatic ^{1}H signals (left) are depicted with a 7-fold scaling for better visibility of the signals. Characteristic resonances corresponding to the consumption of **10** and the formation of **13** are highlighted in dotted frames.

^{1}H NMR analysis shows that the transfer of the methyl group is 92.5 % complete after continuous heating at 160 °C for a total of 162 h.

(5)

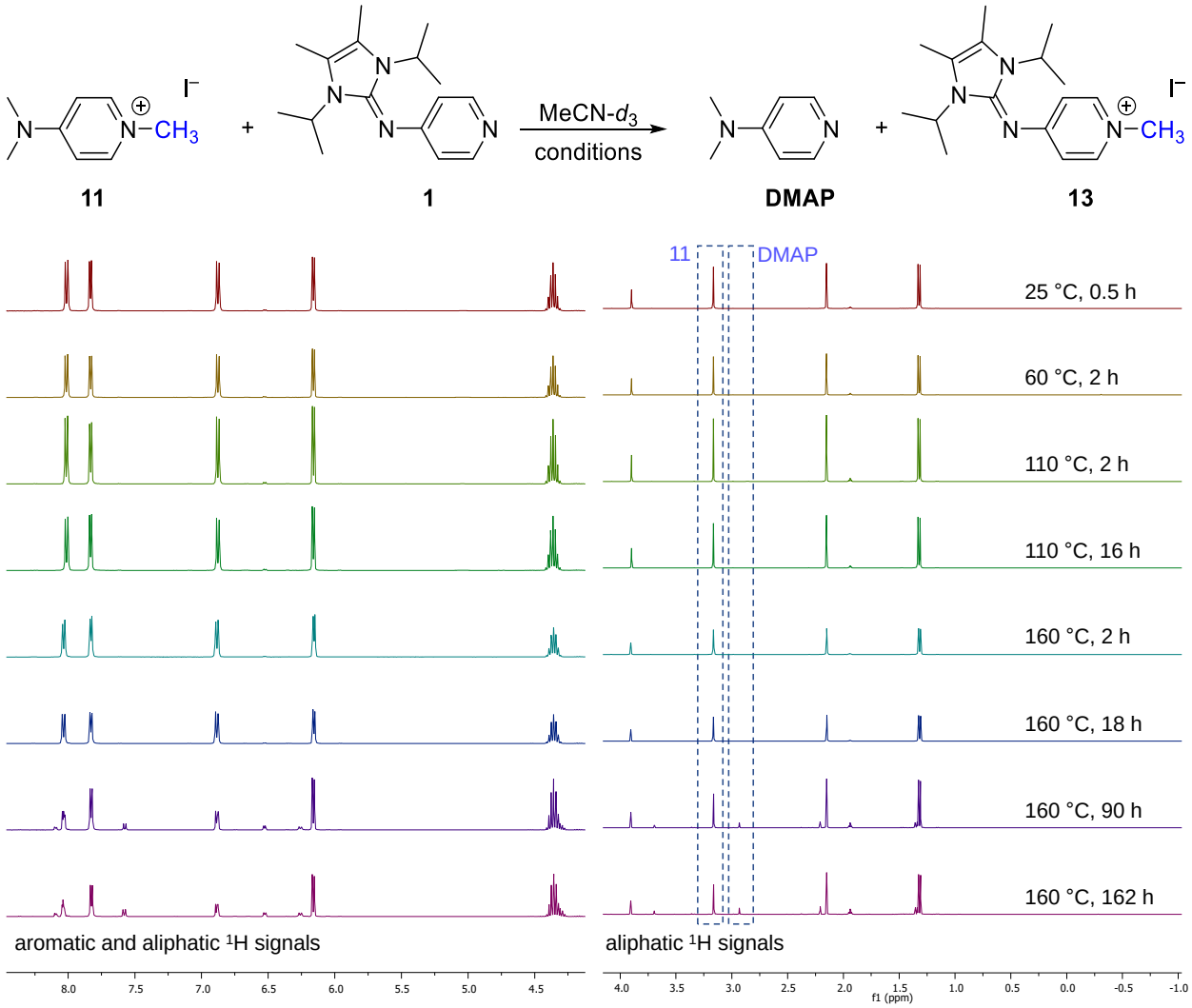

Figure S45: Stacked ^{1}H NMR spectra of the demethylation reaction of **11** using **1** as in MeCN-d_3 recorded after heating at a given temperature for a given time. The aromatic ^{1}H signals (left) are depicted with an 8-fold scaling for better visibility. Characteristic resonances corresponding to the consumption of **11** and the formation of **13** are highlighted in dotted frames.

^{1}H NMR analysis shows that the transfer of the methyl group is 14.8 % complete after continuous heating at 160 °C for a total of 162 h.

(6)

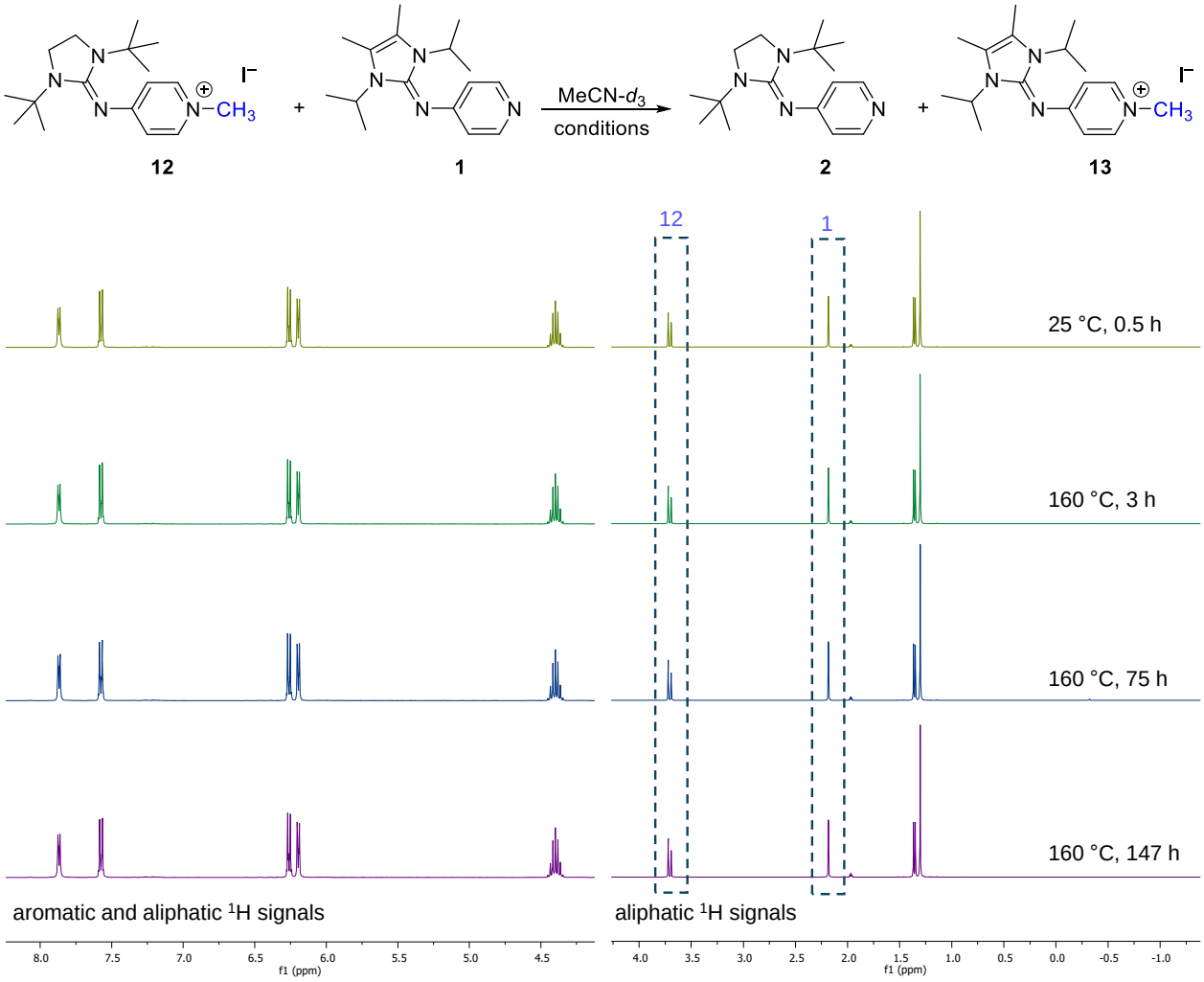

Figure S46: Stacked ^{1}H NMR spectra of the demethylation reaction of **12** using **1** in MeCN-d_3 recorded after heating at a given temperature for a given time. The aromatic and aliphatic ^{1}H signals (left) are depicted with a 10-fold scaling for better visibility of the signals. Characteristic resonances corresponding to the consumption of **12** and **1** are highlighted in dotted frames.

After heating at 160 °C for a total of 147 h, no demethylation of **12** and formation of **13** is observed. The ratio of the relative intensities in the ^{1}H NMR for **1** and **12** remain unchanged.

Determination of the Huynh Electronic Parameter

Determination of HEP of 1

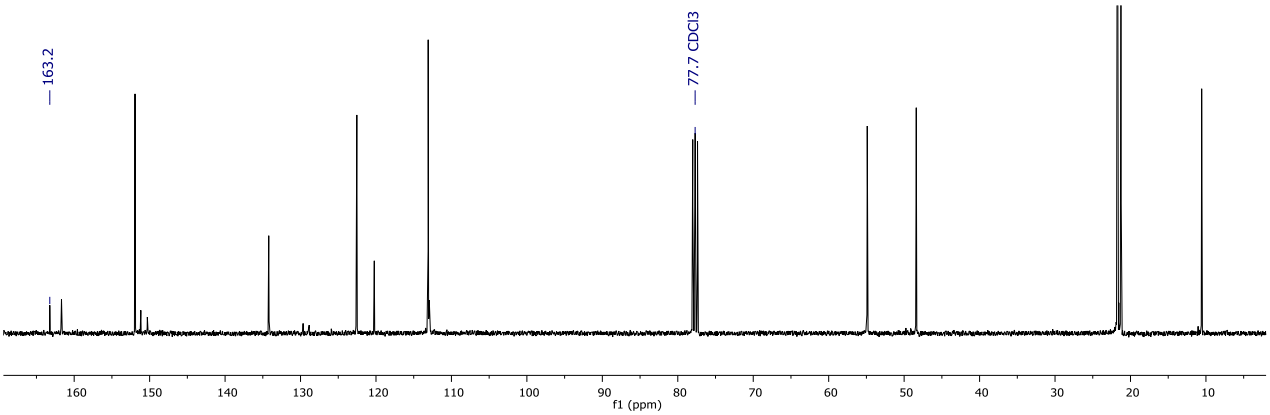

Figure S47: $^{13}C\{^{1}H\}$ NMR spectrum (in $CDCl_3$, 300 K, 100.60 MHz) of **7** internally referenced to the solvent residue signal at 77.7 ppm relative to TMS.

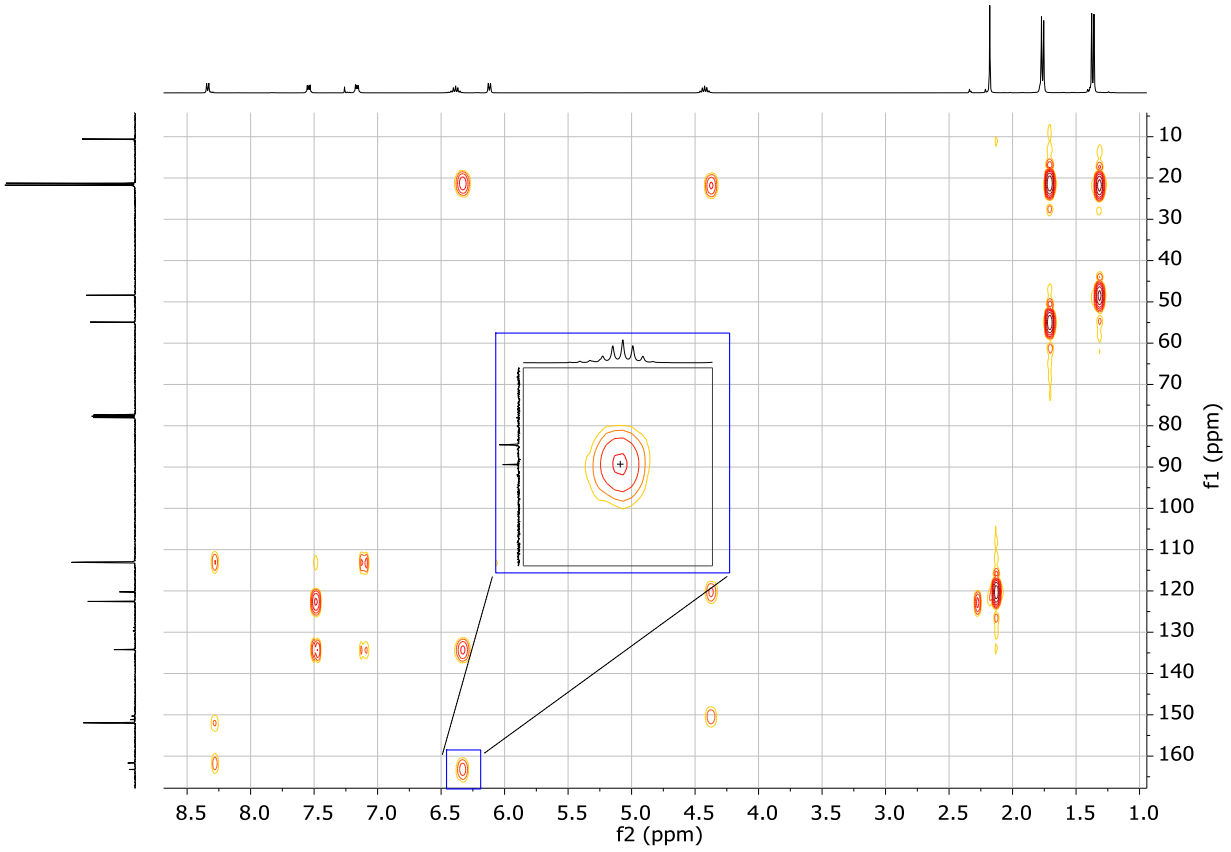

Figure S48: ^{1}H-$^{13}C\{^{1}H\}$ HMBC NMR spectrum (in $CDCl_3$, 298.2 K, 400.03 MHz, 100.60 MHz) of **7** internally referenced to the solvent residue signal of $CDCl_3$ relative to TMS. The $^{3}J_{CH}$ coupling of the CH-isopropyl proton with the carbene carbon atom of the reporter ligand B*i*Pr is highlighted (blue frame), confirming the assignment of the carbene resonance.

Determination of HEP of 2

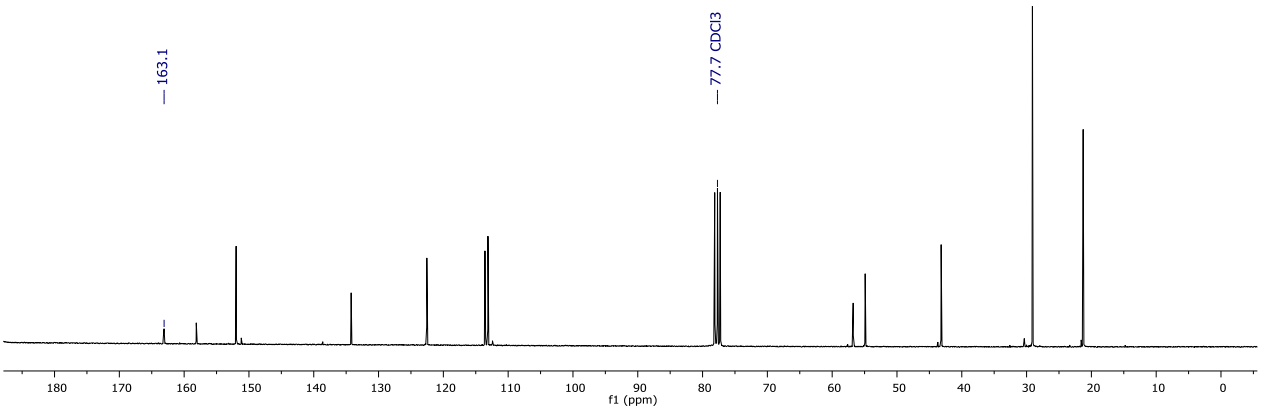

Figure S49: $^{13}C\{^{1}H\}$ NMR spectrum (in $CDCl_3$, 300 K, 100.60 MHz) of **8** internally referenced to the solvent residue signal at 77.7 ppm relative to TMS.

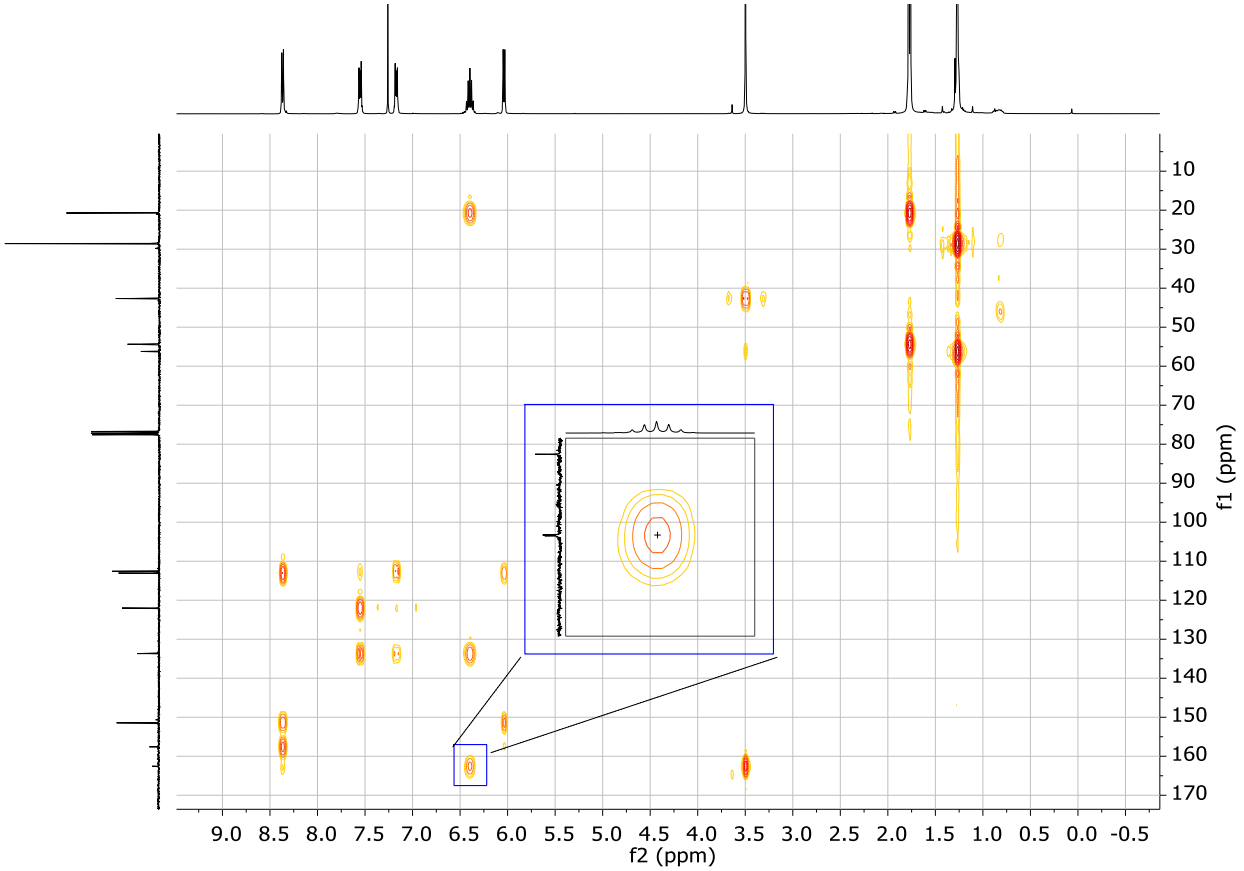

Figure S50: ^{1}H-$^{13}C\{^{1}H\}$ HMBC NMR spectrum (in $CDCl_3$, 298.2 K, 400.03 MHz, 100.6 MHz) of **8** internally referenced to the solvent residue signal of $CDCl_3$ relative to TMS. The $^{3}J_{CH}$ coupling of the CH-isopropyl proton with the carbene carbon atom of the reporter ligand B*i*Pr is highlighted (blue frame), confirming the assignment of the carbene resonance.

Computational Details

Calculation of TEP values of DMAP, 1 and 2:

The TEP values for DMAP, **1** and **2** of the respective [$Ni(CO)_3$**L]** complex were calculated following the procedure reported by Gusev.[10] The calculations were carried out using the mPW1PW91 functional in Gaussian 09[11]. As basis set, 6-311+G(d,p) was used for C, H, N, O and 6-311+G(2d) was used for Ni. Geometry optimizations and frequency calculations were performed using the ultrafine integration grid. The following tables list the XYZ coordinates of the optimized geometries of the respective [$Ni(CO)_3$**L**] complexes.

Table 5: XYZ coordinates of the optimized geometry for [$Ni(CO)_3$**1**].

Atom	X	Y	Z
C	4.17903	1.27055	-0.46486
C	4.74731	0.0422	-0.54451
N	2.88564	1.10494	0.04913
N	3.80825	-0.88102	-0.08299
C	2.67111	-0.22702	0.29714
C	2.03252	2.14462	0.64808
C	2.66771	2.71454	1.91291
H	2.90739	1.9161	2.61694
H	1.96471	3.39476	2.399
H	3.5801	3.27463	1.70186
C	1.60994	3.21678	-0.34825
H	1.13218	1.61251	0.94808
H	2.42599	3.88952	-0.6124
H	0.81729	3.8215	0.09683
H	1.21347	2.77026	-1.26129
C	3.92945	-2.33361	0.08828
C	4.86505	-2.68707	1.23919
H	5.904	-2.42574	1.02725
H	4.82704	-3.76288	1.4238
H	4.55855	-2.17624	2.15329
C	4.26895	-3.05586	-1.20927
H	2.9188	-2.61977	0.38542
H	5.30263	-2.90049	-1.5205
H	3.60813	-2.7389	-2.01783
H	4.13017	-4.12982	-1.06484
N	1.67404	-0.82947	0.90088
C	0.36406	-0.61127	0.63467
C	-0.14861	-0.06954	-0.56668
C	-1.50985	0.05197	-0.74865
N	-2.42703	-0.3126	0.15829

C	-0.61165	-1.01191	1.57185
C	-1.94965	-0.84346	1.29759
Ni	-4.45997	-0.10516	-0.191
C	-4.69921	1.28385	-1.29841
O	-4.92965	2.16205	-1.99345
C	-5.00203	-1.65458	-0.93088
O	-5.40552	-2.61135	-1.40495
C	-5.26131	0.20695	1.38356
O	-5.8377	0.4199	2.34688
C	4.7314	2.57366	-0.92129
C	6.0794	-0.32915	-1.09113
H	0.52025	0.23477	-1.36312
H	-1.89659	0.46005	-1.67488
H	-0.29782	-1.45083	2.50978
H	-2.69422	-1.14754	2.02414
H	4.69607	3.34166	-0.14727
H	4.1976	2.95652	-1.79531
H	5.77553	2.44848	-1.20584
H	6.62422	-0.99855	-0.42427
H	6.68818	0.56484	-1.21969
H	6.00271	-0.81815	-2.06583

Table 6: XYZ coordinates of the optimized geometry for [$Ni(CO)_3$**2**].

Atom	X	Y	Z
C	-4.45938	1.37799	0.88609
C	-4.80486	-0.08095	1.10539
N	-3.14929	1.31651	0.248
N	-4.03205	-0.74077	0.06644
C	-2.92336	0.03839	-0.20514
C	-2.49528	2.59251	-0.17631
C	-3.57626	3.66607	-0.37512
H	-4.27888	3.39196	-1.16546
H	-3.08406	4.5915	-0.67666
H	-4.13558	3.88159	0.53655
C	-1.54066	3.05759	0.92566
H	-2.06788	3.17318	1.87635
H	-1.10573	4.025	0.66329
H	-0.72594	2.34744	1.06332
C	-4.01856	-2.22638	-0.01246
C	-5.39712	-2.73639	0.41647
H	-5.61094	-2.53956	1.46916

H	-5.42724	-3.81781	0.27538
H	-6.19073	-2.29878	-0.19389
C	-2.95279	-2.81643	0.91727
H	-3.10447	-2.48558	1.94877
H	-1.95067	-2.53023	0.60064
H	-3.01398	-3.90715	0.90908
N	-1.90894	-0.44122	-0.84956
C	-0.58922	-0.3001	-0.61394
C	-0.02572	-0.12306	0.66886
C	1.34395	-0.09221	0.82498
N	2.22028	-0.21747	-0.18174
C	0.34162	-0.45491	-1.66232
C	1.69298	-0.40271	-1.40328
Ni	4.2697	-0.17944	0.1428
C	4.58943	0.90988	1.53114
O	4.86939	1.5959	2.40107
C	4.75127	-1.87869	0.49126
O	5.11815	-2.9352	0.71999
C	5.06071	0.4515	-1.33883
O	5.63509	0.85375	-2.24067
H	-0.663	-0.03357	1.5399
H	1.77275	0.0359	1.81227
H	-0.01253	-0.61456	-2.67268
H	2.4045	-0.51628	-2.21257
H	-5.19318	1.84788	0.22489
H	-4.42678	1.94054	1.821
H	-4.4901	-0.41881	2.10279
H	-5.87331	-0.26201	1.00313
C	-1.75662	2.46291	-1.50997
H	-2.38564	1.99686	-2.27035
H	-0.82986	1.90146	-1.43361
H	-1.49958	3.46776	-1.85143
C	-3.79221	-2.66769	-1.46015
H	-4.57156	-2.25653	-2.10604
H	-3.84097	-3.75786	-1.51605
H	-2.82482	-2.33693	-1.82893

Table 7: XYZ coordinates of the optimized geometry for [Ni(CO)$_3$(DMAP)].

Atom	X	Y	Z
C	2.85839	0.01226	0.01471
C	2.11192	1.20739	0.01858
C	0.7344	1.15473	0.02253
N	0.02083	0.02119	0.02376
C	2.10457	-1.17857	0.0137
C	0.72778	-1.11698	0.0181
Ni	-2.05841	-0.00354	-0.00495
C	-2.66331	1.62891	0.42534
O	-3.12915	2.63644	0.69472
C	-2.52983	-0.45882	-1.68109
O	-2.89418	-0.73827	-2.72598
C	-2.59235	-1.21328	1.21124
O	-3.00394	-1.95917	1.9714
N	4.21781	0.008	0.01232
C	4.94625	1.2583	0.00532
H	4.72195	1.85282	-0.88679
H	6.01344	1.04853	0.00867
H	4.71915	1.86263	0.88981
C	4.93863	-1.2467	3.40E-04
H	4.70786	-1.85316	0.88241
H	6.00706	-1.04339	0.00456
H	4.71083	-1.83627	-0.89416
H	2.59197	2.17529	0.01816
H	0.16394	2.07557	0.02419
H	2.57872	-2.14935	0.00937
H	0.14947	-2.0333	0.01606

Calculation of the MCA values of 1, 2 and DBN:

The methyl cation affinity (MCA) represents the reaction enthalpy for the schematic transformation shown in equation (1).

$$LB{-}Me^{\oplus} \xrightarrow{MCA} LB + Me^{\oplus} \qquad (1)$$

MCA values were calculated at the MP2(FC)/6-31+G(2d,p)//B98/6-31G(d) level of theory using Gaussian 09:[11] Geometry optimizations at the B98/6-31G(d) level of theory were performed for the free Lewis Base (LB), the respective methyl-adduct (LB–Me$^+$) and free Me$^+$ cation. By frequency calculations, the optimized structure was verified to only have real harmonic frequencies. The single point energies were calculated at the MP2(FC)/6-31+G(2d,p) level of theory using the optimized geometries. These values were corrected by the "thermal correction to enthalpy" factor obtained from the geometry optimization. For validation of our calculations, we determined the MCA value for DBN (1,5- diazabicyclo(4.3.0)non-5-en) which is known in literature.[12] The obtained MCA values are listed in table 7.

Table 8: Calculated MCA values for DBN, **1** and **2**. Literature value for DBN given in parentheses.

	DBN	**1**	**2**
MCA / kJ mol^{-1}	611.4 (611.3)[12]	659.2	624.8

The XYZ coordinates of the optimized geometries are listed below in the following tables.

Table 9: XYZ coordinates of the optimized geometry for DBN.

Atom	X	Y	Z
N	-0.23229	0.64773	-0.01525
C	-0.19468	-0.73863	0.02563
C	0.97928	1.41423	0.19755
C	2.15305	0.61763	-0.39448
H	1.14352	1.6072	1.27308
H	0.8776	2.39078	-0.29635
C	2.13887	-0.83181	0.13103
H	3.10313	1.11016	-0.15112
H	2.05409	0.61038	-1.4881
N	0.83524	-1.49949	0.06602
H	2.48761	-0.8519	1.17664
H	2.85919	-1.43397	-0.43907
C	-1.63347	-1.23691	0.04742
C	-2.46909	0.01888	-0.28342
H	-1.85732	-1.61196	1.05555
H	-1.77818	-2.06742	-0.64966
C	-1.56886	1.18234	0.18855
H	-3.45013	0.02824	0.20215
H	-2.62443	0.09539	-1.36622
H	-1.75186	1.43036	1.2503
H	-1.71446	2.10066	-0.39632

Table 10: XYZ coordinates of the optimized geometry for DBN–Me^{+}.

Atom	X	Y	Z
N	0.63304	-0.79269	0.0905
C	0.19449	0.46212	0.0347
C	-0.25268	-1.95497	0.19531
C	-1.60664	-1.60057	-0.42872
H	-0.35379	-2.24019	1.25152
H	0.21863	-2.78909	-0.33482
C	-2.12689	-0.27252	0.12776
H	-2.33215	-2.39199	-0.21585
H	-1.50227	-1.53038	-1.51803
N	-1.0919	0.78202	0.04336
H	-2.43884	-0.36819	1.1766

H	-2.99157	0.07265	-0.4484
C	1.35691	1.43027	0.00433
C	2.56963	0.50949	-0.27641
H	1.42953	1.92624	0.98243
H	1.22828	2.20875	-0.75359
C	2.10327	-0.88774	0.17878
H	3.46852	0.83673	0.25087
H	2.78922	0.49958	-1.34865
H	2.3912	-1.11961	1.21281
H	2.45893	-1.69523	-0.46893
C	-1.57656	2.1667	0.02866
H	-0.74922	2.86924	0.12952
H	-2.264	2.31339	0.86896
H	-2.10961	2.3661	-0.90788

Table 11: XYZ coordinates of the optimized geometry for **1**.

Atom	X	Y	Z
C	-1.99863	1.45792	0.24167
C	-2.6056	0.23907	0.22087
N	-0.64959	1.27758	-0.12359
C	-0.41597	-0.06857	-0.35096
N	-1.63241	-0.69854	-0.1541
N	0.64019	-0.70129	-0.80315
C	1.89852	-0.69178	-0.26979
C	3.0137	-0.99152	-1.09216
C	4.28726	-1.0506	-0.53551
N	4.5717	-0.84765	0.76316
C	3.51416	-0.5786	1.54585
C	2.19589	-0.49082	1.10505
H	1.39506	-0.29011	1.81471
H	3.73487	-0.42784	2.60428
H	2.85708	-1.17816	-2.15166
H	5.14147	-1.27666	-1.17568
C	-2.57443	2.80131	0.56909
H	-3.58787	2.6878	0.9653
H	-2.64224	3.45813	-0.30999
H	-1.98059	3.32633	1.32883
C	-4.03765	-0.09667	0.50726
H	-4.54451	0.77525	0.93154
H	-4.13882	-0.91623	1.22862
H	-4.58456	-0.38397	-0.40027
C	-1.7257	-2.16809	-0.23423
C	-2.83428	-2.64418	-1.18587

H	-3.83848	-2.50901	-0.76922
H	-2.7013	-3.71544	-1.37983
H	-2.7774	-2.11649	-2.14476
C	-1.80843	-2.81174	1.16019
H	-0.76143	-2.44139	-0.67588
H	-1.75369	-3.90327	1.06573
H	-2.74454	-2.5679	1.67712
H	-0.97071	-2.48192	1.78497
C	0.24615	2.41849	-0.43514
C	1.03454	2.23063	-1.74187
H	1.85584	1.51784	-1.63838
H	1.45958	3.20185	-2.02425
H	0.3794	1.89312	-2.55255
C	1.14676	2.80412	0.74954
H	-0.44483	3.2508	-0.60655
H	1.67004	3.74037	0.51824
H	1.89583	2.03244	0.9495
H	0.55492	2.96004	1.66

Table 12: XYZ coordinates of the optimized geometry for **1**–Me^{+}.

Atom	X	Y	Z
C	-2.86141	0.38616	0.54031
C	-2.57382	-0.94503	0.42048
N	-1.74273	1.09921	0.09027
C	-0.78023	0.22385	-0.29537
N	-1.26944	-1.03744	-0.09766
N	0.36153	0.57701	-0.92968
C	1.5747	0.34555	-0.44851
C	2.71442	0.67667	-1.26702
C	3.98807	0.48654	-0.81808
N	4.2519	-0.01771	0.42986
C	3.20481	-0.34038	1.24306
C	1.90228	-0.18047	0.85527
H	1.11509	-0.43608	1.55778
H	3.46916	-0.72666	2.22239
H	2.54544	1.08641	-2.25721
H	4.85719	0.72636	-1.4221
C	-4.09283	1.06013	1.06227
H	-4.83349	0.31211	1.35613
H	-4.55922	1.70358	0.30534
H	-3.88106	1.67563	1.94624
C	-3.4208	-2.1199	0.80747
H	-4.42483	-1.77541	1.06905

H	-3.01676	-2.64736	1.68023
H	-3.53002	-2.84556	-0.00553
C	-0.57854	-2.24499	-0.62492
C	-1.24831	-2.74273	-1.91605
H	-2.25687	-3.13051	-1.73882
H	-0.64931	-3.55558	-2.34254
H	-1.30881	-1.93756	-2.65629
C	-0.40624	-3.34049	0.43753
H	0.41698	-1.88349	-0.8922
H	0.29123	-4.09412	0.05467
H	-1.34465	-3.85208	0.66982
H	0.01026	-2.93369	1.36632
C	-1.64938	2.58251	0.00601
C	-1.59575	3.04703	-1.45724
H	-0.68569	2.69105	-1.94866
H	-1.60789	4.14251	-1.48839
H	-2.46432	2.67986	-2.01592
C	-0.49887	3.12984	0.86348
H	-2.58728	2.93462	0.44429
H	-0.57236	4.22259	0.90245
H	0.47603	2.87119	0.44018
H	-0.55525	2.74902	1.89007
C	5.64161	-0.2562	0.84789
H	6.26374	0.59063	0.54637
H	6.02679	-1.17476	0.39212
H	5.67904	-0.34887	1.93518

Table 13: XYZ coordinates of the optimized geometry for **2**.

Atom	X	Y	Z
C	1.45312	1.73E+00	-1.34E+00
C	2.60377	0.90156	-7.53E-01
N	0.26962	1.32934	-5.51E-01
H	1.29122	1.45819	-2.39E+00
H	1.63714	2.80203	-1.29092
C	0.53964	0.00178	-0.11528
N	1.88154	-0.27889	-0.28219
H	3.12554	1.42414	0.06487
H	3.33965	0.64284	-1.51908
N	-0.28169	-0.88475	0.34883
C	-1.63648	-0.96303	0.08045
C	-2.23041	-0.6122	-1.15454
C	-3.59252	-0.83787	-1.34195
N	-4.41519	-1.37429	-0.42599

C	-2.49284	-1.54631	1.03784
C	-3.84278	-1.7162	0.73952
H	-4.50754	-2.15912	1.48227
H	-1.6324	-0.16943	-1.94587
H	-4.05427	-0.57069	-2.29372
H	-2.08915	-1.85714	1.99814
C	-0.27501	2.37963	0.38799
C	0.83267	2.9156	1.33162
H	1.23923	2.10434	1.94899
H	0.41527	3.67327	2.00639
H	1.66017	3.38684	0.78779
C	-0.84373	3.51968	-0.48406
H	-0.07734	4.00606	-1.0992
H	-1.2872	4.29137	0.15678
H	-1.62264	3.1301	-1.14911
C	-1.42074	1.84563	1.26539
H	-1.09333	1.03694	1.92524
H	-2.25897	1.48829	0.66298
H	-1.7786	2.67023	1.89403
C	2.53689	-1.5641	0.10312
C	4.03536	-1.5021	-0.26001
H	4.19494	-1.41894	-1.34195
H	4.50931	-2.43276	0.07178
H	4.55093	-0.67266	0.23914
C	2.40676	-1.77361	1.62902
H	2.90179	-0.95796	2.17266
H	2.8859	-2.71691	1.92033
H	1.35416	-1.80763	1.92095
C	1.90159	-2.74127	-0.67024
H	1.98455	-2.5761	-1.7519
H	0.84741	-2.85795	-0.41162
H	2.43249	-3.66963	-0.4236

Table 14: XYZ coordinates of the optimized geometry for **2**–Me^{+}.

Atom	X	Y	Z
C	2.87877	7.8832	-1.01552
C	2.99983	-0.73173	-0.82306
N	1.62032	1.12785	0.32687
H	2.82E+00	1.06816	-2.07344
H	3.72583	1.31738	-0.56974
C	0.98061	-0.01059	0.04418
N	1.65941	-1.12211	-0.3528
H	3.75633	-0.98685	-0.0684

H	3.25496	-1.24165	-1.75442
N	-0.11606	-0.04781	0.81545
C	-1.37133	-0.02373	0.4142
C	-1.82439	0.01336	-0.9555
C	-3.15875	0.02952	-1.25409
N	-4.12226	0.01843	-0.28643
C	-2.4239	-0.03909	1.39833
C	-3.73711	-0.02024	1.02773
H	-4.54276	-0.03224	1.75467
H	-1.1057	0.02814	-1.76899
H	-3.51805	0.05373	-2.27798
H	-2.16096	-0.06382	2.45059
C	1.40031	2.53772	0.15842
C	2.12599	2.69921	1.51114
H	1.70332	2.01618	2.25693
H	2.01038	3.72521	1.87975
H	3.20057	2.49782	1.42071
C	1.99251	3.4977	-0.89787
H	3.0732	3.38025	-1.02732
H	1.81875	4.52798	-0.57046
H	1.50439	3.36637	-1.87125
C	-0.09149	2.89057	0.31759
H	-0.54621	2.39673	1.17789
H	-0.66156	2.64293	-0.5853
H	-0.16854	3.97236	0.47447
C	1.41893	-2.53078	0.13324
C	2.34558	-3.47357	-0.66501
H	2.14265	-3.42178	-1.74168
H	2.15613	-4.5012	-0.33833
H	3.40819	-3.27238	-0.49283
C	1.75227	-2.61237	1.63767
H	2.79912	-2.34379	1.82755
H	1.60103	-3.63682	1.99764
H	1.10709	-1.94364	2.21673
C	-0.03384	-2.97634	-0.13362
H	-0.33079	-2.75066	-1.16477
H	-0.74485	-2.51548	0.55373
H	-0.09827	-4.06161	0.00429
C	-5.54898	-0.02997	-0.64121
H	-5.68658	0.39374	-1.63827
H	-6.12125	0.56576	0.07431
H	-5.91248	-1.06327	-0.63136

Table 15: XYZ coordinates of the optimized geometry for Me^{+}.

Atom	X	Y	Z
C	0	0.003	0.00001
H	0.94867	0.5464	-0.00001
H	-0.94867	0.54641	-0.00001
H	-0.00001	-1.09464	-0.00001

X-ray Diffraction Studies

General information: Single-crystal X-ray diffraction data were collected on a Bruker APEX-II CCD diffractometer or on a Bruker D8 quest Photon III diffractometer using Mo-K_α radiation (λ = 0.71073 Å). Crystals were selected under oil, mounted on nylon loops and then immediately placed in a cold stream of N_2 on a diffractometer. Using Olex2,[13] the structures were solved with the Superflip[14–16], Olex2.solve[17], ShelXS[18], ShelXD[18] or ShelXT[19] using charge flipping, direct, or dual methods. The refinement was done with ShelXL[19] using Least Squares minimization or Olex2.refine[17] using Gauss-Newton minimization.

Crystallographic data have been deposited with the Cambridge Crystallographic Data Centre as supplementary publication no. CCDC- 2354124 (**1**), CCDC- 2354125 (**2**), CCDC- 2354126 (**3**), CCDC- 2354127 (**4**), CCDC- 2354128 (**5**), CCDC- 2354129 (**6**), CCDC- 2354130 (**7**) and CCDC- 2354131 (**8**), CCDC- 2354132 (**12**) and CCDC- 2354133 (**13**). These data can be obtained free of charge via https://www.ccdc.cam.ac.uk/structures (or from the CCDC, 12 Union Road, Cambridge CB2 1EZ, UK; fax: (+44) 1223-336-033; or deposit@ccdc.cam.ac.uk).

Single-crystal X-ray structure analysis of 1:

Colorless single crystals of **1** were obtained by storing an *n*-hexane solution of **1** at –34 °C. The single-crystal X-ray structure analysis revealed that **1** crystallizes in the orthorhombic space group $P2_12_12_1$. The asymmetric unit contains one molecule of **1**.

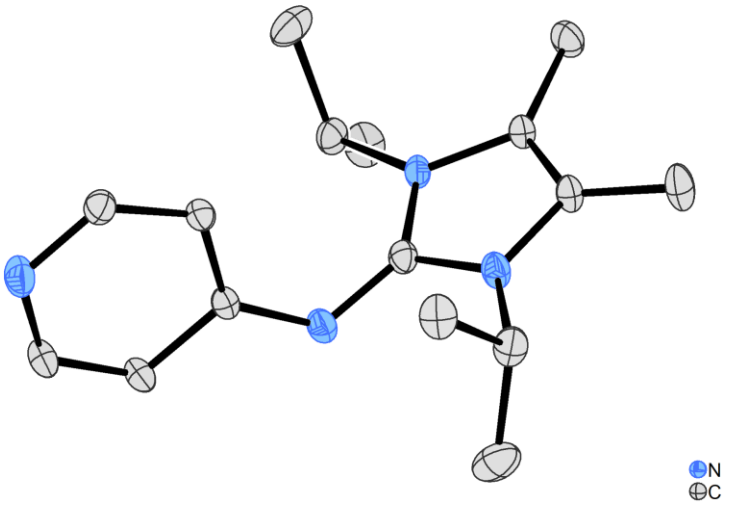

Figure S51: Molecular view of **1** in the solid state with thermal ellipsoid plot at the 50% levels of probability. Hydrogen atoms are omitted for clarity.

Identification code	**2354124**	μ/mm^{-1}	0.073
Empirical formula	$C_{16}H_{24}N_4$	F(000)	592.0
Formula weight	272.39	Crystal size/mm^3	0.42 × 0.11 × 0.11
Temperature/K	100.01	Radiation	MoKα (λ = 0.71073)
Crystal system	orthorhombic	2Θ range for data collection	6.89 to 59.182°
Space group	$P2_12_12_1$	Index ranges	$-13 \le h \le 12$, $-15 \le k \le 15$, $-19 \le l \le 19$
a/Å	9.74140(10)	Reflections collected	15931
b/Å	11.2691(2)	Independent reflections	4280 [R_{int} = 0.0191, R_{sigma} = 0.0178]
c/Å	13.8933(2)	Data/restraints/parameters	4280/0/187
α/°	90	Goodness-of-fit on F^2	1.081
β/°	90	Final R indexes [I>=2σ (I)]	R_1 = 0.0400, wR_2 = 0.1120
γ/°	90	Final R indexes [all data]	R_1 = 0.0413, wR_2 = 0.1131
Volume/Å^3	1525.16(4)	Largest diff. peak/hole / e Å^{-3}	0.51/-0.25
Z	4	Flack parameter	-0.2(4)
ρ_{calc}g/cm^3	1.186		

Single-crystal X-ray structure analysis of 2:

Colorless single crystals of **2** were obtained by storing an *n*-hexane solution of **2** at –34 °C. The single-crystal X-ray structure analysis revealed that **2** crystallizes in the monoclinic space group $P2_1/c$. The asymmetric unit contains one molecule of **2**.

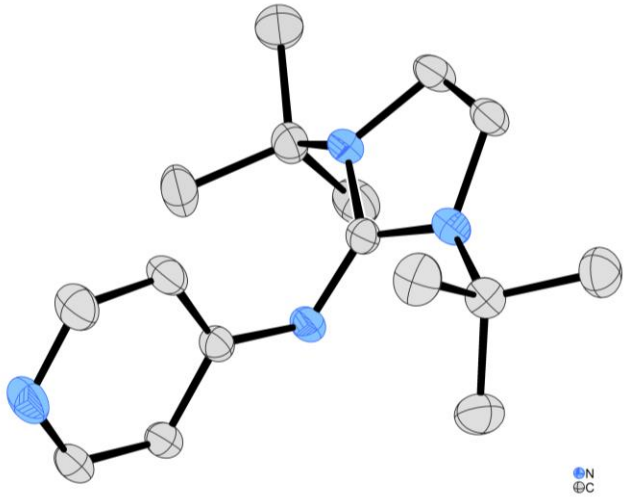

Figure S52: Molecular view of **2** in the solid state with thermal ellipsoid plot at the 50% levels of probability. Hydrogen atoms are omitted for clarity.

Identification code	**2354125**	ρ_{calc}g/cm^3	1.163
Empirical formula	$C_{16}H_{26}N_4$	μ/mm^{-1}	0.071
Formula weight	274.41	F(000)	600.0
Temperature/K	173.00	Crystal size/mm^3	0.15 × 0.13 × 0.11
Crystal system	monoclinic	Radiation	MoKα (λ = 0.71073)
Space group	$P2_1/n$	2Θ range for data collection/°	4.392 to 55.004
a/Å	6.2718(2)	Index ranges	$-8 \le h \le 8$, $-17 \le k \le 17$, $-24 \le l \le 24$
b/Å	13.4687(6)	Reflections collected	38299
c/Å	18.5555(8)	Independent reflections	3589 [R_{int} = 0.0660, R_{sigma} = 0.0273]
α/°	90	Data/restraints/parameters	3589/0/187
β/°	91.4840(10)	Goodness-of-fit on F^2	1.037
γ/°	90	Final R indexes [I>=2σ (I)]	R_1 = 0.0503, wR_2 = 0.1110
Volume/Å^3	1566.91(11)	Final R indexes [all data]	R_1 = 0.0650, wR_2 = 0.1186
Z	4	Largest diff. peak/hole / e Å^{-3}	0.22/-0.20

Single-crystal X-ray structure analysis of 3:

Colorless single crystals of **3** were obtained by the diffusion of *n*-hexane into a $CHCl_3$ solution of **3** at –34 °C. The single-crystal X-ray structure analysis revealed that **3** crystallizes in the orthorhombic space group *Pna*2_1. The asymmetric unit contains one molecule of **3**. One BF_4^- anion is disordered over two positions (occupancy 0.8 : 0.2).Compound **3** was refined as a 2-component inversion twin (BASF 0.3(10)).

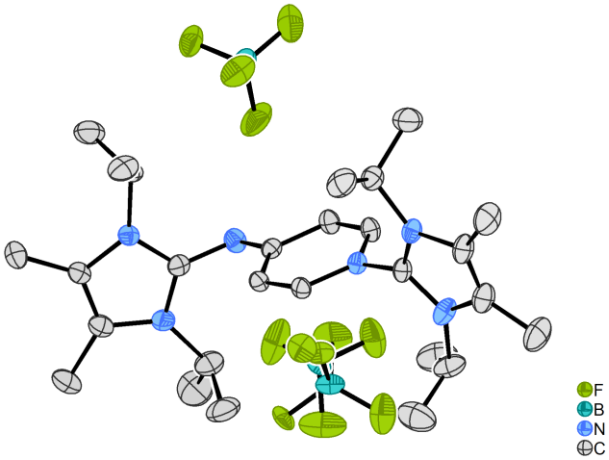

Figure S53: Molecular view of **3** in the solid state with thermal ellipsoid plot at the 50% levels of probability. Hydrogen atoms are omitted for clarity.

Identification code	**2354126**	ρ_{calc}g/cm^3	1.290
Empirical formula	$C_{27}H_{43}B_2F_8N_6$	μ/mm^{-1}	0.109
Formula weight	625.29	F(000)	1316.0
Temperature/K	100.02	Crystal size/mm^3	0.32 × 0.22 × 0.06
Crystal system	orthorhombic	Radiation	MoKα (λ = 0.71073)
Space group	*Pna*2_1	2Θ range for data collection	6.408 to 56.588°
a/Å	15.6898(5)	Index ranges	$-20 \le h \le 19$, $-11 \le k \le 11$, $-32 \le l \le 32$
b/Å	8.5225(3)	Reflections collected	35131
c/Å	24.0701(7)	Independent reflections	7933 [R_{int} = 0.0504, R_{sigma} = 0.0494]
α/°	90	Data/restraints/parameters	7933/19/446
β/°	90	Goodness-of-fit on F^2	1.050
γ/°	90	Final *R* indexes [$I>=2\sigma(I)$]	R_1 = 0.0631, wR_2 = 0.1775
Volume/Å^3	3218.57(18)	Final *R* indexes [all data]	R_1 = 0.0685, wR_2 = 0.1827
Z	4	Largest diff. peak/hole / e Å^{-3}	0.68/-0.23

Single-crystal X-ray structure analysis of 4:

Colorless single crystals of **4** were obtained by the diffusion of *n*-hexane into a THF solution of **4** at ambient temperature. The single-crystal X-ray structure analysis revealed that **4** crystallizes in the monoclinic space group *C*2/*c*. The asymmetric unit contains one molecule of **4** and half a THF molecule. One *iso*-propyl group is disordered over two positions (occupancy 0.7:0.3).

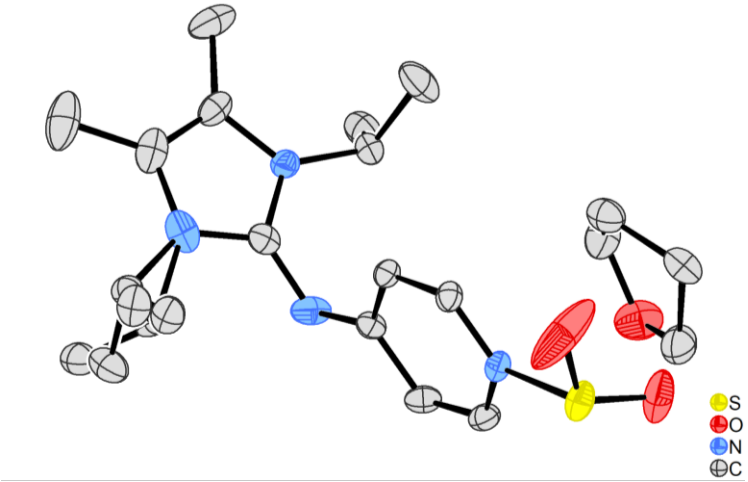

Figure S54: Molecular view of **4** in the solid state with thermal ellipsoid plot at the 50% levels of probability. Hydrogen atoms are omitted for clarity.

Identification code	**2354127**	ρ_{calc}g/cm^3	1.291
Empirical formula	$C_{18}H_{28}N_4O_{2.5}S$	μ/mm^{-1}	0.191
Formula weight	372.50	*F*(000)	1600.0
Temperature/K	100	Crystal size/mm^3	0.49 × 0.45 × 0.03
Crystal system	monoclinic	Radiation	MoKα (λ = 0.71073)
Space group	*C*2/*c*	2Θ range for data collection/°	7.1 to 59.228°
a/Å	20.7329(3)	Index ranges	$-28 \le h \le 28$, $-14 \le k \le 14$, $-24 \le l \le 24$
b/Å	10.41810(10)	Reflections collected	32208
c/Å	17.8347(2)	Independent reflections	5386 [R_{int} = 0.0237, R_{sigma} = 0.0157]
α/°	90	Data/restraints/parameters	5386/0/267
β/°	95.7146(6)	Goodness-of-fit on F^2	1.020
γ/°	90	Final *R* indexes [$I>=2\sigma(I)$]	R_1 = 0.0553, wR_2 = 0.1371
Volume/Å^3	3833.10(8)	Final *R* indexes [all data]	R_1 = 0.0606, wR_2 = 0.1412
Z	8	Largest diff. peak/hole / e Å^{-3}	0.98/-0.69

Single-crystal X-ray structure analysis of 5:

Colorless single crystals of **5** were obtained by the diffusion of *n*-pentane into a DCM solution of **5** at –34 °C. The single-crystal X-ray structure analysis revealed that **5** crystallizes in the monoclinic space group $P2_1/m$. The asymmetric unit contains half a molecule of **5**.

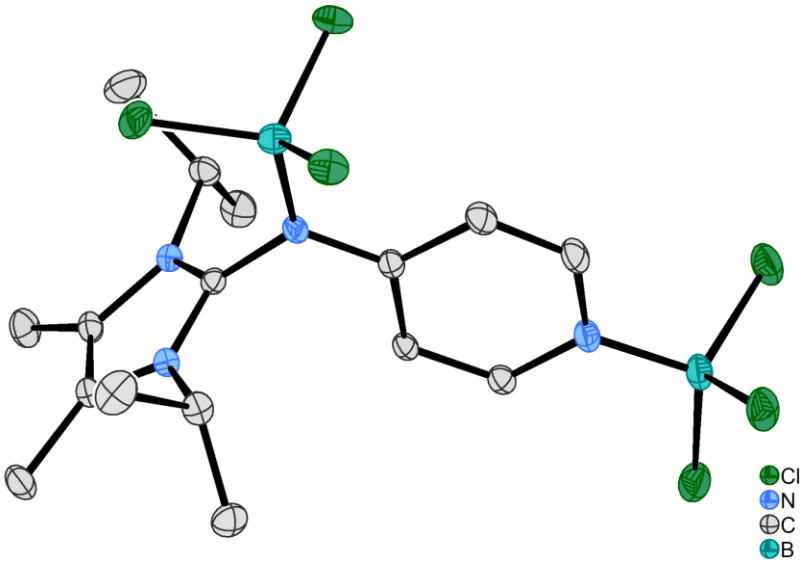

Figure S55: Molecular view of **5** in the solid state with thermal ellipsoid plot at the 50% levels of probability. Hydrogen atoms are omitted for clarity.

Identification code	**2354128**	ρ_{calc}g/cm^3	1.423
Empirical formula	$C_{16}H_{24}B_2Cl_6N_4$	μ/mm^{-1}	0.737
Formula weight	506.71	F(000)	520.0
Temperature/K	100	Crystal size/mm^3	0.14 × 0.12 × 0.02
Crystal system	monoclinic	Radiation	MoKα (λ = 0.71073)
Space group	$P2_1/m$	2Θ range for data collection/°	6.928 to 57.492°
a/Å	7.52560(10)	Index ranges	$-10 \le h \le 10$, $-18 \le k \le 18$, $-16 \le l \le 16$
b/Å	13.7012(2)	Reflections collected	15766
c/Å	12.0051(2)	Independent reflections	3191 [R_{int} = 0.0247, R_{sigma} = 0.0195]
α/°	90	Data/restraints/parameters	3191/0/148
β/°	107.2128(8)	Goodness-of-fit on F^2	1.104
γ/°	90	Final R indexes [I>=2σ (I)]	R_1 = 0.0349, wR_2 = 0.0913
Volume/Å^3	1182.40(3)	Final R indexes [all data]	R_1 = 0.0411, wR_2 = 0.0951
Z	2	Largest diff. peak/hole / e Å^{-3}	0.45/-0.26

Single-crystal X-ray structure analysis of 6:

Yellow single crystals of **6** were obtained by the diffusion of *n*-hexane into a THF solution of **6** at –34 °C. The single-crystal X-ray structure analysis revealed that **6** crystallizes in the monoclinic space group $P2_1/c$. The asymmetric unit contains half a molecule of **6**. One *iso*-propyl group is disordered over two positions (occupancy 0.8 : 0.2).

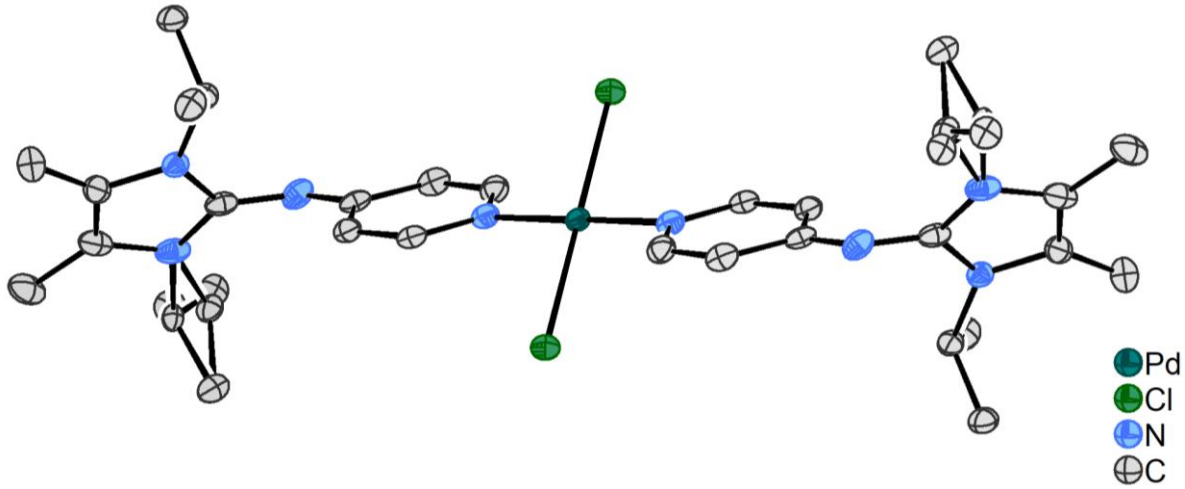

Figure S56: Molecular view of **6** in the solid state with thermal ellipsoid plot at the 50% levels of probability. Hydrogen atoms are omitted for clarity.

Identification code	**2354129**	ρ_{calc}g/cm^3	1.415
Empirical formula	$C_{32}H_{48}N_8Cl_2Pd$	μ/mm^{-1}	0.740
Formula weight	722.08	F(000)	752.0
Temperature/K	100	Crystal size/mm^3	0.27 × 0.03 × 0.03
Crystal system	monoclinic	Radiation	MoKα (λ = 0.71073)
Space group	$P2_1/c$	2Θ range for data collection/°	6.358 to 56.768°
a/Å	6.6684(2)	Index ranges	$-8 \le h \le 8$, $-18 \le k \le 18$, $-25 \le l \le 25$
b/Å	13.6481(4)	Reflections collected	24127
c/Å	18.8863(5)	Independent reflections	4236 [R_{int} = 0.0497, R_{sigma} = 0.0366]
α/°	90	Data/restraints/parameters	4236/12/221
β/°	99.5077(18)	Goodness-of-fit on F^2	1.030
γ/°	90	Final R indexes [I>=2σ (I)]	R_1 = 0.0321, wR_2 = 0.0687
Volume/Å^3	1695.25(8)	Final R indexes [all data]	R_1 = 0.0449, wR_2 = 0.0744
Z	2	Largest diff. peak/hole / e Å^{-3}	0.47/-0.61

Single-crystal X-ray structure analysis of 7:

Yellow single crystals of **7** were obtained by the diffusion of *n*-hexane into a $CDCl_3$ solution of **7** at –34 °C. The single-crystal X-ray structure analysis revealed that **7** crystallizes in the monoclinic space group $P2_1/c$. The asymmetric unit contains one molecule of **7** and two $CDCl_3$ molecules.

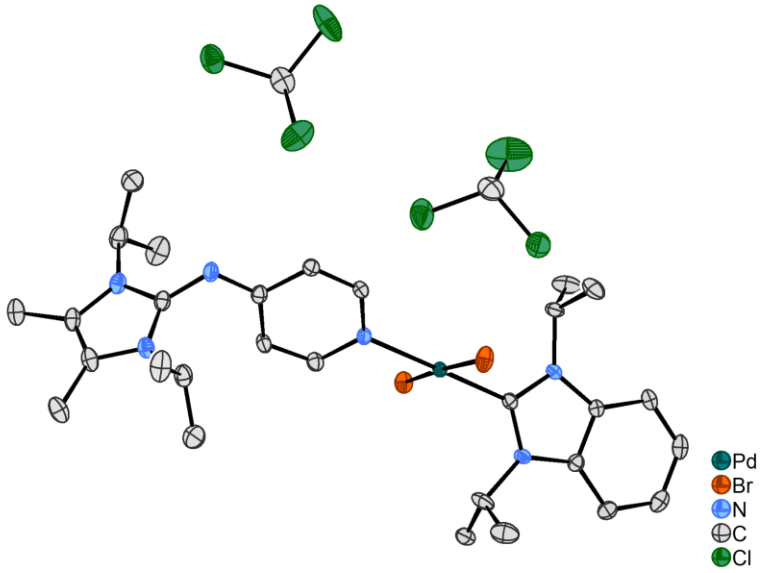

Figure S57: Molecular view of **7** in the solid state with thermal ellipsoid plot at the 50% levels of probability. Hydrogen atoms are omitted for clarity.

Identification code	**2354130**	ρ_{calc}g/cm^3	1.615
Empirical formula	$C_{31}H_{44}Br_2Cl_6N_6Pd$	μ/mm^{-1}	2.872
Formula weight	979.64	F(000)	1960.0
Temperature/K	100	Crystal size/mm^3	0.31 × 0.2 × 0.02
Crystal system	monoclinic	Radiation	MoKα (λ = 0.71073)
Space group	$P2_1/c$	2Θ range for data collection/°	3.466 to 60.12°
a/Å	10.4329(2)	Index ranges	$-14 \le h \le 14$, $-17 \le k \le 17$, $-42 \le l \le 42$
b/Å	12.7505(3)	Reflections collected	62658
c/Å	30.4283(6)	Independent reflections	11775 [R_{int} = 0.0396, R_{sigma} = 0.0299]
α/°	90	Data/restraints/parameters	11775/0/425
β/°	95.4543(10)	Goodness-of-fit on F^2	1.045
γ/°	90	Final R indexes [I>=2σ (I)]	R_1 = 0.0337, wR_2 = 0.0763
Volume/Å^3	4029.39(15)	Final R indexes [all data]	R_1 = 0.0445, wR_2 = 0.0807
Z	4	Largest diff. peak/hole / e Å^{-3}	0.98/-1.24

Single-crystal X-ray structure analysis of 8:

Yellow single crystals of **8** were obtained by the diffusion of *n*-hexane into a DCM/$CHCl_3$ solution of **8** at –34 °C. The single-crystal X-ray structure analysis revealed that **8** crystallizes in the orthorhombic space group *P*ca2_1. The asymmetric unit contains one molecule of **8** and one DCM molecule.

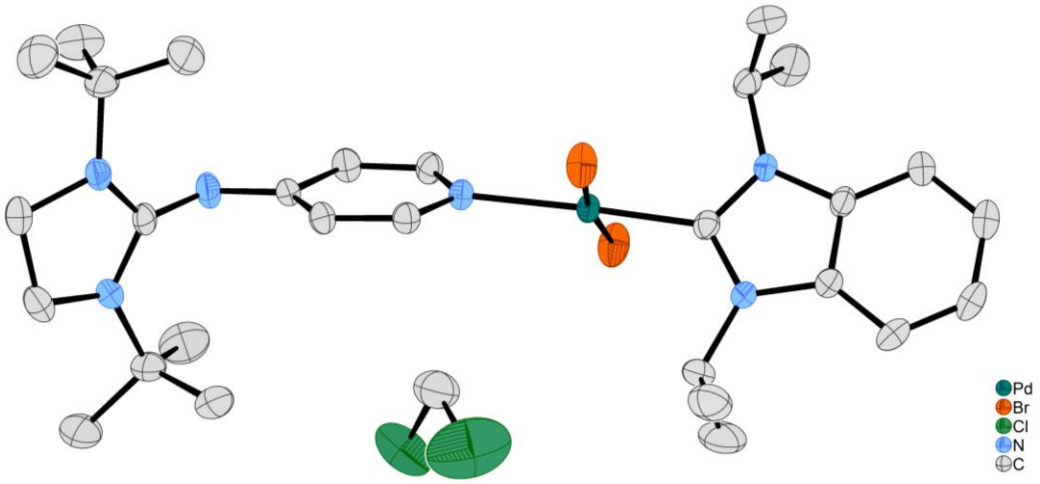

Figure S58: Molecular view of **8** in the solid state with thermal ellipsoid plot at the 50% levels of probability. Hydrogen atoms are omitted for clarity.

Identification code	**2354131**	μ /mm^{-1}	2.902
Empirical formula	$C_{30}H_{46}Br_2Cl_2N_6Pd$	*F*(000)	1672.0
Formula weight	827.85	Crystal size/mm^3	0.21 × 0.19 × 0.09
Temperature/K	183.00	Radiation	MoKα (λ = 0.71073)
Crystal system	orthorhombic	2Θ range for data collection/°	4.584 to 55.046
Space group	*P*ca2_1	Index ranges	$-23 \le h \le 23$, $-24 \le k \le 24$, $-14 \le l \le 14$
a/Å	17.7755(4)	Reflections collected	87916
b/Å	18.4999(4)	Independent reflections	8120 [R_{int} = 0.0411, R_{sigma} = 0.0219]
c/Å	10.9830(2)	Data/restraints/parameters	8120/1/380
α/°	90	Goodness-of-fit on F^2	1.024
β/°	90	Final *R* indexes [$I>=2\sigma(I)$]	R_1 = 0.0205, wR_2 = 0.0485
γ/°	90	Final *R* indexes [all data]	R_1 = 0.0219, wR_2 = 0.0492
Volume/Å^3	3611.70(13)	Largest diff. peak/hole / e Å^{-3}	0.70/-0.49
Z	4	Flack parameter	0.001(3)
ρ_{calc}g/cm^3	1.522		

Single-crystal X-ray structure analysis of 12:

Colorless single crystals of **12** were obtained by the diffusion of Et_2O into a MeCN solution of **12** at ambient temperature. The single-crystal X-ray structure analysis revealed that **12** crystallizes in the monoclinic space group $P2_1/c$. The asymmetric unit contains one molecule of **12**. The methyl groups of the *tert*-butyl group (occupancy 0.8 : 0.2) and the iodide anion (occupancy 0.66 : 0.34) are disordered over two positions, respectively.

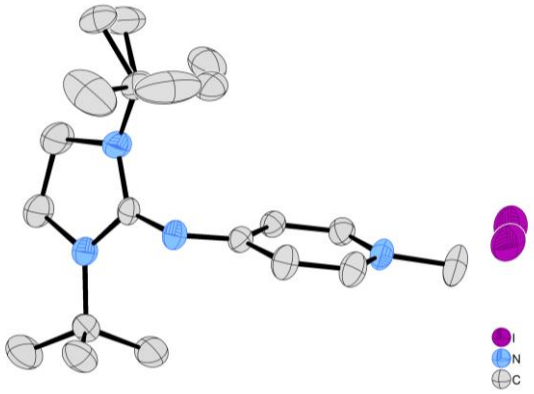

Figure S59: Molecular view of **12** in the solid state with thermal ellipsoid plot at the 50% levels of probability. Hydrogen atoms are omitted for clarity.

Identification code	**2354132**	ρ_{calc}g/cm^3	1.398
Empirical formula	$C_{17}H_{29}IN_4$	μ/mm^{-1}	1.622
Formula weight	416.34	F(000)	848.0
Temperature/K	173.0	Crystal size/mm^3	0.35 × 0.21 × 0.19
Crystal system	monoclinic	Radiation	MoKα (λ = 0.71073)
Space group	$P2_1/c$	2Θ range for data collection/°	4.404 to 53.61
a/Å	8.5821(3)	Index ranges	$-10 \le h \le 10$, $-15 \le k \le 15$, $-22 \le l \le 23$
b/Å	12.4611(4)	Reflections collected	41828
c/Å	18.6160(6)	Independent reflections	4168 [R_{int} = 0.0321, R_{sigma} = 0.0176]
α/°	90	Data/restraints/parameters	4168/0/245
β/°	96.4610(10)	Goodness-of-fit on F^2	1.059
γ/°	90	Final R indexes [I>=2σ (I)]	R_1 = 0.0241, wR_2 = 0.0662
Volume/Å^3	1978.20(11)	Final R indexes [all data]	R_1 = 0.0252, wR_2 = 0.0672
Z	4	Largest diff. peak/hole / e Å^{-3}	0.28/-0.49

Single-crystal X-ray structure analysis of 13:

Colorless single crystals of **13** were obtained by the diffusion of Et_2O into a DCM/*n*-hexane solution of **13** at ambient temperature. The single-crystal X-ray structure analysis revealed that **13** crystallizes in the monoclinic space group $P2_1/c$. The asymmetric unit contains one molecule of **13** and one molecule of DCM.

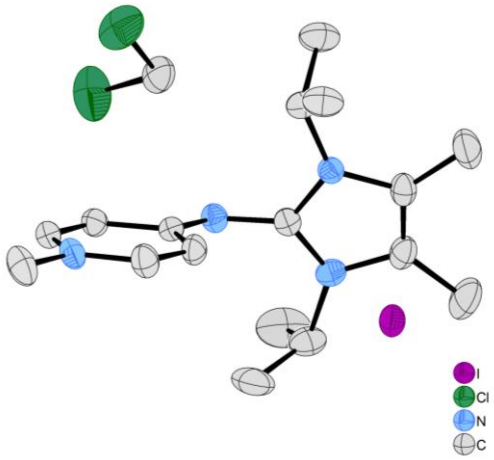

Figure S60: Molecular view of **13** in the solid state with thermal ellipsoid plot at the 50% levels of probability. Hydrogen atoms are omitted for clarity.

Identification code	**2354133**	ρ_{calc}g/cm^3	1.454
Empirical formula	$C_{18}H_{29}Cl_2IN_4$	μ/mm^{-1}	1.647
Formula weight	499.25	F(000)	1008.0
Temperature/K	150.0	Crystal size/mm^3	0.24 × 0.12 × 0.09
Crystal system	monoclinic	Radiation	MoKα (λ = 0.71073)
Space group	$P2_1/c$	2Θ range for data collection/°	4.43 to 61.06
a/Å	9.6460(5)	Index ranges	$-13 \leq h \leq 13$, $-34 \leq k \leq 34$, $-14 \leq l \leq 14$
b/Å	23.9946(12)	Reflections collected	64820
c/Å	10.3357(5)	Independent reflections	6934 [R_{int} = 0.0848, R_{sigma} = 0.0404]
α/°	90	Data/restraints/parameters	6934/0/233
β/°	107.612(2)	Goodness-of-fit on F^2	1.047
γ/°	90	Final R indexes [I>=2σ (I)]	R_1 = 0.0362, wR_2 = 0.0695
Volume/Å^3	2280.1(2)	Final R indexes [all data]	R_1 = 0.0535, wR_2 = 0.0795
Z	4	Largest diff. peak/hole / e Å^{-3}	0.77/-1.08

References

1 Y. Han; H. V. Huynh; G. K. Tan, *Organometallics*, **2007**, *26*, 6447–6452.
2 H. V. Huynh; Y. Han; R. Jothibasu; J. an Yang, *Organometallics*, **2009**, *28*, 5395–5404.
3 Q. Teng; P. S. Ng; J. N. Leung; H. V. Huynh, *Chem. Eur. J*, **2019**, *25*, 13956–13963.
4 R. A. Kunetskiy; S. M. Polyakova; J. Vavřík; I. Císařová; J. Saame; E. R. Nerut; I. Koppel; I. A. Koppel; A. Kütt; I. Leito; I. M. Lyapkalo, *Chem. Eur. J.*, **2012**, *18*, 3621–3630.
5 X. Zhou; K.-C. Lau; B. J. Petro; R. F. Jordan, *Organometallics*, **2014**, *33*, 7209–7214.
6 H. V. Huynh; Y. Han; R. Jothibasu; J. an Yang, *Organometallics*, **2009**, *28*, 5395–5404.
7 A.-C. C. Carlsson; J. Gräfenstein; A. Budnjo; J. L. Laurila; J. Bergquist; A. Karim; R. Kleinmaier; U. Brath; M. Erdélyi, *J. Am. Chem. Soc.*, **2012**, *134*, 5706–5715.
8 H. Xiao; K. Xin; H. Dou; G. Yin; Y. Quan; R. Wang, *Chem. Commun.*, **2015**, *51*, 1442–1445.
9 S. Lall; V. Behaj; D. Mancheno; R. Casiano; M. Thomas; A. Rikin; J. Gaillard; R. Raju; A. Scumpia; S. Castro; R. Engel; J. I. Cohen, *Synthesis*, **2002**, 1530–1540.
10 D. G. Gusev, *Organometallics*, **2009**, *28*, 6458–6461.
11 Frisch, M.J., Trucks, G.W., Schlegel, H.B., Scuseria, G.E., Robb, M.A., Cheeseman, J.R., Scalmani, G., Barone, V., Mennucci, B., Petersson, G.A., Nakatsuji, H., Caricato, M., Li, X., Hratchian, H.P., Izmaylov, A.F., Bloino, J., Zheng, G., Sonnenberg, J.L., Hada, M., Ehara, M., Toyota, K., Fukuda, R., Hasegawa, J., Ishida, M., Nakajima, T., Honda, Y., Kitao, O., Nakai, H., Vreven, T., Montgomery Jr., J.A., Peralta, J.E., Ogliaro, F., Bearpark, M., Heyd, J.J., Brothers, E., Kudin, K.N., Staroverov, V.N., Kobayashi, R., Normand, J., Raghavachari, K., Rendell, A., Burant, J.C., Iyengar, S.S., Tomasi, J., Cossi, M., Rega, N., Millam, J.M., Klene, M., Knox, J.E., Cross, J.B., Bakken, V., Adamo, C., Jaramillo, J., Gomperts, R., Stratmann, R.E., Yazyev, O., Austin, A.J., Cammi, R., Pomelli, C., Ochterski, J.W., Martin, R.L., Morokuma, K., Zakrzewski, V.G., Voth, G.A., Salvador, P., Dannenberg, J.J., Dapprich, S., Daniels, A.D., Farkas, O., Foresman, J.B., Ortiz, J.V., Cioslowski, J. and Fox, D.J, Gaussian, Inc., Wallingford CT, 2013.
12 Y. Wei; G. N. Sastry; H. Zipse, *Journal of the American Chemical Society*, **2008**, *130*, 3473–3477.
13 O. V. Dolomanov; L. J. Bourhis; R. J. Gildea; J. A. K. Howard; H. Puschmann, *J. Appl. Crystallogr.*, **2009**, *42*, 339–341.
14 L. Palatinus; G. Chapuis, *J. Appl. Crystallogr.*, **2007**, *40*, 786–790.
15 L. Palatinus; A. van der Lee, *J. Appl. Crystallogr.*, **2008**, *41*, 975–984.
16 L. Palatinus; S. J. Prathapa; S. van Smaalen, *J. Appl. Crystallogr.*, **2012**, *45*, 575–580.
17 L. J. Bourhis; O. V. Dolomanov; R. J. Gildea; J. A. K. Howard; H. Puschmann, *Acta crystallogr. A*, **2015**, *71*, 59–75.
18 G. M. Sheldrick, *Acta crystallogr. A*, **2008**, *64*, 112–122.
19 G. M. Sheldrick, *Acta crystallogr. A*, **2015**, *71*, 3–8.